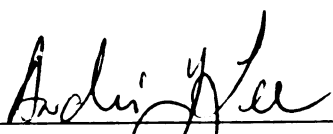




This is to certify that the
thesis entitled
Hygrothermal Effects on the Epoxy Resins
Influenced by the Network Topology
presented by
JinKyu Choi
has been accepted towards fulfillment
of the requirements for
Master's degree in Materials Science


Major professor

Date May 7, 1996

LIBRARY

Michigan State University

PLACE IN RETURN BOX to remove this checkout from your record.
TO AVOID FINES return on or before date due.

DATE DUE	DATE DUE	DATE DUE
JAN 26 1998 100		

**HYGROTHERMAL EFFECTS ON THE EPOXY RESINS
INFLUENCED BY THE NETWORK TOPOLOGY**

By

JinKyu Choi

A THESIS

Submitted to
Michigan State University
in partial fulfillment of the requirements
for the degree of

MASTER OF SCIENCE

Department of Materials Science and Mechanics

1996

ABSTRACT

The hygrothermal effects on the epoxy resins influenced by the network topology were investigated. In this study, the 3-dimensional epoxy network structures were altered by using di-functional, tri-functional, and tetra-functional epoxy resins cured with a di-functional amine, respectively. The samples were immersed in distilled water at isothermal temperature ranging from 45° C to 90° C for over 2000 hours. Moisture absorption was monitored gravimetrically as a function of time. Weight gain percentage was curve fitted against time by using non-linear least-squared curve fitting from which the diffusivity and weight gain percentage at saturation were obtained. The diffusion coefficients were found to be inversely related to the difference between the glass transition temperature (T_g) and the conditioned temperature. The glass transition temperatures were measured by a length dilatometer. Plasticization of the polymer was evident. Positron Annihilation Lifetime Spectroscopy (PALS) provided a great deal of information regarding the nature of water molecules occupying free volume between the polymer molecules. Available hydroxyl sites in the epoxy network, however, proved to be the dominant factor controlling the moisture absorption. Tensile testing results showed that hygrothermal degradation significantly reduced mechanical properties of the epoxy glass. Results from the cross-polarization ^1H solid state NMR in rotating frame and quadrupole echo deuterium ^1H NMR showed that there were no physical evidence of chemical bonding between the water molecules and the crosslink network.

DEDICATION

To

my parents

F

ac

an

the

the

in a

Uni

sper

num

willi

Rook

who

resea

and th

becam

ACKNOWLEDGMENTS

Financial support for this research was provided by the Research Excellence Fund of the State of Michigan.

Upon completion of this research, many people deserve to be thanked and acknowledged.

I would like to thank my advisor, Dr. Andre Lee, for his guidance, support, and most of all, abundant patience throughout this research. I also would like to thank the members of my committee, Dr. Kalinath Mukherjee and Dr. Roger J. Morgan for their input and guidance. I am also grateful to Dr. James P. Lucas for his generosity in allowing me to use the moisture chambers, and for his input on this research.

There are some other members of the College of Engineering at Michigan State University whose help I deeply appreciate. Those include Dr. Kermit Johnson, who spent a number of hours to assist me on operating and analyzing NMR spectra, and numerous discussions with him on NMR are invaluable; Mr. Mike Rich, who was willing to answer any questions I had regarding experimental techniques; Mr. Brian Rook, who patiently instructed me on operating various equipments; Mr. Jiming Zhou, who shared many articles, ideas and friendship with me during the course of this research.

I deeply thank my parents and family for their emotional and financial support, and their never-ending encouragement throughout my education.

Last, but not least, I would like to thank my wife, Sora who “officially” became a part of my life during this research, for her patience, love and support.

LI

LI

1.

1

1

1

2. M

2.

2.

2.

2.

Table of Content

LIST OF TABLES	ix
LIST OF FIGURES	x
1. INTRODUCTION.....	1
1.1 Problems	1
1.2 Outline.....	3
1.3 General Background	5
1.3.1 “Volumetric” and “Interaction” Approach.....	7
1.3.2 Spectroscopy	9
1.4 Overview	10
2. MATERIALS AND SAMPLE PREPARATIONS	12
2.1 Materials.....	12
2.2 Sample Mixing	17
2.2.1 Weight fraction of DGEBA, MY510, MY721, and D230.....	17
2.2.2 Mixing	17
2.3 Curing Cycle	19
2.3.1 DGEBA/D230	19

2

3.1

3

3.

3.

3.

3.5

4. M

4.1

4.2

4.3

4

2.3.2 MY510/D230	19
2.3.3 MY721/D230	20
2.4 Sample Storage.....	20
3. MOISTURE ABSORPTION.....	21
3.1 Diffusion	21
3.2 Sample Preparations	23
3.3 Experimental Procedure.....	23
3.4 Results and Discussion	26
3.4.1 Sorption behaviors	26
3.4.2 Thickness effects on the sorption behavior	36
3.4.3 Hydroxyl Sites Dependency	42
3.5 Summary.....	44
4. MOISTURE EFFECTS ON PHYSICAL PROPERTIES.....	45
4.1 Dilatometry	45
4.2 Experimental Procedure	46
4.3 Results and Discussion	52
4.3.1 Glass Transition Temperature (T_g)	52

4.3.2 Coefficients of Thermal Expansion (CTE)	62
4.4 Positron Annihilation Lifetime Spectroscopy (PALS)	67
4.4.1 Background	67
4.4.2 PALS	69
4.4.3 Experimental Procedures	71
4.4.4 Results and Discussions	71
4.5 Summary	76
5. MOISTURE EFFECTS ON MECHANICAL PROPERTIES	78
5.1 Experimental Procedures	78
5.2 Samples	78
5.3 Results and Discussions	79
5.3.1 Oxidation and Degradation	79
5.4 Summary	92
6. NUCLEAR MAGNETIC RESONANCE SPECTROSCOPY	93
6.1 Introduction	93
6.2 The Spin-Lattice Relaxation Time (T_1)	104
6.3 Cross-Polarization (CP)	106

6

6

6.

6.

6.

6.

7. C

8. R

6.4 Proton Spin-Lattice Relaxation Times in the Rotating Frame.....	111
6.4.1 The rotating frame	111
6.4.2 Proton spin-lattice relaxation times in the rotating frame.....	116
6.5 Sample Preparation for the T_{CH} and $^H T_{1\rho}$ Experiment.....	117
6.6 Experimental Procedure	117
6.7 Results and Discussion	118
6.7.1 ^1H Spin-Lattice Relaxation Times in the Rotating Frame	118
6.8 Quadrupole Echo Deuterium NMR Experiment.....	124
6.8.1 Results and Discussion	125
6.9 Summary.....	129
7. CONCLUSIONS.....	130
8. REFERENCES.....	133

LIST OF TABLES

Table 2-1: The stoichiometric mixing ratio of epoxies and a diamine.	18
Table 3-1: Changes in M_{∞} and diffusivity due to the functionality difference and moisture absorption.	30
Table 3-2: Activation energy and diffusion coefficients of the epoxy systems	35
Table 3-3: Thickness effects on M_{∞} and D	41
Table 3-4: Number of hydroxyl groups in each epoxy.	43
Table 4-1: Change of the glass transition temperatures due to moisture saturation.	53
Table 4-2: Correlation between $\Delta T = T_g - T_g $ and the diffusivities of the epoxy glasses.	55
Table 4-3: Thermal Expansion Coefficients of DGEBA/D230, MY510/D230, and MY721/D230.	64
Table 4-4: Thermal Expansion Coefficient of DGEBA/D230, MY510/D230, and MY721/D230 after the moisture has been desorbed at 100°C for 3 days.	66
Table 4-5: τ_3 and I_3 results on epoxy systems.	74
Table 4-6: Conditioned-temperature effects on the free volume. Presented here are data obtained on DGEBA/D230 epoxy network.	75
Table 5-1: Tensile testing results on DGEBA/D230 epoxy systems.	84
Table 5-2: Tensile testing results on MY510/D230 epoxy systems.	85
Table 5-3: Tensile testing results on MY721/D230 epoxy systems.	86
Table 6-1: T_{CH} and $^H T_{I\rho}$ of DGEBA/D230	119
Table 6-2: T_{CH} and $^H T_{I\rho}$ of MY510/D230	120
Table 6-3: T_{CH} and $^H T_{I\rho}$ of MY721/D230	121

Fig

Fig

Fig

Fig

Fig

Fig

Fig

Fig

Fig

Fig

Fig

Fig

LIST OF FIGURES

Figure 2-1: Diglycidyl ether of bisphenol A (DER 332).....	13
Figure 2-2: Diglycidyl ether of para-aminophenol (Araldite MY510).....	14
Figure 2-3: N,N,N',N',-Tetraglycidyl-4,4'-methylenebisbenzenamine (Araldite MY721).....	15
Figure 2-4: The chemical structure of diamine.....	16
Figure 3-1: The variation of M_t/M_∞ with time. Exact (solid line): Eq. 3-4; approximate (dotted line): Eq. 3-5.....	24
Figure 3-2 (a): Moisture absorption curve of DGEBA/D230. Samples were saturated with water at 45°C, 60°C, 75°C, and 90°C for 2254 hours. Lines represent theoretical curves. Symbols represent experimental data at different temperatures.....	27
Figure 3-2 (b): Moisture absorption curve of DGEBA/D230. Samples were saturated with water at 45°C, 60°C, 75°C, and 90°C for 2254 hours. Lines represent theoretical curves. Symbols represent experimental data at different temperatures.....	28
Figure 3-2 (c): Moisture absorption curve of DGEBA/D230. Samples were saturated with water at 45°C, 60°C, 75°C, and 90°C for 2254 hours. Lines represent theoretical curves. Symbols represent experimental data at different temperatures.....	29
Figure 3-3 (a): $\ln D$ vs. $1/T$ curve of DGEBA/D230, where D is the diffusivity (cm^2/sec) and T is the temperature (K).....	32
Figure 3-3 (b): $\ln D$ vs. $1/T$ curve of MY510/D230, where D is the diffusivity (cm^2/sec) and T is the temperature (K).....	33
Figure 3-3 (c): $\ln D$ vs. $1/T$ curve of MY721/D230, where D is the diffusivity (cm^2/sec) and T is the temperature (K).....	34
Figure 3-4 (a): Sorption curves for DGEBA/D230 with different thickness; S1 and S2. Hollow symbols represent thick samples (S1). Filled symbols represent thin samples (S2).	38

Figure 3-4 (b): Sorption curves for MY510/D230 with different thickness; S1 and S2. Hollow symbols represent thick samples (S1). Filled symbols represent thin samples (S2).	39
Figure 3-4 (c): Sorption curves for MY721/D230 with different thickness; S1 and S2. Hollow symbols represent thick samples (S1). Filled symbols represent thin samples (S2).	40
Figure 4-1: A length dilatometer built by Omega Co.	48
Figure 4-2: Strain versus Temperature ($^{\circ}\text{C}$) of the DGEBA/D230 epoxy resin. Samples have been saturated with distilled water at 45°C , 60°C , 75°C , and 90°C for 2254 hours.	49
Figure 4-3: Strain versus Temperature ($^{\circ}\text{C}$) of the MY510/D230 epoxy resin. Samples have been saturated with distilled water at 45°C , 60°C , 75°C , and 90°C for 2254 hours.	50
Figure 4-4: Strain versus Temperature ($^{\circ}\text{C}$) of the MY721/D230 epoxy resin. Samples have been saturated with distilled water at 45°C , 60°C , 75°C , and 90°C for 2254 hours.	51
Figure 4-5: Change of the strain between the dry and moisture desorbed samples of the DGEBA/D230 epoxy resin were plotted against temperature ($^{\circ}\text{C}$).	59
Figure 4-6: Change of the strain between the dry and moisture desorbed samples of the MY510/D230 epoxy resin were plotted against temperature ($^{\circ}\text{C}$).	60
Figure 4-7: Change of the strain between the dry and moisture desorbed samples of the MY721/D230 epoxy resin were plotted against temperature ($^{\circ}\text{C}$).	61
Figure 4-8: Schematic illustration of the variation of the specific volume, V , of a polymer with temperature, T . The free volume is represented by the shaded area. (<i>Adapted from R. J. Young, Introduction to Polymers, 1st ed., 1981.</i>)	68
Figure 5-1: Comparison of the color change between dry and moisture saturated samples. As the soaking temperature increases, the color of the sample becomes darker. Shown here are DGEBA/D230 epoxy resins.	80

Figure

Figure

Figure

Figure

Figure

Figure

Figure 6

Figure 6

Figure 6

Figure 6

Figure 6

Figure 5-2: Comparison of the color change between dry and moisture saturated samples on MY510/D230 epoxy resins.	81
Figure 5-3: Comparison of the color change between dry and moisture saturated samples on MY721/D230 epoxy resins.	82
Figure 5-4: Change of % strain at break (%) are shown here.	89
Figure 5-5: Change of load at break (kN) are shown here.	90
Figure 5-6: Change of Young's modulus (MPa) are shown here.	91
Figure 6-1: A spinning proton generates a magnetic field, called its magnetic moment. This magnetic field (H_o) resembles that of a small bar magnet. <i>Adapted from [43]</i>	94
Figure 6-2: An external magnetic field (H_o) applies a force to a small bar magnet, twisting the bar magnet to align it with the external field. The arrangement of the bar magnet aligned <i>with</i> the field is lower in energy than the arrangement aligned <i>against</i> the field. <i>Adapted from [43]</i>	95
Figure 6-3: In the presence of an external magnetic field (H_o), a proton has a spin quantum number (I) of either $+1/2$ or $-1/2$. The state with spin $I = +1/2$ is called the α -spin state, aligned with the external magnetic field. The state with spin $I = -1/2$ is called the β -spin state, aligned against the external field. The β -spin state is higher in energy than the α -spin state. <i>Adapted from [43]</i>	97
Figure 6-4: The nuclear spin generates a small magnetic field, and in the absence of an applied magnetic field, the orientation of these dipoles is random (a). When a sample is placed in a homogenous magnetic field, the dipoles will align themselves with the lines of induction or force of the applied magnetic field (b). However, thermal motion does not allow the alignment to remain, and the average alignment is at a small angle to the magnetic field (c). The magnetic moment precesses about the magnetic field at the Larmor frequency (d). <i>Adapted from [43]</i>	100
Figure 6-5: Quantized energies of nuclei in a magnetic field. <i>Adapted from [43]</i>	102
Figure 6-6: A nucleus in "in resonance" when it is irradiated with radio-frequency photons having energy equal to the energy difference between the spin states. Under these conditions, a proton in the α -spin state can absorb a photon and change to the β -spin state. <i>Adapted from [44]</i>	103

Figure

Figure

Figure

Figure

Figure

Figure

Figure

Figure 6-7: The timing sequence for the cross-polarization experiment. <i>Adapted from [43]</i>	109
Figure 6-8: Diagram to show the motion of a spinning nucleus in a magnetic field of direction z. <i>Adapted from [48]</i>	113
Figure 6-9: Changing coordinates to the rotating frame: (a) rotation of magnetic moment μ about laboratory coordinates; (b) change of coordinates to rotating frame and application of a radio-frequency induced magnetic field along x' ; (c) after application of field H_1 along x' (note the vector M moves through the $z'y'$ plane by 90° to become colinear with y'); (d) after changing the phase of the irradiation field so that H_1 is colinear with M and y' . <i>Adapted from [48]</i>	115
Figure 6-10: The change in carbon magnetization with contact time for the cross-polarization experiment. The initial rise is due to the cross-polarization contact time, T_{CH} , and the relaxation decrease is governed by the $^H T_{1\rho}$	122
Figure 6-11: Quadrupole echo deuterium 1H NMR spectrum of D_2O . The sharp peak at $\delta 16000$ is indicating the chemical shift of pure deuterium. .	126
Figure 6-12: Quadrupole echo deuterium 1H NMR spectra of samples saturated with D_2O at $90^\circ C$; (a) DGEBA/ D_2O ; (b) MY510/ D_2O ; and (c) MY721/ D_2O	127
Figure 6-13: Quadrupole echo deuterium 1H NMR spectra of D_2O desorbed samples ($100^\circ C$ for 4 days); (a) DGEBA/ D_2O ; (b) MY510/ D_2O ; and (c) MY721/ D_2O	128

matrix

to ex

mech

to mo

enviro

behav

moistu

and pa

effect

interac

behavi

conten

to the

1.1 Pr

the am

hardene

1. INTRODUCTION

Epoxy resins are widely used as structural adhesives and composite matrices in both the aerospace and automotive industries, and are often exposed to extreme environments. Such service environment raises some concern that the mechanical properties of such materials may suffer when the material is exposed to moisture for long periods of time. The durability of epoxies in such service environments is difficult to predict without a knowledge of the structure, and behaviors of deformation and failure.

Many investigation have been conducted to address various aspects of moisture induced behavior in part to understand the structure [1, 4~40, 61, 62] and partly to understand the behaviors of mechanical response due to the moisture effect [56, 58, 59, 60]. Until now, the explanations on (i) how the moisture interact with the epoxy network and (ii) how its structure and mechanical behavior were influenced by the moisture were based upon varying the amine content. Moisture uptake was monitored as a function of the amine's mole ratio to the epoxy, of the different amine types, or of the curing time.

1.1 Problems

Most of the sorption kinetics studies have been performed either by varying the amine content, or by changing cure conditions. Synthesizing epoxides and hardeners with off-stoichiometric ratio will produce excess amount of either

epoxie

their s

group

until t

temper

other h

absorb

These

bondin

of the

bisphen

diamine

states

PDA is

would

behavio

extent

they or

Morel

epoxides or hardeners in the system. Carfagna *et al.* discussed this problem in their studies [11]. If excess amount of epoxide is present, the secondary hydroxyl groups, formed in the previous reaction, could add to the remaining epoxide rings until the glass transition temperature of the forming network exceeds the curing temperature and the unfavored reaction becomes diffusion controlled. On the other hand, when the resin is crosslinked with a large excess of hardener, the resin absorbs more water than that crosslinked with stoichiometric amount of hardener. These findings suggest that the presence of unreacted amines provide hydrogen bonding sites, resulting in increased moisture absorption.

Another effect discussed by Diamant *et al.* [4] is due to the resin polarity of the hardener. In order to increase crosslink density, diglycidyl ether of bisphenol A (DGEBA) was cured with *m*-phenylenediamine (*m*-PDA) and parts of diamine was replaced with aniline. The *m*-PDA molecule has more resonative states which allocate a higher negative charge on the benzene ring such that *m*-PDA is highly soluble in water whereas aniline is almost insoluble. Thus, *m*-PDA would attract moisture more than aniline.

Curing condition is another contributing factor in moisture absorption behavior. Danieleley *et al.* [10] found that the water uptake increases with the extent of cure, and concluded that hydroxyl groups play a predominant role since they originate from epoxide-amine reactions. However, a question was raised by Morel *et al.* [7] that epoxide-epoxide and epoxide-alcohol side reactions in

TGM

obtain

exten

the de

crossl

polym

affect

sorpti

water

crossl

sites

amoun

conte

1.2

mater

hydro

differe

$h l \ll$

TGMDA-DDS system are also important, because the higher degree of cure is obtained with a relatively low hardener concentration. Thus, it is to a certain extent difficult to speculate on the hydroxyl build-up in the final stage of cure [7].

Moy and Karasz [12] also argued the moisture absorption dependency on the degree of curing. Curing at higher temperatures is expected to increase the crosslink density as well as increasing the number of hydroxyl groups in the polymer such that the equilibrium sorption of water in the resin is markedly affected by the curing conditions. It was found that a decrease in the rate of sorption with increasing cure temperature suggests that sorption and transport of water vapor in the glassy state of the epoxy is predominantly controlled by the crosslink density rather than by the increase in the number of possible sorption sites. These arguments, however, ignore a possibility that uncured or excess amount of hardener would react with water resulting in an increased moisture content in the epoxy resin.

1.2 Outline

Chemical structure, processing conditions, and sample storage of the materials were presented in Chapter 2.

In Chapter 3, the moisture sorption behaviors in relation to the available hydroxyl sites were investigated. Moisture uptakes of the materials under different hygrothermal conditions were monitored as a function of time. Since the $h/l \ll 1$ and $h/w \ll 1$ (h is the thickness, l is the length, and w is the width of the

sample

on the

various

variati

(PALS

mecha

intensi

PALS

expans

studied

prepare

distille

temper

worsen

discuss

network

were pr

this stu

sample), 1-dimensional diffusion was assumed, neglecting "edge effects". Based on the solution of Fick's second law, diffusion coefficients of the samples at various conditioning temperatures were obtained. The effect of the thickness variation on the sorption behavior was also discussed.

In Chapter 4, by using the positron annihilation lifetime spectroscopy (PALS) and length dilatometry, moisture effects on the change of physical and mechanical properties were discussed. Measurements of the free volume size and intensity change of the free volume upon moisture absorption were measured by PALS. Change of glass transition temperatures and coefficient of thermal expansion were measured by the dilatometer.

In Chapter 5, the mechanical response due to the moisture absorption was studied by using a screw-driven Instron tensile testing machine. Few tables were prepared to report tensile testing results. After prolonged immersion in the distilled water at elevated temperatures, surface discoloration was evident. As the temperature of the immersion increased, the degree of discoloration became worsen. Reasonings in conjunction with the effect of chemical degradation were discussed.

To conduct a microscopic investigation on the moisture in the epoxy networks, nuclear magnetic resonance spectroscopy was employed and its results were presented in Chapter 6. It is noteworthy that the NMR technique used in this study was ^{13}C NMR spin-lattice relaxation times supplemented by cross-

polariz

moistur

echo de

on the n

T

results o

1.3 Gen

T

perform

involve

interacti

response

be safe t

hundreds

Gr

moisture

different

one with

revealed

diffusion-e

polarization. Delay of the relaxation time, $^H T_{1\rho}$, and its relationship to the moisture mobility in the epoxy network were discussed. In addition, a quadrupole echo deuterium NMR study was also conducted to provide additional information on the nature of the moisture in the epoxy networks.

The last chapter, Chapter 7, contains conclusions of the experimental results of this study.

1.3 General Background

The sorption of solvent in polymeric composites and their effects on the performance of the composites are highly complicated issues. Their studies involve the implications of (i) the polymer science; focusing on molecular-level interactions, and (ii) the applied mechanics; mainly dealing with mechanical response. An extensive review of this subject is a profound task such that it may be safe to assume that the total number of papers regarding this subject run into hundreds, maybe even thousands.

Gupta, Drzal, and Rich [5] conducted an experiment characterizing the moisture transport through a di-functional epoxy resin (DGEBA) cured with different amounts of metaphenylene diamine (m-PDA), using two cure cycles i.e., one with standard cure and the other with additional post cure. The sorption data revealed that moisture sorption proceeded with having two stages. The initial diffusion-controlled linear region showed considerable temperature dependence.

The t

highly

sampl

less d

appea

tempe

moistu

that t

determ

i.e., at

in con

on th

differe

condu

bisphe

fillers

nonline

point.

coeffic

increas

The temperature dependence of the initial region was relatively small for the most highly crosslinked, high T_g samples and was high for the less crosslinked, low T_g samples. At longer times, however, the moisture uptake appeared to be rather less dependent on temperature. The temperature dependence in this region also appeared to be large for samples of low crosslink density, low T_g . At room temperature, the most highly crosslinked samples absorbed the maximum moisture, while at 100°C they absorbed the least. From these findings, they noted that the specific volume and the free volume played a. important role in determining the moisture absorption characteristics of the post-cured samples, i.e., at room temperature, there were small differences in specific volume resulting in considerable differences in their diffusion coefficient. At higher temperature, on the other hand, large differences in specific volume lead to only small differences in diffusion coefficient.

Similar results can be found in other papers. De'Nève and Shanahan [19] conducted an experiment of water sorption based on the diglycidyl ether of bisphenol A (DGEBA), crosslinked with dicyandiamide (DDA), and contained fillers (Ciba-Geigy XB3131). At the start of water uptake, the curve was nonlinear and rather it was more like sigmoidal in shape with a single inflection point. This type of curve was explained by using a history-dependent diffusion coefficient. Rising penetrant concentration was assumed to lead to an immediate increase in diffusion coefficient, followed by a slow drift towards an equilibrium

value a

noted t

depend

the sign

V

an offs

insuffici

undergo

oxidatio

N

showed

water th

weight

between

one is d

and the

diffusio

1

B

resides

"volumic

value as a result of a relaxation process characteristic of the glassy state. They noted that the value of the diffusion coefficient in any element of the system depended on the concentration history of the element. They also concluded that the sigmoidal behavior was evident in the case of an excess of hardener.

Wong and Broutman [45, 46] also discussed in their papers that there was an offset between the theoretical and experimental diffusion curves for an insufficiently cured epoxy network (DGEBA/m-PDA) and was caused by the resin undergoing further postcuring in the sorption process. They also noted that oxidation of the resin during sorption also caused the offset between the curves.

Moy and Karasz [12] found that the sorption curve they have constructed showed a non-linearity during the initial sorption process. The diffusion of the water through the resin is found to increase with the concentration of water from weight gain rates at various partial pressures. Their reasoning for the mismatch between the theoretical and experimental diffusion curves consists of two effects; one is due to the irreversible chemical reaction taking place between the polymer and the water, forming hydrogen bonds. The other is due to decoupling of the diffusion to a relaxation process at T_g .

1.3.1 “Volumetric” and “Interaction” Approach

Besides the arguments on the kinetics of fluid sorption, how the moisture resides within the epoxy network is another controversial issue; one is the “volumic” approach and the other is the “interaction” approach.

which

molecu

that th

microv

free vo

interact

has been

the ava

microv

offer pr

T

are nei

morphol

hydroph

types of

that the

of the ep

C

stoichion

of amine

The free volume, by definition, is the space in a solid or liquid sample which is not occupied by polymer molecules, i.e. the 'empty-space' between molecules [50]. Researchers based upon the free volume approach are claiming that the absorbed moisture takes up the free volume, 'empty-space' and microvoids, and is relatively free to travel through the free-volume voids [6]. The free volume approaches, however, often neglect the existence of specific interactions between water and hydrophilic sites of the network. For instance, it has been suggested that the water equilibrium concentration is mainly governed by the available free volume [6, 8], or that water molecules occupy essentially the microvoids, internodular areas and other morphological defects [4, 5] which can offer preferential ways for their diffusion.

The "interaction" approaches, on the other hand, state that water molecules are neither distributed randomly in the network nor concentrated in its morphological defects, but rather linked by strong hydrogen bonds to some hydrophilic loci, mainly hydroxyls [10] or amines [11]. The contribution of both types of groups could be interdependent [7]. Some researchers also suggested that the degree of curing takes an important role in the morphology and chemistry of the epoxy-water system.

Carfagna et al. [11] conducted a sorption experiment by altering stoichiometric ratio of amine and found that the epoxies with the excess amount of amine had higher equilibrium water uptake level than the epoxies with less

amount of amine. It was proposed that the presence of unreacted amines contributed to increasing the equilibrium water uptake level by providing more hydrogen bonding sites.

It is noteworthy that in the volumic approach, the behavior of the water-epoxy system is mainly controlled by the physical state of the polymer, while in the interaction approach, the chemical structure plays a dominant role and often this approach was accounted for by spectrometric observations such as FT-IR [13, 40, 64] and NMR [9, 12, 41, 50, 51].

1.3.2 Spectroscopy

Using FT-IR spectroscopy, Ghorbel and Valentin [13] revealed that there was a modification in the intensities and shape of the peaks in polyester and vinylester resins due to reactions such as the decrease in the styrene content and the hydrolysis. In addition, Koenig [43] showed that the frequency of the in-plane bending mode of water in epoxy resins lies between the frequencies of liquid and mobile water proposing that the sorbed water was clutched within the epoxy resin by hydrogen bonding.

Nuclear magnetic resonance is another sensitive technique of probing the molecular interaction between two components. Moy and Karasz [12], in their results, suggested that at low concentration, the water may be interacting with adjacent bond sites so that not only translational but rotational movement becomes hindered as well. At higher concentrations, however, secondary layers

of water

Similar

proton

became

noted t

scale, g

the dia

that a n

than ag

present

Karasz

interact

that (r)

water,

the wa

1.4 Ov

curing

functio

epoxide

of Texa

of water molecules were able to rotate freely and line narrowing was observed. Similar results were reported by Schadt and Vanderhart [41] by using solid state proton NMR. It was noted that at higher water concentrations, linewidth became narrower, indicating that the water mobility was increased. It was also noted that they found no evidence of a uniform distribution of crosslinks on a scale, greater than 4 nm, which possessed a mobility gradient. This suggests that the diameter of a void is no larger than 40 angstroms. In conclusion, they stated that a majority of water molecules were molecularly dispersed in the epoxy rather than aggregated in a water like state within voids, suggesting that if voids are present, they can only accommodate one or two molecules. In different papers, Karasz and co-workers [50, 51] reported the nature of the epoxy-water molecule interactions using quadrupole echo deuterium NMR spectroscopy. They stated that (i) the movement of water is impeded in epoxy resin; (ii) there is no free water; (iii) there is no evidence for tightly bound water; and (iv) it is unlikely that the water disrupts the hydrogen-bond network in the epoxy resin.

1.4 Overview

In this study, instead of varying amine contents or tempering with the curing conditions, the entire experiments were carried out based upon varying the functionalities of the epoxy resins only, such that *di*-, *tri*-, and *tetra*-functional epoxides were cured with an amine terminated PPO (Jeffamine D230, designation of Texaco Chemical Company). Also, by having the mole ratio of the epoxide to

amine

fully c

two co

concer

(ii) th

monom

inconsi

enable

the ep

diffusio

morpho

amine to that of the stoichiometric ratio, it was assumed that the epoxies were fully cured pertaining the highest crosslink density as much as possible. These two conditions, as well as using more flexible hardener like PPO, eliminated concerns evolved from (i) the further curing during the hygrothermal treatment, (ii) the interaction between the water molecules and an excess amount of monomers, (iii) diffusion controlled secondary amine reaction, and (iv) an inconsistent free volume distributions. It is believed that these conditions will enable a thorough investigation on the physical nature of the water absorption in the epoxy networks. The moisture absorption behavior, characterization of diffusion process, moisture effects on physical and mechanical properties, and morphological characterization by using solid state NMR were also presented.

2.1

dia

are

Cha

ph

epo

cro

desi

epo

2. MATERIALS AND SAMPLE PREPARATIONS

2.1 Materials

Sample having different polymer network topologies cured with PPO diamines have been investigated. The commercially available epoxy resins studied are based on di-functional pure diglycidyl ether of bisphenol A (DER 332, Dow Chemical, USA); tri-functional low viscosity epoxy resin based on para amino phenol (Araldite MY510, Ciba-Geigy Corporation); and tetra-functional liquid epoxy based on methylene dianiline (Araldite MY721, Ciba-Geigy Corporation) crosslinked with an amine terminated poly(propylene oxide) (Jeffamine D230, designation of Texaco Chemical Company). The chemical structures of the three epoxies mentioned on the above are described in Figure 2-1 through Figure 2-4.

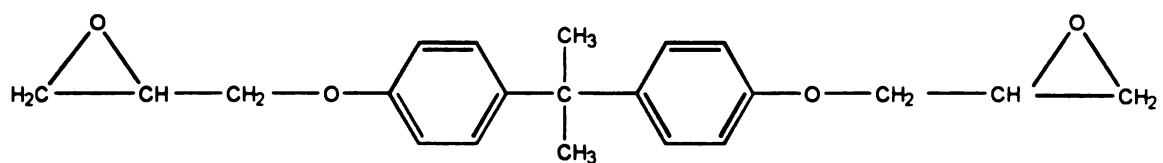


Figure 2-1: Diglycidyl ether of bisphenol A (DER 332)

Fig

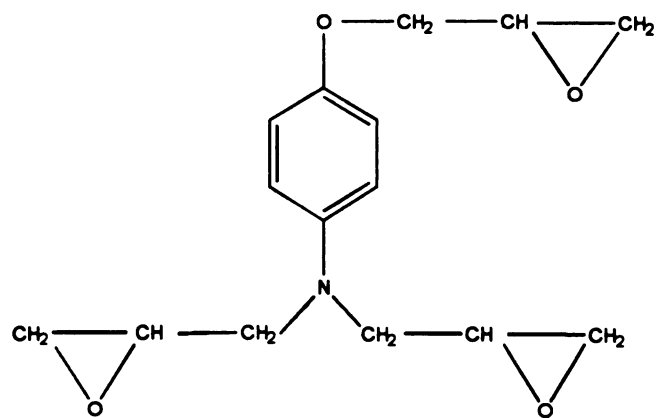


Figure 2-2: Diglycidyl ether of para-aminophenol (Araldite MY510)

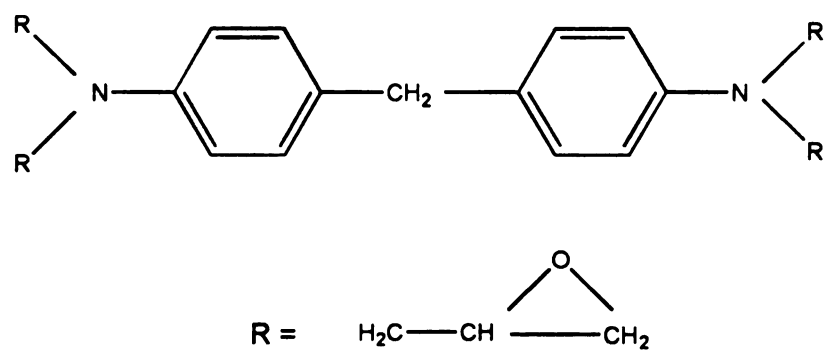


Figure 2-3: N,N,N',N',-Tetraglycidyl-4,4'-methylenebisbenzenamine (Araldite MY721)

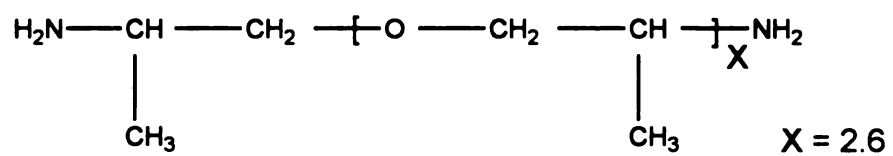


Figure 2-4: The chemical structure of diamine.

Jeffamine D-230 Polyoxypropylenediamine

2.2 Sam

2.

DO

M

M

D2

2.2

Epo

(Jeffamine

stoichiome

using a gra

and the mi

The mixtu

temperature

each sample

2.2 Sample Mixing

2.2.1 Weight fraction of DGEBA, MY510, MY721, and D230

DGEBA: 170 g / epoxy group (e.g.)

MY510: 100 g / e.g.

MY721: 110 g / e.g.

D230: 57.5 g / e.g.

2.2.2 Mixing

Epoxies (DGEBA, MY510, and MY721) were mixed with diamine (Jeffamine D230) and the mole ratio of epoxide to amine was that of stoichiometric ratio, as shown in Table 2-1. After the weights were measured by using a gravimetric balance with 0.1 mg resolution, diamine was added to epoxies and the mixtures were stirred with wooden stirrers until they became clear liquid. The mixtures were then placed in a vacuum oven for degassing at room temperature for 30 to 40 min. Weighing, mixing, degassing were performed on each sample, separately.

Epoxy
DGEE
MY51
MY72

Table 2-1: The stoichiometric mixing ratio of epoxies and a diamine.

Epoxies	g/epoxy group	Total weight (g) (epoxy+diamine)	Wt. fraction of D230	Wt. fraction of epoxies
DGEBA	170	$170 + 57.5$ $= 227.5$	$57.5 / 227.5$ $= 0.2527$	$170 / 227.5$ $= 0.7473$
MY510	101	$101 + 57.5$ $= 158.5$	$57.5 / 158.5$ $= 0.3628$	$101 / 158.5$ $= 0.6372$
MY721	110	$110 + 57.5$ $= 167.5$	$57.5 / 110$ $= 0.3433$	$110 / 167.5$ $= 0.6567$

hou

the

moie

mixt

degr

remo

silico

and 6

24 ho

allowe

hours t

the dia

stoichic

homoge

30 to 40

2.3 Curing Cycle

2.3.1 DGEBA/D230

The DGEBA, di-functional epoxide monomer, was preheated at 60°C for 2 hours to melt any crystals present. The amine was then added to the epoxide and the mixture was stirred by a wooden tongue until it becomes a clear mixture. The mole ratio of the epoxide to amine was that of the stoichiometric ratio. The mixture was degassed at room temperature for 30 to 40 minutes, depending on the degree of the bubbles present on top of the mixture's surface, under vacuum to remove all the air bubbles as much as possible. Then, the mixture was cast into silicon molds with dimensions of $7.62\text{ cm} \times 0.32\text{ cm} \times 1.27\text{ cm}$ rectangular strips and $6.0\text{ cm} \times 0.16\text{ cm} \times 1.0\text{ cm}$ tensile testing coupons, and cured at 100°C for 24 hours. After the drying cycle, the molds were removed from the oven and allowed to cool slowly at room temperature over night.

2.3.2 MY510/D230

The MY510, tri-functional epoxide monomer, was preheated at 60° C for 2 hours to melt any crystals left in the epoxide. Then the epoxide was mixed with the diamine, D230, where the mole ratio of the epoxide to amine was that of the stoichiometric ratio. The mixture was stirred by a wooden stirrer until it became homogeneous viscous liquid. The mixture was degassed at room temperature for 30 to 40 minutes under vacuum to allow all the bubbles to escape. The mixture

was

of t

curr

tem

2 h

epo

epo

at r

for c

allow

2.4

temp

bega

was then cast into a silicon mold and cured at 130° C for 24 hours. Dimensions of the specimens were identical to that of the DGEBA/D230 specimens. After the curing, the mold was removed from the oven and allowed to cool slowly at room temperature over night.

2.3.3 MY721/D230

The MY721, tetra-functional epoxide monomer, was preheated at 60°C for 2 hours to melt any crystals that might be trapped in the epoxide. The MY721 epoxide was then mixed with diamine (Jeffamine D230). The mole ratio of the epoxide to amine was that of the stoichiometric ratio. The mixture was degassed at room temperature for 30 to 40 minutes under vacuum, then cast into the mold for curing at 157° C for 24 hours. The molds were removed from the oven and allowed to cool slowly at room temperature over night.

2.4 Sample Storage

After the curing cycle, the samples were stored in ziploc bags at room temperature until the experiments were begun. Before the moisture experiment began, the samples had been dried in a vacuum oven at 60° C for 17 days.

3.1 Dif

T

the hypo

a section

section,

where J

concentra

componen

As

volume V

Therefore

componen

Mass Con.

3. MOISTURE ABSORPTION

3.1 Diffusion

The mathematical theory of diffusion in isotropic substance is based upon the hypotheses that the rate of transfer of diffusing substance through unit area of a section is proportional to the concentration gradient measured normal to the section, i.e.

$$J_i = -D_i \nabla C_i$$

Eq. 3-1

where J is the rate of transfer per unit area of section by component i , C the concentration of diffusing substance, and D is called the diffusion coefficient of component i [47].

Assume that the surface is a closed, continuous surface that encloses a volume V . Classically, we assume that mass is not created or destroyed. Therefore, mass flowing out of the surface must result in a decrease in the mass of component i , in the volume V enclosed by the surface. This is called *the Law of Mass Conservation*. This assumption leads to a mass continuity equation, i.e.

$$\text{div} \vec{J} = -\frac{\partial C_i}{\partial t}$$

Eq. 3-2

wh

of c

can

law

solut

where t is time.

If the diffusion coefficient is constant, $D \neq D(C)$, and if there is a gradient of concentration only along the x-axis, by substituting Eq. 3-2 into Eq. 3-1, one can discuss the diffusion phenomena by using a simple solution of Fick's second law as

$$\frac{\partial C}{\partial t} = D \frac{\partial^2 C}{\partial x^2}$$

Eq. 3-3.

For diffusion occurs through both sides of surface, as depicted below, solution of Eq. 3-3 can be written as



$$\frac{M_t}{M_\infty} = 1 - \frac{8}{\pi^2} \sum_{i=0}^{\infty} \exp \left[\frac{-(2i+1)^2 \pi^2 \left(\frac{Dt}{h^2} \right)}{(2i+1)^2} \right] = G(t)$$

Eq. 3-4

where M

saturated

Eq

and the co

the approx

non-linear

3.2 Samp

After

obtain over

for 17 days

3.3 Exper

The

chambers o

moisture up

mg resolution

weight gain

where M_t is the initial diffusant content absorbed in the system at $t=t$, M_∞ the saturated diffusant content at $t=\infty$, and h is the thickness of the sample.

Eq. 3-4 can be approximated [1] by the expression

$$\frac{M_t}{M_\infty} = 1 - \exp\left[-7.3\left(\frac{Dt}{h^2}\right)^{0.75}\right] = H(t)$$

Eq. 3-5

and the comparison between Eq. 3-4 and Eq. 3-5 is shown in Figure 3-1. Since the approximate curve is in well agreement with the theoretical curve, by using non-linear least-square curve fitting, the diffusivity can be obtained.

3.2 Sample Preparations

After being discharged from the molds, samples were carefully polished to obtain overall flat surface. Samples then dried in an oven at 60°C under vacuum for 17 days to achieve dry states from which reference points were collected.

3.3 Experimental Procedure

The specimens from each epoxy system were immersed in distilled water chambers of temperatures set at 45°C, 60°C, 75°C, and 90°C for 2254 hours. The moisture uptake was measured periodically by using an analytical balance with 0.1 mg resolution. Assuming that weight gain was due to the moisture uptake, the weight gain percentage was obtained by Eq. 3-6,

0
0
G(t)
H(t)
-- 0
0

Figure 3-1

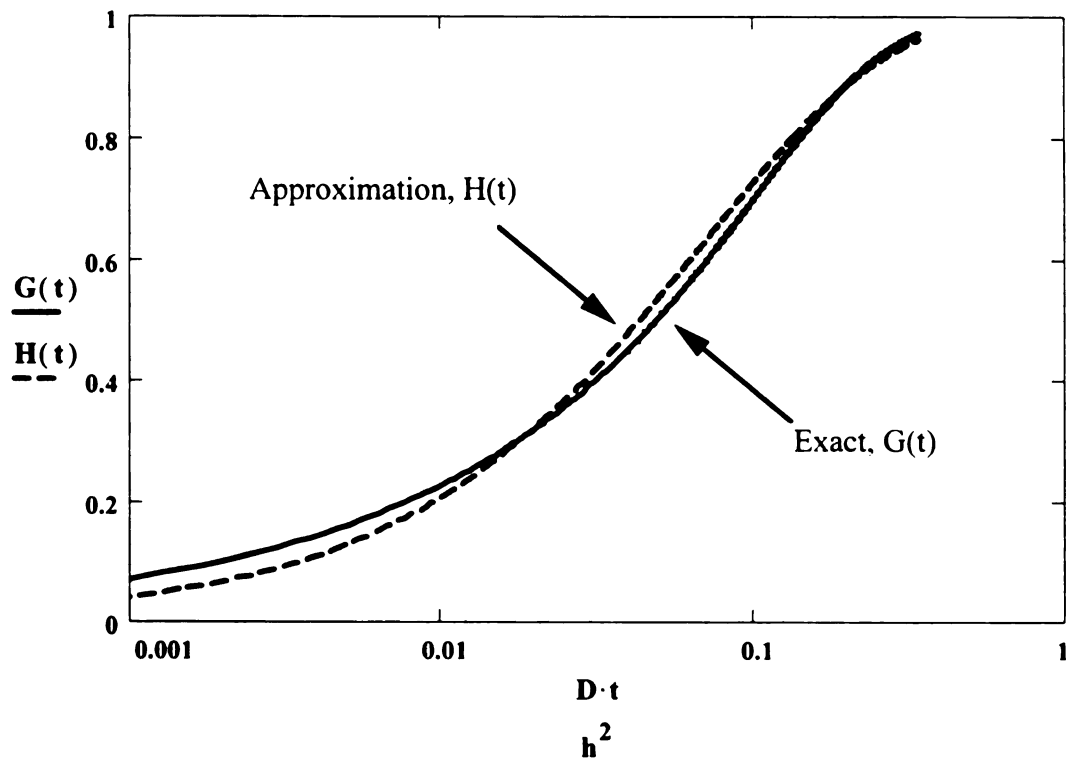


Figure 3-1: The variation of M_t/M_∞ with time. Exact (solid line): Eq. 3-4; approximate (dotted line): Eq. 3-5.

where

is the

thickness

The thin

(sec) m

linear le

3-5 to

tabulate

fitting v

and to l

guessing

C

approxim

slopes of

was plott

$$M = \frac{W_t - W_i}{W_i} \times 100$$

Eq. 3-6

where M is percentage weight gain (%), W_t weight of the sample at time t , and W_i is the initial weight of the sample obtained from dry samples.

In addition, during sorption experiment, samples with two different thicknesses were used to investigate the thickness effect on the sorption process. The thicknesses were 0.32 cm and 0.159 cm, denoted as S1 and S2, respectively.

After sufficient amount of data were collected, % weight gain versus time (sec) moisture absorption profiles were plotted, as shown in Figure 3-2. Non-linear least-squared curve fitting was performed on experimental data by using Eq. 3-5 to obtain M_∞ s and diffusion coefficients of the samples. The results were tabulated in Table 3-1. The reason for using the non-linear least-squared curve fitting was to use the actual data as much as possible, to obtain the diffusivities and to let M_∞ to be decided mathematically by the curve fit value, rather than guessing from curves.

Conventional method of obtaining diffusivities was to use a short-time approximated diffusion equation from which diffusivities were obtained by taking slopes of the linear region of the sorption curves where weight gain percentage was plotted against $t^{1/2}$. This method, however, tends to ignore data points after

the lin

the so

and di

spread

the en

param

3.4 R

entire

realistic

Table 3

inverse

system.

process

crosslin

soaking

diffusivi

the linear region, using only a portion of data. Also, one must assume M_{∞} from the sorption curves in order to obtain the diffusivity.

Non-linear least-squared curve fitting, however, allows one to obtain M_{∞} and diffusivity right out of the approximation by solving the equation, aided by a spread sheet software program. Therefore, this method uses not a portion of but the entire range of data. One must be careful, however, choosing the correct parameter for calculating the equation.

3.4 Results and Discussion

3.4.1 Sorption behaviors

Non-linear least-square curve fitting by using Eq. 3-5 allows to use the entire range of data to obtain the diffusivities such that it provides much more realistic results. Results from the moisture sorption process, as illustrated in Table 3-1, suggests that the magnitude of the diffusivity of the epoxy network is inversely related to its functionality such that the tetra-functional epoxy resin system, MY721/D230, revealed the lowest diffusivity. It is clear that the diffusion process of the crosslinked epoxy of a higher functionality is hindered by its higher crosslink density. In addition, the diffusivity of the epoxy glass increased as the soaking temperature increased, showing the temperature dependence of the diffusivity, as expected.

3.

3.

2.

% weight gain
2.
1.

1.

0.5

0.0

Figure 3
saturated
obtained

DGEBA/D230

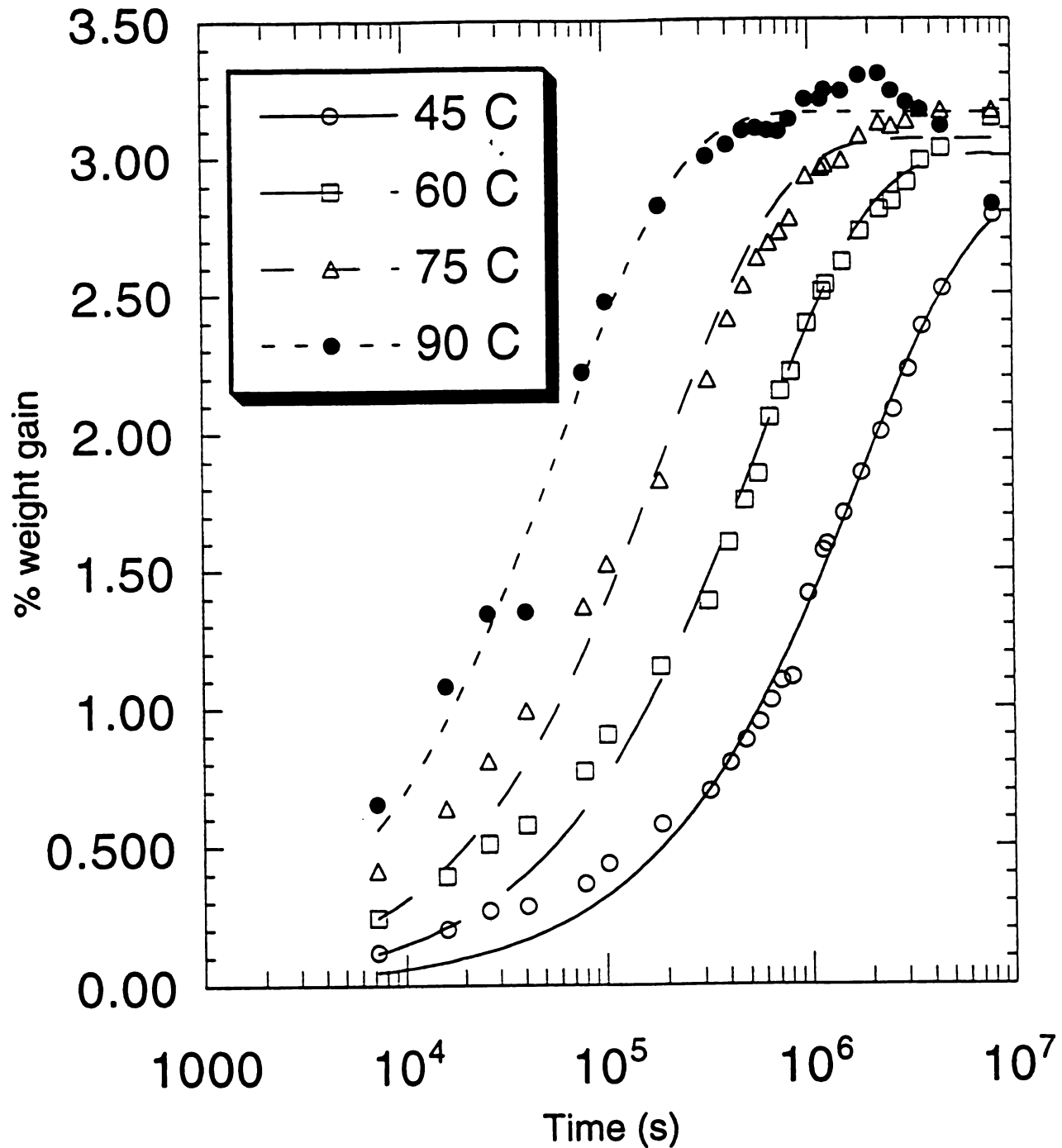


Figure 3-2 (a): Moisture absorption curve of DGEBA/D230. Samples were saturated with water at 45°C, 60°C, 75°C, and 90°C for 2254 hours. Lines were obtained from non-linear least-squared curve fitting, by using Eq. 3-5.

% weight gain

Figure
satur
obtai

MY510/D230

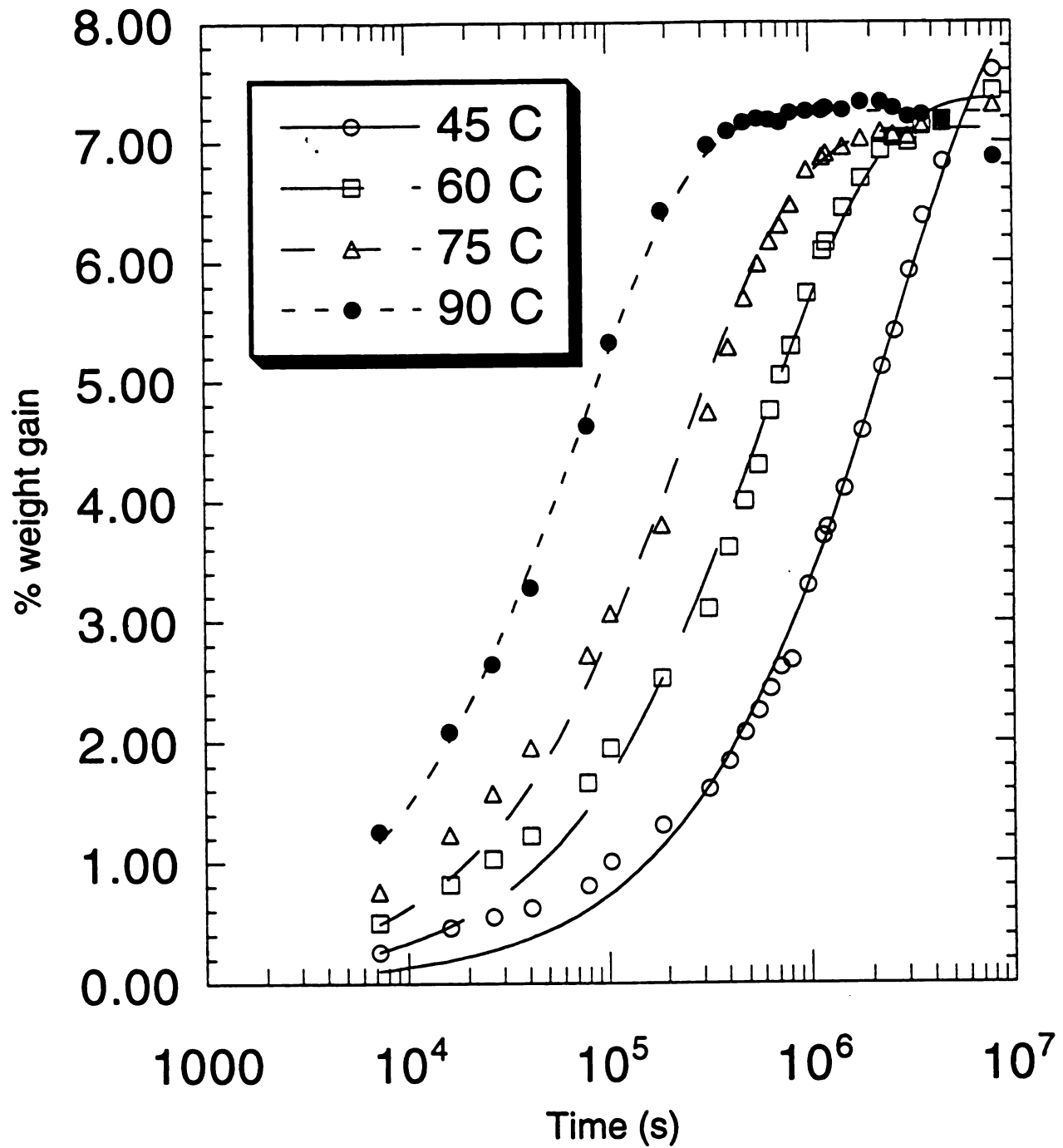


Figure 3-2 (b): Moisture absorption curve of MY510/D230. Samples were saturated with water at 45°C, 60°C, 75°C, and 90°C for 2254 hours. Lines were obtained from non-linear least-squared curve fitting, by using Eq. 3-5

% weight gain

2

1

0

Figure
saturat
obtaine

MY721/D230

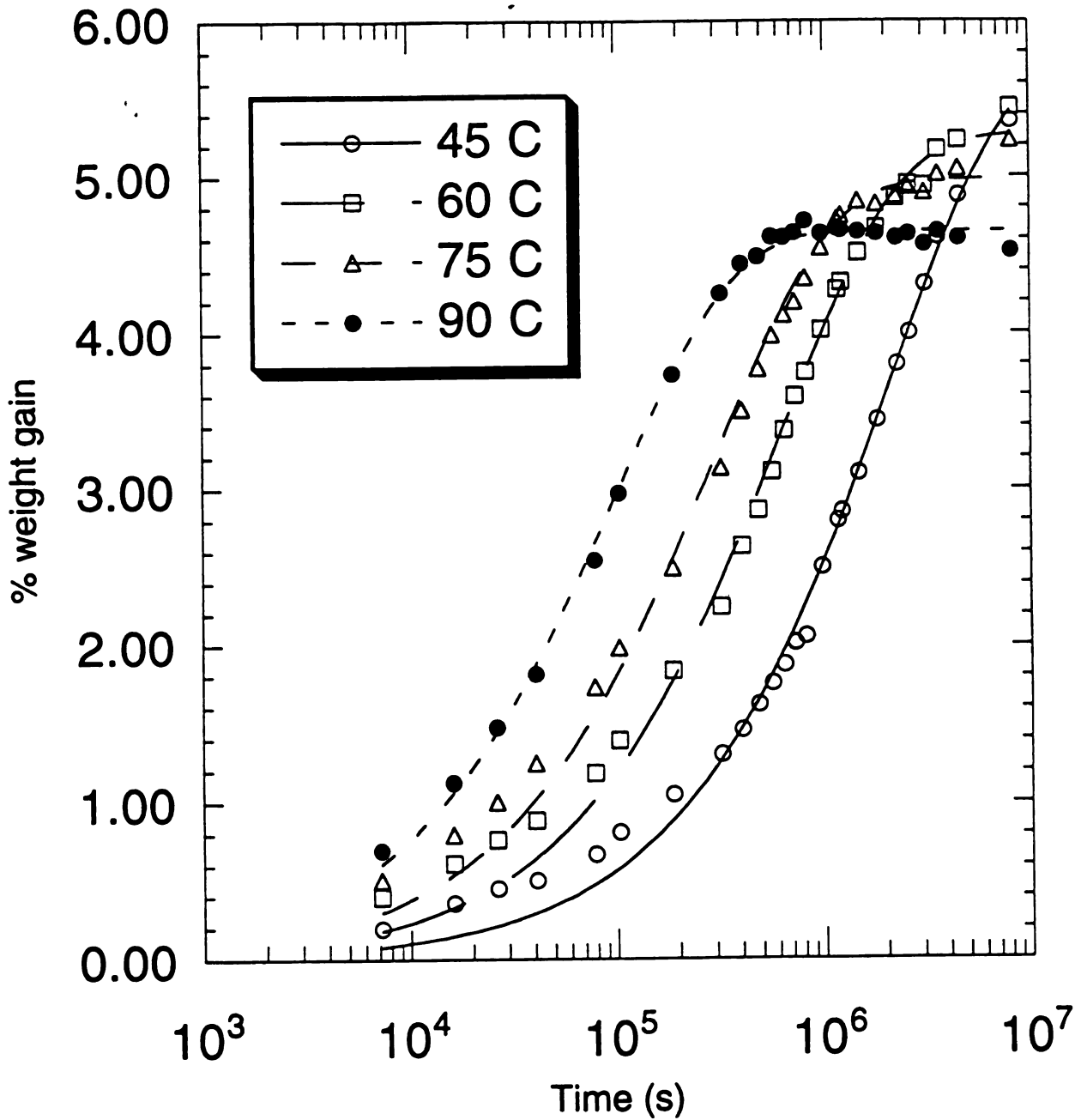


Figure 3-2 (c): Moisture absorption curve of MY721/D230. Samples were saturated with water at 45°C, 60°C, 75°C, and 90°C for 2254 hours. Lines were obtained from non-linear least-squared curve fitting, by using Eq. 3-5

Table 3-1

M
DGE (di-fu
MY5 (tri-fu
MY7 (fun

$D ($

M_{mc}

M_x

Table 3-1: Changes in M_{∞} and diffusivity due to the functionality difference and moisture absorption.

Materials	T_g (°C) (dry)	T (°C) (cond. temp.)	M_{max} (g)	M_{∞} (%)	$D \times 10^{-8}$ (cm^2/sec)
DGEBA/D230 (di-functional)	80	Dry (as cast)	-----	0.00	-----
		45	0.0997	2.88	0.39
		60	0.1127	3.01	1.32
		75	0.1111	3.06	2.63
		90	0.1157	3.16	8.21
MY510/D230 (tri-functional)	98	Dry (as cast)	-----	0.00	-----
		45	0.2323	8.50	0.206
		60	0.2275	7.37	0.829
		75	0.2228	7.05	2.165
		90	0.2231	7.28	6.534
MY721/D230 (tetra-functional)	136	Dry (as cast)	-----	0.00	-----
		45	0.1398	5.76	0.19
		60	0.1420	5.27	0.62
		75	0.1351	4.98	1.33
		90	0.1211	4.65	3.84

$D (\times 10^{-8} cm^2/sec) =$ Diffusivity.

$M_{max} =$ Maximum weight gain in gram.

$M_{\infty} =$ Maximum weight gain in percentage.

T
temperat
regressio
obtained
shown i
agreeme
behavior

where D_0
of the ma
(K).

Ac
the mate
polymer
closer to
less energ
and the d
MY721/D

The diffusivities obtained by using Eq. 3-5 at different sorption temperatures were plotted as $\ln D$ vs. $1/T$ in Figure 3-3. By extrapolating the regression line to the y-axis, D_o was obtained. The activation energy, Q , was also obtained by taking the slope of the regression line. The values of D_o and Q are shown in Table 3-2. It can be seen from Figure 3-3 that there is a good agreement between the variation of D with temperature and the Arrhenius behavior,

$$D = D_o \exp\left(-\frac{Q}{RT}\right)$$

Eq. 3-7

where D_o is the diffusivity at a temperature (cm^2/sec), Q is the activation energy of the material (J/mol), R is the gas constant ($J/mol \cdot K$), and T is the temperature (K).

Activation energy is an energy required for a diffusant to diffuse through the material from one site to another. If the system is a highly crosslinked polymer network, the diffusion sites (either hydroxyl sites or free volume) will be closer to each other so that the water molecules can easily hop around (requiring less energy) and occupy the site. Table 3-2 illustrated the activation energy (Q) and the diffusion constant (D_o) of the each epoxy networks. It is shown that MY721/D230 has the lowest activation energy and the highest diffusion constant.

-15.0
-16.0
-17.0
InD
-18.0
-19.0
-20.0
0.

Figure 3-
($cm^2 sec$)

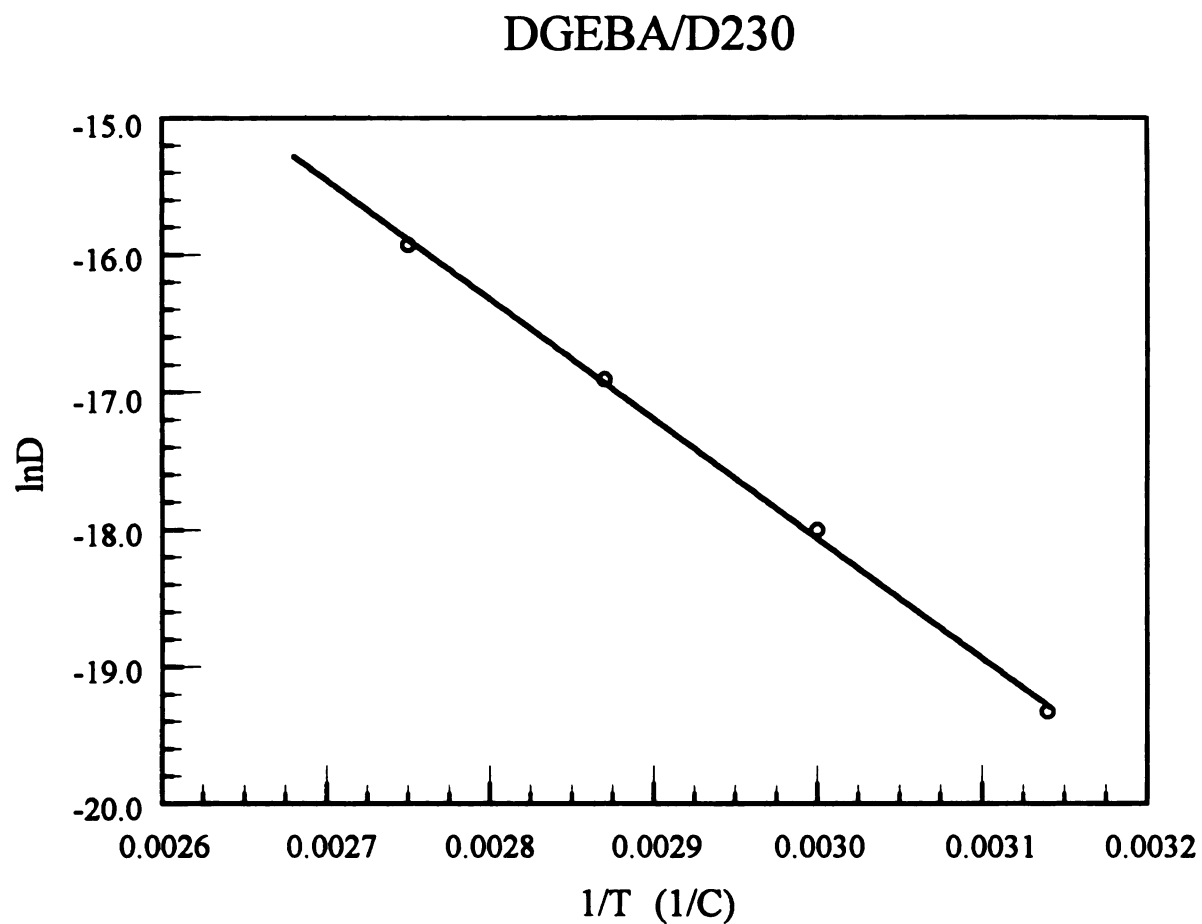


Figure 3-3 (a): $\ln D$ vs. $1/T$ curve of DGEBA/D230, where D is the diffusivity (cm^2/sec) and T is the temperature (K).

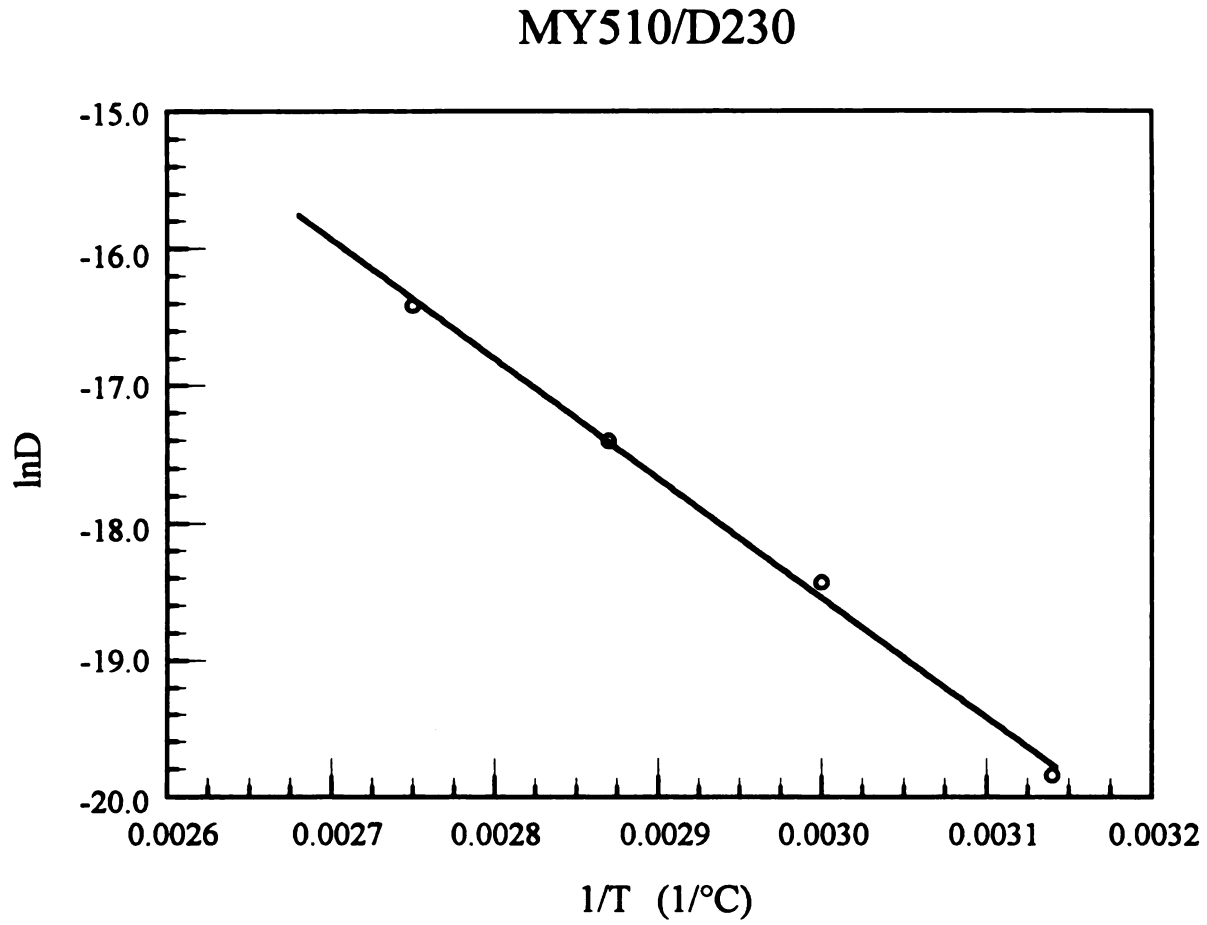


Figure 3-3 (b): $\ln D$ vs. $1/T$ curve of MY510/D230, where D is the diffusivity (cm^2/sec) and T is the temperature (K).

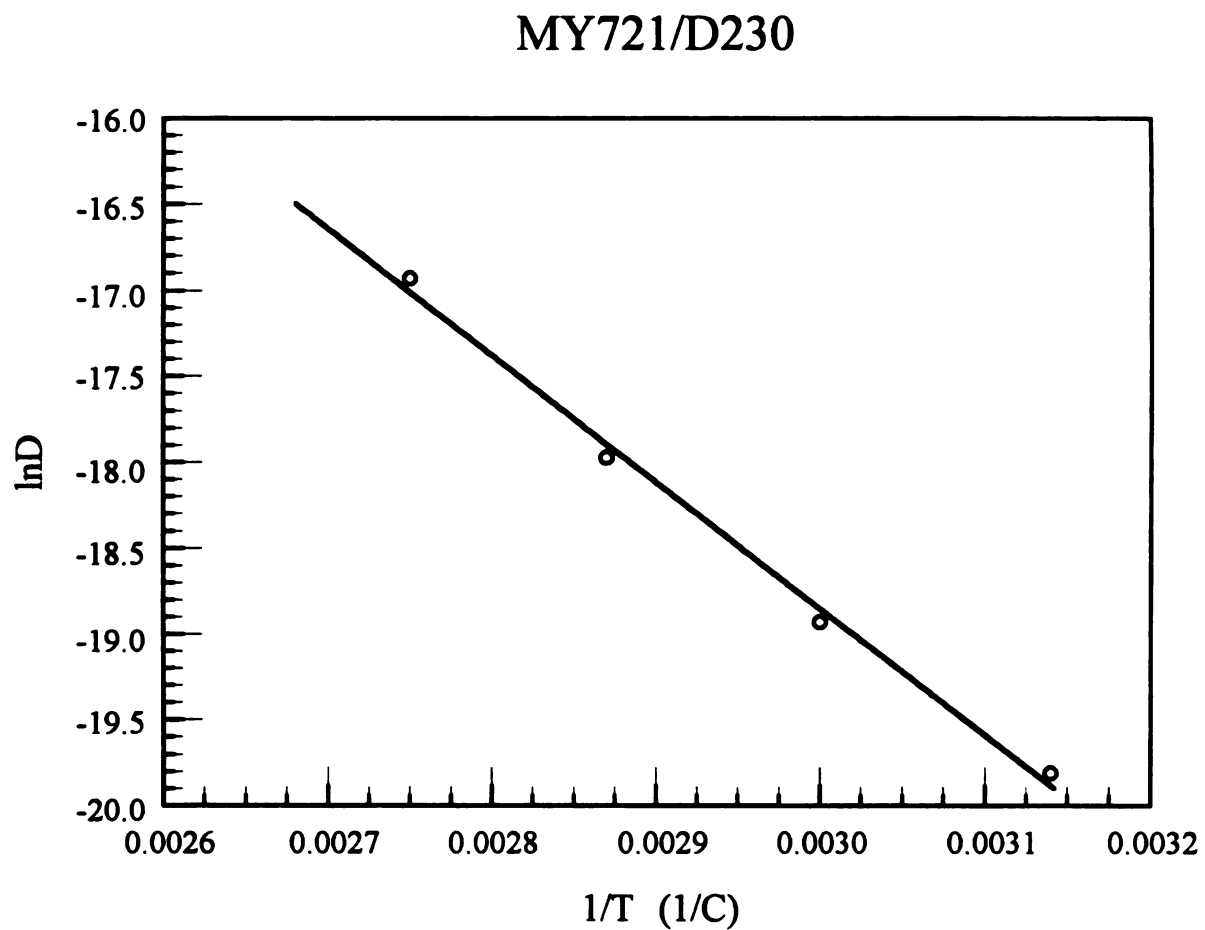


Figure 3-3 (c): $\ln D$ vs. $1/T$ curve of MY721/D230, where D is the diffusivity (cm^2/sec) and T is the temperature (K).

Table 3-2: Activation energy and diffusion coefficients of the epoxy systems

Materials	Q (kJ/mol)	D_o (cm ² /sec)
DGEBA/D230	69.5	1.05×10^{-3}
MY510/D230	72.5	1.72×10^{-3}
MY721/D230	62.8	0.39×10^{-2}

3.4.2 Thickness effects on the sorption behavior

In this experiment, in order to investigate the thickness effects on the sorption behavior, samples with two different thicknesses were used; 0.32 *cm* (S1) and 0.159 *cm* (S2). The result, as depicted in Figure 3-4, indicates that thickness variation affects the sorption such that during the initial sorption process, thinner samples (S2) absorbed moisture at a rate faster than for the thicker samples (S1). This is shown in Table 3-3 where the diffusivity of the thin specimens are higher than that of thick specimens. In addition, the magnitude of the saturation point (M_{∞}) for the thinner specimens is smaller than that for the thicker samples suggesting that in a epoxy glass, M_{∞} as well as diffusivity are depended upon the thickness of the specimen.

Consider the concentration profiles in the thickness direction of thin and thick samples, since the length and the width of the two samples are assumed to be the same. As moisture absorption proceeds from the surface towards the center of specimen, at a given time, water concentration in the thickness direction of the thin samples will be higher than that of the thick samples since the distance between the surfaces are shorter for thin samples such that the distance that water molecules have to travel through the matrix to the center is shorter. However, for thick samples, as opposed to thin samples, the distance between surfaces are longer such that it requires longer time for water molecules to diffuse through the matrix. In addition, assume that at a given time such that the thin samples are

completely saturated, only the outer surface and some distance towards the center of the thick samples will be saturated. Consequently, some degree of swelling will be observed on the surface of the thick samples, as a result, diffusion process will be hindered by the swelled structure and while being saturated, due to the swelling effect, equilibrium moisture content, M_{∞} , will be higher than that of thin samples. This is exactly what happened as shown in Figure 3-4 where weight gain percentages were plotted against time, normalized by the thickness. The results, Table 3-3, showed that the diffusion coefficients of thick samples were lower than those of thin samples and the equilibrium moisture content, M_{∞} , of thick samples, on the other hand, were higher than that of thin samples. As discussed on the above, those results can be said of due to swelling effect. Similar results were also observed elsewhere [6, 45, 46] that the distribution of water between the less dense and dense specimens were explained by the swelling phenomena.

DGEBA/D230

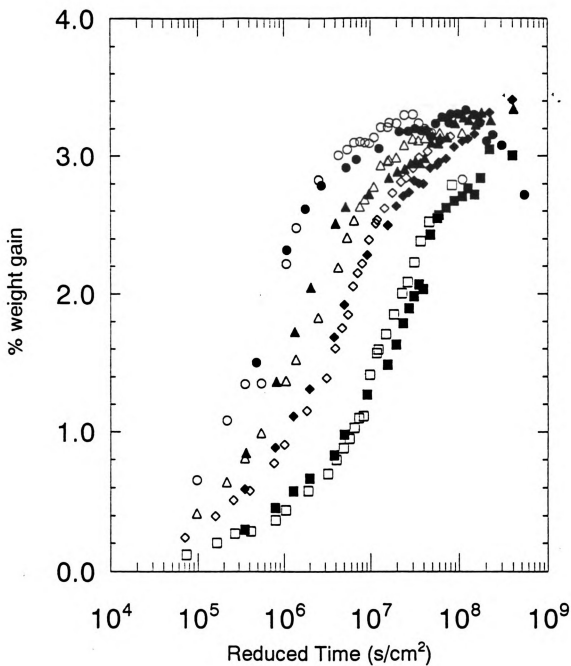


Figure 3-4 (a): Sorption curves for DGEBA/D230 with different thickness; S1 and S2. Hollow symbols represent thick samples (S1). Filled symbols represent thin samples (S2). (\square) 45°C, (\diamond) 60°C, (Δ) 75°C, (\circ) 90°C.

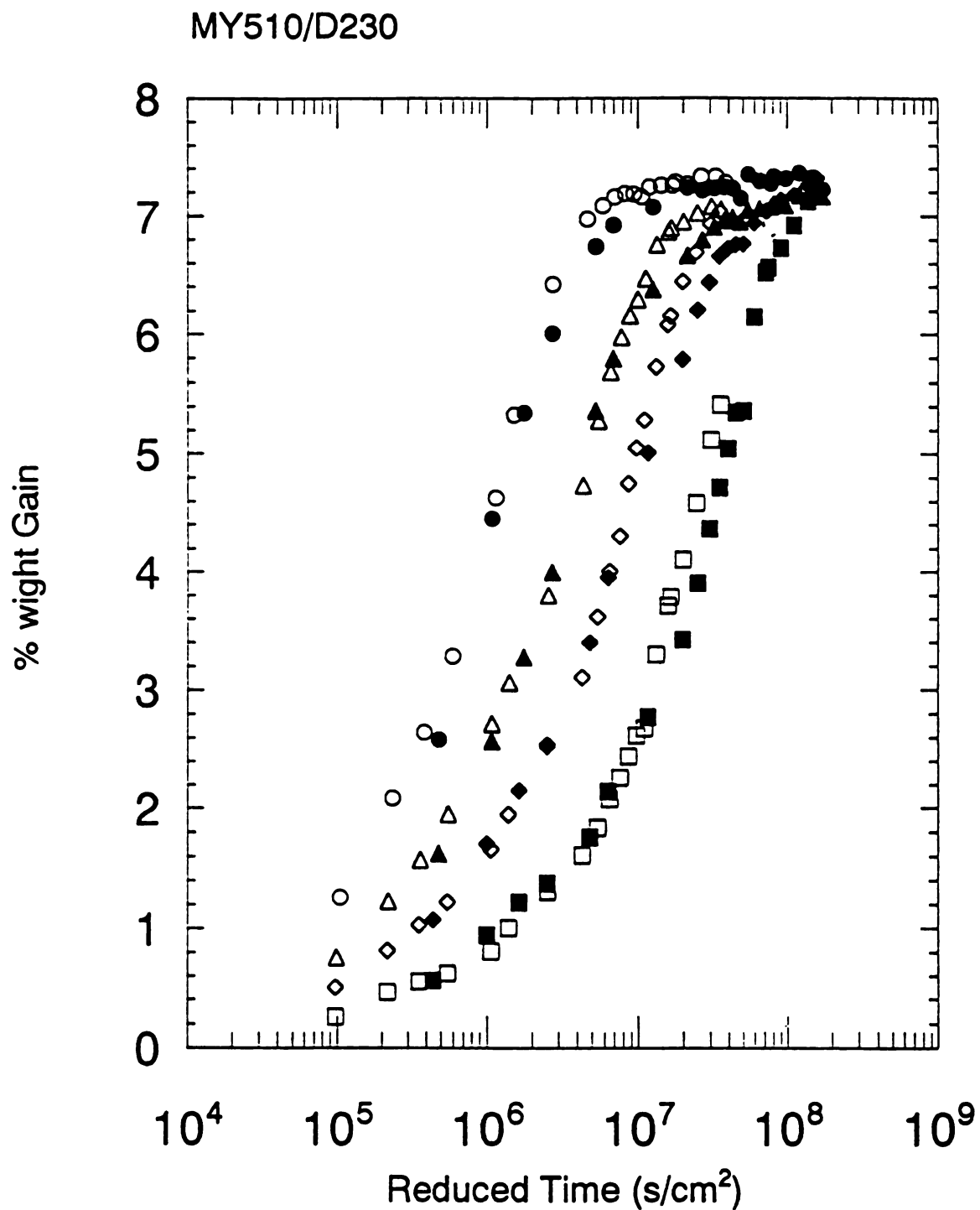


Figure 3-4 (b): Sorption curves for MY510/D230 with different thickness; S1 and S2. Hollow symbols represent thick samples (S1). Filled symbols represent thin samples (S2). (\square) 45°C, (\diamond) 60°C, (Δ) 75°C, (\circ) 90°C.

MY721/D230

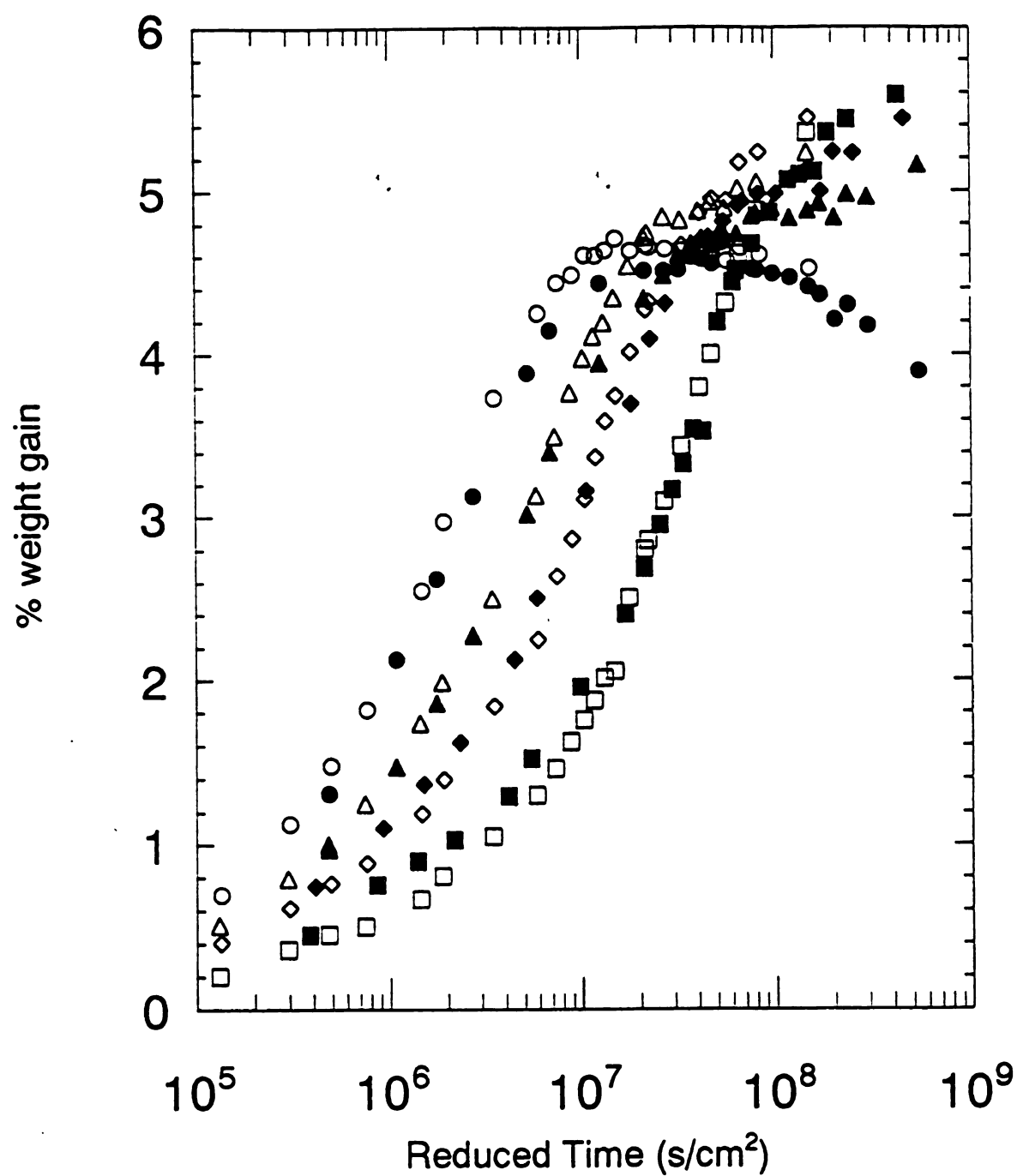


Figure 3-4 (c): Sorption curves for MY721/D230 with different thickness; S1 and S2. Hollow symbols represent thick samples (S1). Filled symbols represent thin samples (S2). (\square) 45°C, (\diamond) 60°C, (Δ) 75°C, (\circ) 90°C.

Table 3-3: Thickness effects on M_{∞} and D .

Epoxy system	Cond. temp. (°C)	Specimens	M_{∞} (%)	D ($\times 10^{-8}$ cm ² /sec)
DGEBA/D230	45	S1 (thick)	2.89	0.39
		S2 (thin)	2.87	0.31
	60	S1	3.01	1.32
		S2	3.01	1.38
	75	S1	3.06	2.63
		S2	3.09	3.67
	90	S1	3.16	8.21
		S2	3.16	8.23
MY510/D230	45	S1	8.5	0.206
		S2	7.58	0.209
	60	S1	7.37	0.829
		S2	7.06	0.852
	75	S1	7.05	2.120
		S2	7.02	2.123
	90	S1	7.28	6.53
		S2	7.24	5.57
MY721/D230	45	S1	5.76	0.19
		S2	5.45	0.21
	60	S1	5.27	0.62
		S2	5.07	0.66
	75	S1	4.98	1.33
		S2	4.83	1.34
	90	S1	4.65	3.54
		S2	4.44	3.84

3.4.3 Hydroxyl Sites Dependency

Non-linear least-squared curve fitting, by using Eq. 3-5 deduced M_{∞} for the epoxy glasses under study. The sorption curves showed that a tri-functional epoxy network manifested a saturation level of approximately 7.5 %, followed by a tetra-functional (≈ 5.2 %), and a di-functional epoxy resin absorbing the least (≈ 3.2 %). To provide an analytical results, hydroxyl group affinity of the epoxy network was examined by calculating the numbers of hydroxyl groups present in each epoxy network. The results, as presented in Table 3-4 show that the tri-functional epoxy resin (MY510) having 6.309×10^{-3} mole of [OH]/g contains the highest hydroxyl groups per mole and the di-functional epoxy resin (DGEBA) having 4.396×10^{-3} mole of [OH]/g contains the lowest. The chemical nature of the penetrant versus that of the polymer determines the penetrant-polymer affinity. The relatively high water absorption capacity of epoxy resins derives from the presence in the epoxy chains of [OH] groups attracting the polar water molecules.

Therefore, it is suffice to say that the epoxy network having the highest number of hydroxyl sites available in its network will attract and accommodate water more readily than the epoxy network having a lower number of hydroxyl sites available in its network.

Table 3-4: Number of hydroxyl groups in each epoxy

Epoxy System	g / mole of [OH]	mole of [OH] / g
MY510/D230	158.5	6.309×10^{-3}
MY721/D230	167.5	5.970×10^{-3}
DGEBA/D230	227.5	4.396×10^{-3}

3.5 Summary

Diffusion process for an epoxy glass is directly related to the functionality of the epoxy resin such that an epoxy glass formed by a resin having a higher functionality will produce a highly crosslinked epoxy network, resulting in hindrance in diffusion process. The results showed that the diffusivity of MY721/D230 epoxy glass was the lowest while DGEBA/D230 having the highest diffusivity. As expected, diffusion process in polymer network was also sensitive to the temperature of the environment such that the diffusion rate increased with the soaking temperature.

Thickness variation also affects the diffusion process. Swelling appears to be the main cause for the thickness variation effects where thin specimens showed higher diffusion coefficients than thick specimens and thick specimens retained higher equilibrium moisture content. As for the thick samples, due to swelling effect at the surface, diffusion process was disturbed and overall equilibrium moisture content was raised by the addition of moisture in swelled structure at the surface of the specimen.

Finally, the epoxy resin containing the highest number of hydroxyl groups per mole creates more hydroxyl sites for water molecules to react, resulting in a higher moisture weight gain. As a result, MY510/D230 epoxy system absorbed more moisture than any other epoxy systems studied.

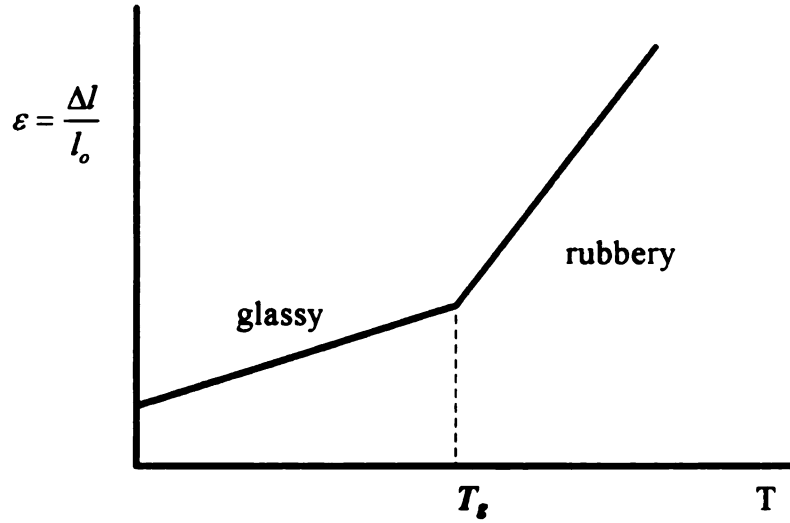
4. MOISTURE EFFECTS ON PHYSICAL PROPERTIES

4.1 Dilatometry

Dilatometry is used to study and to measure dimensional changes of matter. Dimensional changes in polymers occur as a result of a variety of stimuli, e.g. absorption of fluids; mechanical stresses; chemical reactions (polymerization and cross-linking); and effects of time (aging of glasses and crystallization). For processing and engineering applications of polymeric materials, the study of dimensional changes bears great technical significance. In addition, dilatometry is also used to study the physical and chemical phenomena in conjunction with dimensional changes, such as melting, crystallization, secondary transitions, glass formation, polymerization, cross-linking reactions, fluid sorption, formation of voids and crazes during mechanical deformation, and many others. Linear dimensional changes are most useful in situations where it may be assumed that the shape of the test specimen remains unchanged.

In this study, dilatometry was used on dry and moisture saturated samples to monitor the change of the glass transition temperatures such that one can examine the deviation of the glass transition temperature with respect to different conditioning temperatures. Moisture desorbed samples were also examined by a dilatometer; (i) to investigate if there were any changes in the glass transition temperatures among the dry, saturated, and moisture desorbed samples; (ii) to examine any change in the network conformation affected by the moisture.

By definition, the temperature at which the polymer undergoes the transformation from a rubber to a glass is known as the glass transition temperature, T_g .



The linear thermal expansion coefficient

$$\alpha_L = \frac{1}{l_o} \frac{\Delta l}{\Delta T}$$

Eq. 4-1

for either α_g or α_l is obtained by taking the slope of the glassy or rubbery region, respectively.

4.2 Experimental Procedure

The glass transition temperatures of the moisture saturated and desorbed samples were measured by a length dilatometer manufactured by Omega shown in

Figure 4-1. The heating rate during the experiment was 2°C/min. Samples saturated with distilled water were cut from their initial dimension of 7.62 *cm* × 0.32 *cm* × 1.27 *cm* into 2.54 *cm* long specimens, and the change of the sample length with respect to the temperature increase was measured by a LVDT (Linear Variable Differential Transducer). From the output voltage collected from the dilatometer, the strain, ε , was calculated by Eq. 4-2,

$$\varepsilon = 0.023 \times \left(\frac{mV}{l_o} \right)$$

Eq. 4-2

where ε = Strain

mV = Output voltage from the dilatometer.

l_o = Initial length of the sample (*cm*).

0.023 = A calibration constant determined by the deformation of LVDT with a known length change (*cm/mV*).

Strain versus temperature curves are shown in Figure 4-2 through Figure 4-7.

The T_g was determined as an onset point of the strain versus temperature curve.



Figure 4-1: A length dilatometer built by Omega Co.

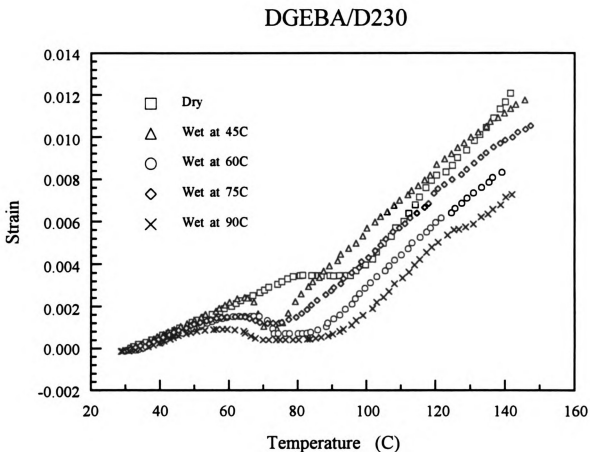


Figure 4-2: Strain versus Temperature (°C) of the DGEBA/D230 epoxy resin. Samples have been saturated with distilled water at 45°C, 60°C, 75°C, and 90°C for 2254 hours.

0.01
0.01
0.00
0.00
0.00
0.00
-0.00

Figure
Sample:
for 225.

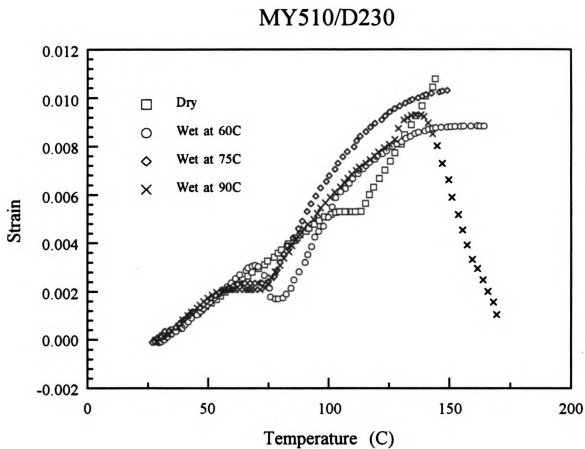


Figure 4-3: Strain versus Temperature (°C) of the MY510/D230 epoxy resin. Samples have been saturated with distilled water at 45°C, 60°C, 75°C, and 90°C for 2254 hours.

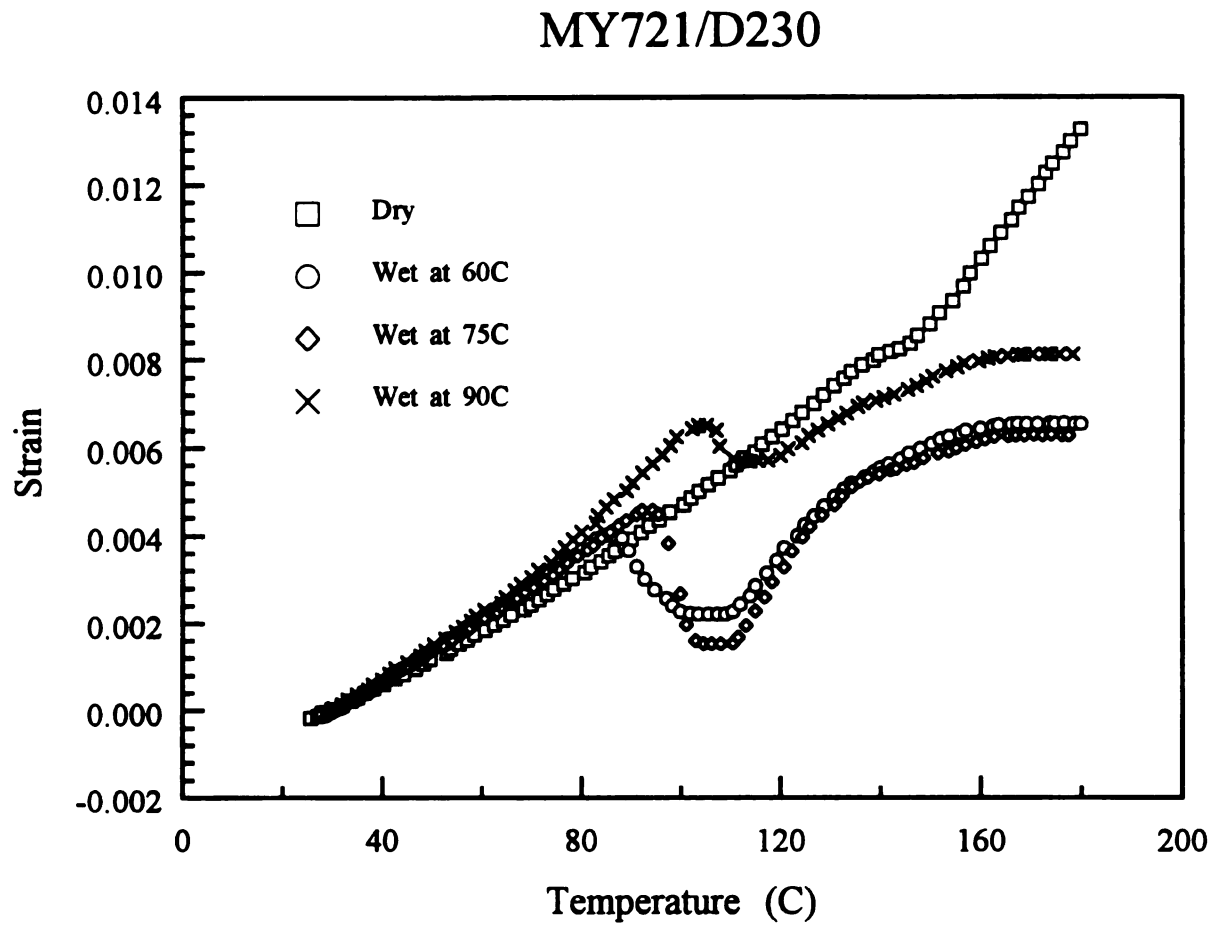


Figure 4-4: Strain versus Temperature (°C) of the MY721/D230 epoxy resin. Samples have been saturated with distilled water at 45°C, 60°C, 75°C, and 90°C for 2254 hours.

For the desorption of the samples, $2.54\text{ cm} \times 0.32\text{ cm} \times 1.27\text{ cm}$ wet samples were dried in an oven at 100°C for 24 hours under vacuum. Then the samples have undergone T_g evaluation by the dilatometer, heating rate at $2^{\circ}\text{C}/\text{min}$.

4.3 Results and Discussion

4.3.1 Glass Transition Temperature (T_g)

4.3.1.1 Moisture Absorbed Samples

From Table 4-1, for DGEBA/D230 and MY510/D230 samples, the glass transition temperatures decreased as the soaking temperatures increased. Due to the moisture presence in the network, substantial molecular rearrangement of the epoxy network occurred during the sorption process. Over the many years of research on the moisture absorption, it is believed that the decrease in the glass transition temperatures is due to the water acting as a plasticizer.

In a highly crosslinked sample, MY721/D230, the glass transition temperature of the sample saturated at 60°C decreased substantially, compared to that of the dry sample. As the soaking temperature increased, however, the glass transition temperature increased gradually from 83°C to 99°C . This phenomenon is in disagreement with the results obtained from other epoxy systems of which the glass transition temperatures decreased consistently as the soaking temperatures increased. Because the water molecules is polar, it is capable of

Table 4-1: Change of the glass transition temperatures due to moisture saturation.

Conditioned Temperatures	T_g of DGEBA/D230	T_g of MY510/D230	T_g of MY721/D230
Dry	80°C	98°C	136°C
45°C	62°C	-----	-----
60°C	57°C	68°C	83°C
75°C	53°C	58°C	91°C
90°C	49°C	54°C	99°C

forming hydrogen bonds with hydroxyl groups of the epoxy network, resulting in a stiffer network. Higher the soaking temperature, the concentration of the water would be higher due to the increased rate of the mass transport through the matrix; therefore, more water molecules become available for the epoxy network to form hydrogen bonding. Having the highly crosslinked epoxy network, the crosslink density of the MY721/D230 was intensified by hydrogen bonding formed between the absorbed water and the epoxy network. Not only translational, but also rotational movement of the chain was hindered, resulting in the increase of glass transition temperature.

It is noteworthy that, as shown in Table 4-2 under the constant conditioning temperature, as $\Delta T = |T_e - T_g|$ increases, the diffusion coefficient decreased (T_e is an experiment temperature). In other words, as the conditioning temperature is further away from the T_g , the epoxy resin tends to be more stiff such that it will be more difficult for the diffusants to penetrate through the epoxy network.

Table 4-2: Correlationship between $\Delta T = |T_g - T_c|$ and the diffusivities of the epoxy glasses.

Materials	T_g (°C)	T_c (°C) (cond. temp.)	$D \times 10^{-8}$ (cm^2/sec)
DGEBA/D230 (di-functional)	80	Dry (as cast)	-----
	62	45	0.39
	57	60	1.32
	53	75	2.63
	49	90	8.21
MY510/D230 (tri-functional)	98	Dry (as cast)	-----
	---	45	0.206
	68	60	0.829
	58	75	2.165
	54	90	6.534
MY721/D230 (tetra-functional)	136	Dry (as cast)	-----
	---	45	0.19
	83	60	0.62
	91	75	1.33
	99	90	3.84

$D (\times 10^{-8} cm^2/sec) = \text{Diffusivity.}$

4.3.1.2 Moisture Desorbed Samples

Dilatometry results on the samples that have been conditioned through the desorption process show that the behaviors of recovering the glass transition temperatures were different among DGEBA/D230, MY510/D230, and MY721/D230 epoxy networks. For instance, the recovery of the glass transition temperatures was not observed in any of MY721/D230 epoxy resin regardless of their soaking temperatures, even though MY510/D230 and some of DGEBA/D230 samples did recover their T_g .

The glass transition temperatures of the DGEBA/D230 samples saturated at 45°C, 60°C, and 75°C returned to, or returned close to the inherent glass transition temperature which is 80°C. As shown in Figure 4-5 through Figure 4-7, one exception was found in the sample saturated at 90°C for which the glass transition temperature of the desorbed sample reached only to 70°C. The saturation temperatures of 45°C, 60°C, and 75°C were lower than the glass transition temperature of the DGEBA/D230 epoxy. The saturation temperature of 90°C, however, is higher than the glass transition temperature of the DGEBA/D230 epoxy network, so that during the sorption process, the material was in a rubbery state. As the sorption process proceeded, the molecular rearrangement of the epoxy network was readily achieved. During the desorption process, the polymer network would not have enough time for long range molecular motion to restore its original molecular arrangement. After the

desorption, the epoxy would exhibit a network structure in which the newly formed molecular conformation is “frozen in”, providing the network more room to relax. This would result in the suppression of the glass transition temperature, as partially discussed elsewhere [45].

From the sorption curve in Figure 3-2, tri-functional epoxy (MY510/D230) absorbed the moisture the most. Higher percentage of the moisture uptake can be explained such that in addition to its higher hydrophilic sites, the tri-functional epoxy system has a greater mobility in its segmental chain movement. The conformational change of the network after the moisture introduced to the network through the sorption process can be readily compensated by the segmental chain rearrangements. After the desorption process, the chain segments were able to return to its original conformation such that the glass transition temperatures of the samples, regardless of their soaking temperatures returned to the initial T_g (98°C).

MY721/D230 epoxy is a highly crosslinked epoxy resin. When the system was in the sorption process, it experienced the molecular rearrangement as other epoxy systems (DGEBA/D230 and MY510/D230) encountered. The mobility of the chain segment, however, was likely to be hindered due to its higher crosslink density. Low chain mobility due to the higher crosslink density required more time, or made even impossible for the molecular chains to recover its original chemical conformation. Therefore, even though the desorbed samples showed

their glass transition temperatures in agreement at approximately 112°C, the initial glass transition temperature (136°C) was not recovered.

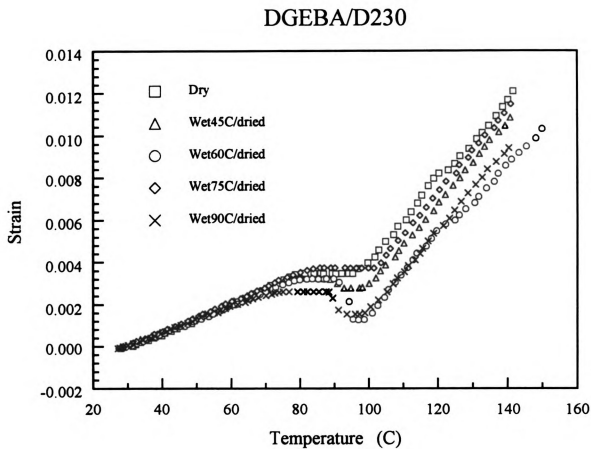


Figure 4-5: Change of the strain between the dry and moisture desorbed samples of the DGEBA/D230 epoxy resin were plotted against temperature (°C).

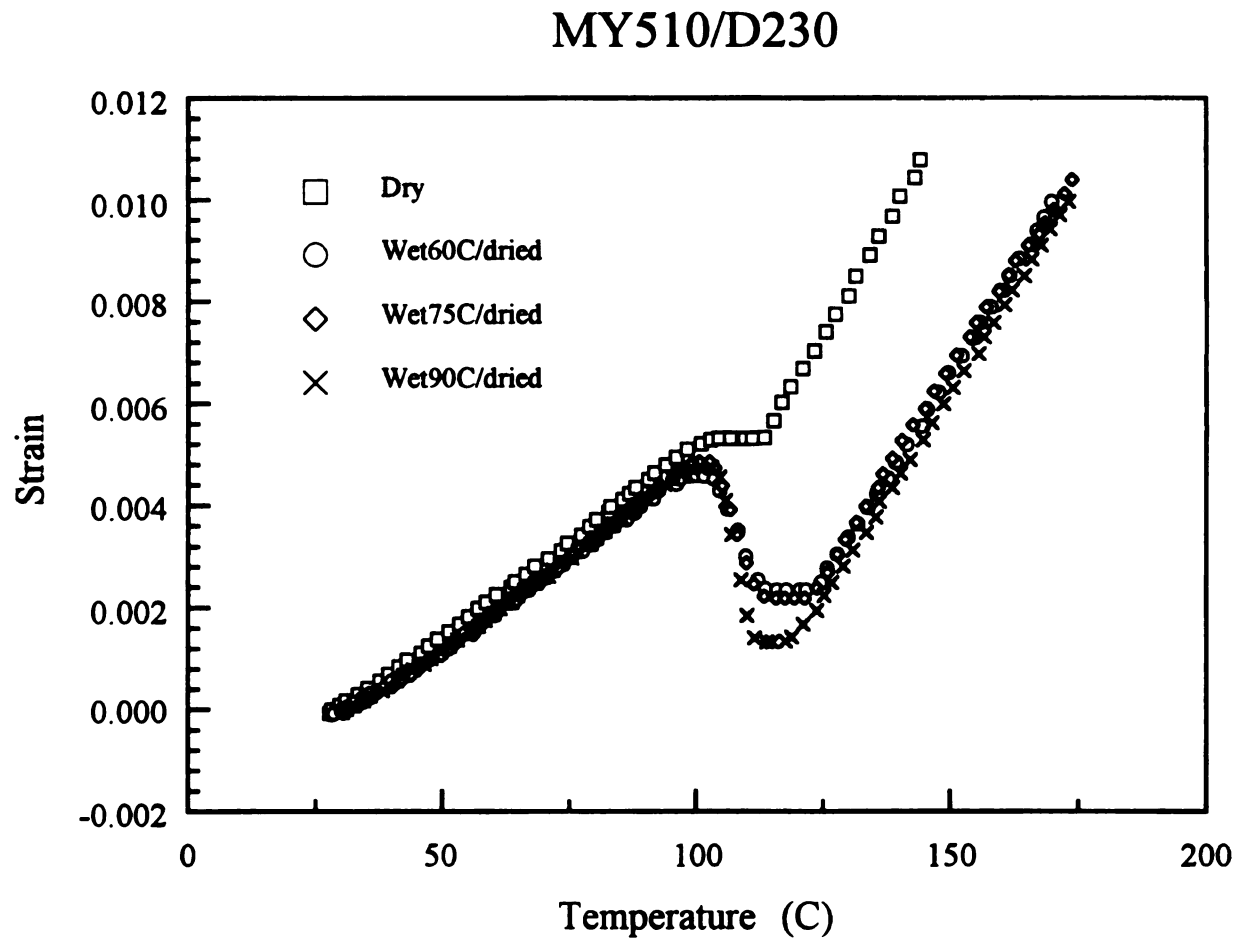


Figure 4-6: Change of the strain between the dry and moisture desorbed samples of the MY510/D230 epoxy resin were plotted against temperature (°C).

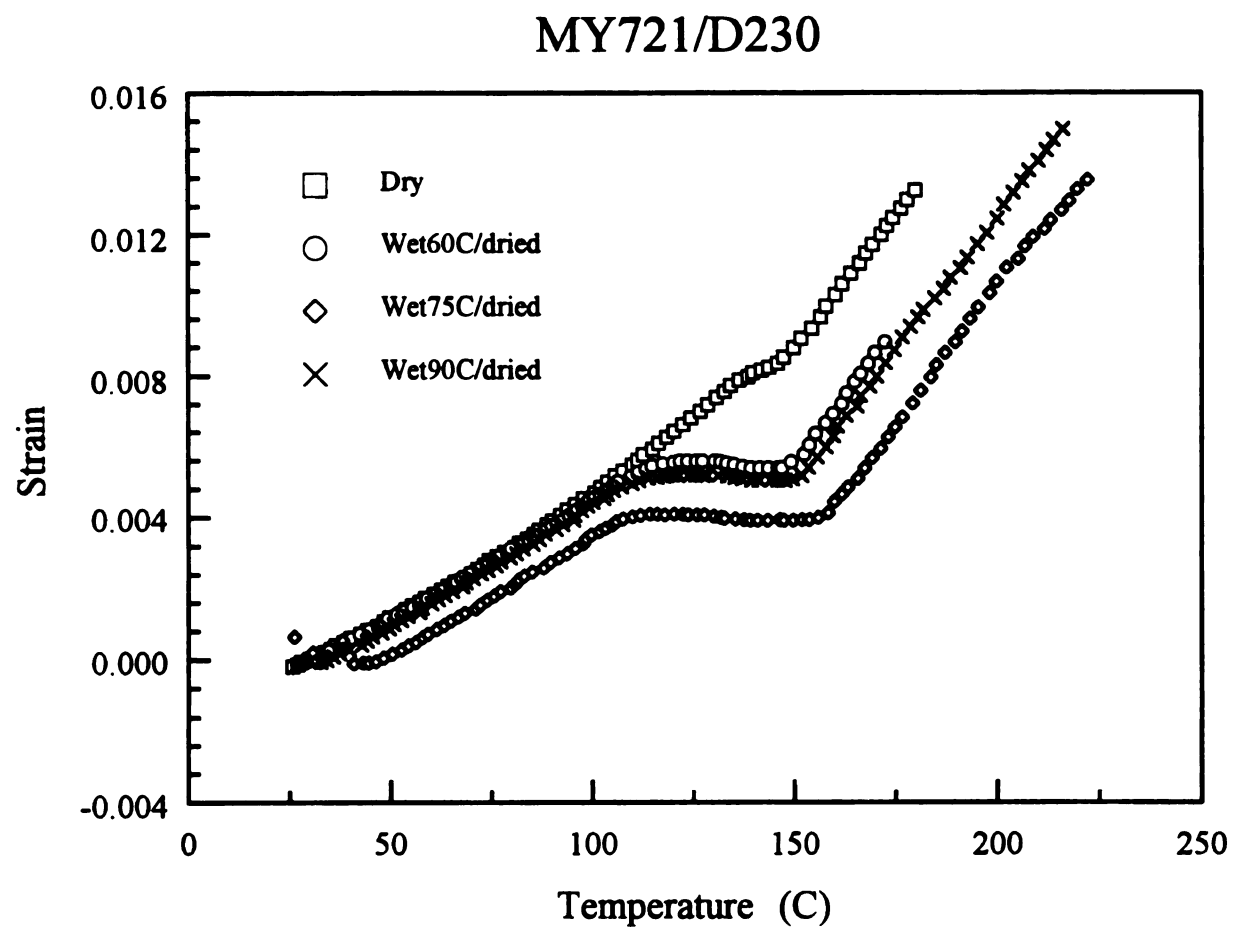


Figure 4-7: Change of the strain between the dry and moisture desorbed samples of the MY721/D230 epoxy resin were plotted against temperature (°C).

4.3.2 Coefficients of Thermal Expansion (CTE)

4.3.2.1 Moisture Saturated Samples

The thermal expansion coefficients of glass region, α_g , and of liquid region, α_l , were obtained by taking the slopes of the glass and the rubbery regions of strain versus temperature curves, respectively. The coefficient of thermal expansion is one way of manifesting the mobility of the molecular chain segment. Its implication with the molecular chain segment mobility draws an attention that how the molecular mobility would be affected by the sorption process.

In the glassy state, the coefficients of thermal expansion, α_g , for the various wet samples are not very different; however, the comparison of the coefficients of thermal expansion among each epoxy network shows that the magnitude of the CTE follows the same order as the moisture absorption behaviors such that MY510/D230 having the highest α_g , followed by MY721/D230, and DGEBA/D230 having the lowest α_g , refer to Table 4-3. Higher CTE means higher molecular mobility. As shown from the previous chapter of this study, MY510/D230 absorbed about 7.5 wt% of moisture, the highest among three, because it has more hydroxyl groups available in the network. It was also said that the absorbed water is acting as a plasticizer in the polymer network. The epoxy resin that has higher number of hydroxyl groups per mole in the network absorbed more moisture, which plasticizes the material;

therefore, MY510/D230 possesses the highest α_g followed by MY721/D230 and DGEBA/D230.

In the rubbery state, it appears that in comparing α_f between the dry and wet samples, wet samples of all three epoxy systems showed a decrease in their α_f . When the water molecules were introduced to the crosslink network, the “voids” between the polymer molecules were filled with water molecules such that the mobility of the polymer chains were hindered. This restriction of the chain mobility resulted in the decrease of α_f . Figure 4-2 through Figure 4-4 well illustrated these effects where α_f portions of the curves were leaning towards the x-axes. Further reasoning of this phenomena was attempted microscopically by using positron annihilation lifetime spectroscopy (PALS). Detailed discussions on this subject were presented in section 4.4.

Table 4-3: Thermal Expansion Coefficients of DGEBA/D230, MY510/D230, and MY721/D230.

	$\alpha_g (10^{-4} \text{ } ^\circ\text{C}^{-1})$			$\alpha_l (10^{-4} \text{ } ^\circ\text{C}^{-1})$		
Temperature (° C)	DGEBA/ D230	MY510/ D230	MY721/ D230	DGEBA/ D230	MY510/ D230	MY721/ D230
Dry (23° C)	0.6824	0.736	0.704	1.8854	1.7430	1.5218
45° C	0.6338	-----	-----	1.4473	-----	-----
60° C	0.6157	0.8585	0.7364	1.4562	1.9360	1.3937
75° C	0.6399	0.7511	0.7398	1.3463	1.8875	1.7778
90° C	0.5871	0.8820	0.8738	1.3407	1.5056	0.7102

4.3.2.2 Moisture Desorbed Samples

The coefficients of thermal expansion of moisture desorbed samples were presented in Table 4-4. Even though there were some variations in T_g , the results showed that the difference between the coefficients of thermal expansion of dry samples and that of moisture saturated samples was negligible.

Water molecules occupying the “voids” between the polymer molecules were eventually dried out after the desorption cycle such that the polymer network recovered (maybe not 100% but somewhat close) its conformation. More detailed explanations were presented in section 4.4 with supporting evidence comprised of PALS results.

Table 4-4: Thermal Expansion Coefficient of DGEBA/D230, MY510/D230, and MY721/D230 after the moisture has been desorbed at 100°C for 3 days.

	α_g ($10^{-4} \text{ }^{\circ}\text{C}^{-1}$)			α_l ($10^{-4} \text{ }^{\circ}\text{C}^{-1}$)		
Temperature ($^{\circ}\text{C}$)	DGEBA/D230	MY510/D230	MY721/D230	DGEBA/D230	MY510/D230	MY721/D230
Dry (23 $^{\circ}\text{C}$)	0.6824	0.736	0.704	1.8854	1.7430	1.5218
45 $^{\circ}\text{C}$ /dried	0.662	-----	-----	1.965	-----	-----
60 $^{\circ}\text{C}$ /dried	0.640	0.717	0.667	1.697	1.630	1.575
75 $^{\circ}\text{C}$ /dried	0.674	0.762	0.674	1.967	1.594	1.523
90 $^{\circ}\text{C}$ /dried	0.624	0.731	0.686	1.954	1.620	1.532

4.4 Positron Annihilation Lifetime Spectroscopy (PALS)

4.4.1 Background

The free-volume theory has long been assumed to explain the molecular motion and physical behavior of glassy and rubbery states [6, 16, 22~25, 27]. The theory has been widely adopted among the polymer scientists because it is conceptually simple and intuitively plausible for understanding many polymer properties at a molecular level.

The free volume, by definition, is the space in a solid or liquid sample which is not occupied by polymer molecules, i.e. the 'empty space' between molecules [50]. In the liquid state, it is supposed that the free volume will be sensitive to the change in temperature and that most of the thermal expansion of the polymer rubber or melt can be explained by a change in the free volume. As the temperature of the melt is decreased, the free volume will be reduced until eventually there will not be enough free volume to allow molecular rotation or translation to take place. The temperature at which this happens corresponds to T_g as below this temperature, the polymer glass is effectively 'frozen'. The situation is illustrated schematically in Figure 4-8. The free volume is represented as a shaded area. It is assumed to be constant at V_f^* below T_g and to increase as the temperature is raised above T_g . The total sample volume V_t , therefore, consists of volume occupied by molecules V_o and free volume V_f such that

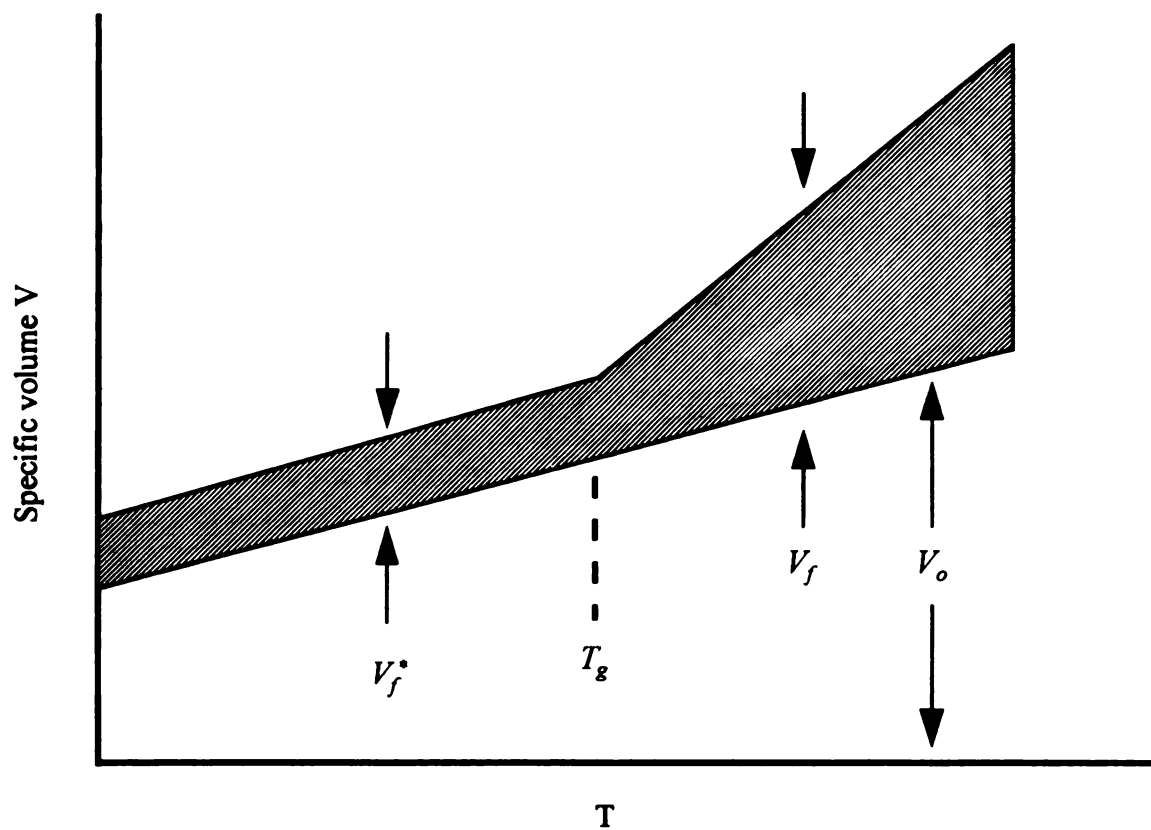


Figure 4-8: Schematic illustration of the variation of the specific volume, V , of a polymer with temperature, T . The free volume is represented by the shaded area. (Adapted from R. J. Young, *Introduction to Polymers*, 1st ed., 1981.)

$$V_t = V_o + V_f$$

Eq. 4-3.

One of the challenging issues in polymer research is in quantifying the relationship between the molecular motion and free-volume properties. In the early stage of development, the free volume was merely considered to be a theoretical concept, something that could not be measured directly. In the last two decades, however, the PALS method has become a more and more powerful tool for studying the molecular structure of polymeric materials in general [52].

To take advantage of this notable technique, PALS method was utilized in this study to examine the nature of the moisture in the polymer network.

4.4.2 PALS

The method makes use of the interactions between the positrons (emitted, usually, from a radioactive material such as ^{22}Na) and the electrons from the material under study. One employs the anti-electron, the positron, as a probe and monitors the lifetime of the positron and positronium, Ps (a bound atom which consists of an electron and the positron) in the host material. Ps is formed when a positron is injected into a solid, it captures an electron from the surrounding medium forming the neutral atom, positronium (Ps). At the present time, however, the positronium formation process in polymeric materials is not well understood.

Due to the positive-charged nature of the positron, the positron and Ps are repelled by the core electrons of polymers and trapped in open spaces, for instance holes, the free volume, and voids. The positron and Ps are localized in these preexisting local holes and the free volume in polymers [32]. The annihilation photons come mainly from these open spaces.

Typically, the lifetime of positron is in the range of 0.3 ~ 0.5 ns, while the lifetime of the Ps depends upon the spin state [51]. Depending on the spin configuration, two ground states of Ps exist: the singlet state called *para*-Ps (*p*-Ps) and the triplet state called *ortho*-Ps (*o*-Ps). In vacuum, *o*-Ps and *p*-Ps have lifetimes of 140 ns and 125 ps, respectively [33]. It has been found that the lifetimes and relative intensities of the positron itself and *p*-Ps are not directly related to the materials characteristics. On the other hand, the lifetime (τ_3) and relative intensity (I_3) of the *o*-Ps are influenced by the structure of the material under study [52]. The lifetimes of the *p*-Ps (τ_1) and e^+ (τ_2) are much shorter (0.125 ns and 0.5~0.6 ns, respectively) than the vacuum lifetime of *o*-Ps (~140 ns).

In molecular substances, the repulsion between the electron in *o*-Ps and the electrons in the surrounding medium localizes the *o*-Ps in regions with lower electron densities or 'voids'. *o*-Ps annihilates through a process called 'pick off' annihilation where the positron of *o*-Ps annihilates with one of the bound electrons with opposite spin. As a result of the 'pick-off' annihilation, the lifetimes

decrease considerably, and for most amorphous polymers are in the range 1.5~3 ns. The lifetime of *o*-Ps (τ_3) is correlated to the size of the void where *o*-Ps is situated at the instant of annihilation, while the intensity of the *o*-Ps lifetime (I_3) is related to the concentration of voids in the polymer.

4.4.3 Experimental Procedures

Three different conditions of samples - dry, conditioned at 75°C, and moisture desorbed at 100°C in vacuum for 24 hours - were prepared from each epoxy systems. The PALS measurements were carried out by using a conventional fast-timing coincidence method in a temperature-controlled chamber at a constant temperature of $25 \pm 1^\circ\text{C}$. The positron source [$\sim 1 \times 10^4$ Bq (~ 30 μCi) of ^{22}Na] was deposited on the surface of an annealed single-crystal copper disc. As a result, I_3 measured was approximately half of that determined with the source sandwiched between two samples. The spectra were acquired and stored in a MicroVAX (Digital model 3100) based multichannel analyzer. Each spectrum was acquired for about 3 hrs. The lifetime spectra were resolved into three or four components by using the PFPOSFIT program.

4.4.4 Results and Discussions

The results shown in Table 4-5 indicated that between dry and wet samples of all three epoxy systems, there were no significant changes in the lifetime of *o*-Ps (τ_3) (τ_3 of wet samples decreased in the range of 0.53~1.91%). The intensity

of the *o*-Ps lifetime (I_3), however, showed noticeable changes between dry and wet samples (10.94~17.3% decrease). From these findings, one can suspect that when the water molecules were introduced into the epoxy network, they occupied the 'voids' between the polymer molecules such that even though there were no significant changes in τ_3 (related to the size of the 'voids'), I_3 (related to the concentration of 'voids') decreased substantially for water molecules occupying the voids. This reasoning was also supported, in previous sections in this Chapter, by the dilatometry results shown in Figure 4-2 through Figure 4-4 where the α_l curves of moisture saturated samples were leaning towards the x-axis.

After the samples went through the desorption cycle, again, PALS measurements were taken on all three epoxy systems. Overall, no distinct changes in τ_3 and I_3 were observed between dry and moisture desorbed samples. It is noteworthy, however, that unlike DGEBA and MY510 epoxy systems, in MY721/D230, there were slight increase in τ_3 and I_3 . MY721/D230 epoxy network, being a highly crosslinked system, sustained elevated internal stress by the water molecules occupying the free volume. After prolonged immersion in the moisture bath, the crosslinked molecular chains may have been ruptured, increasing the size and the concentration of the voids in the polymer network.

4.4.4.1 Conditioned-temperature effects

In order to investigate how the free volume physically respond to the moisture, absorbed at different temperatures, another set of an experiment was

conducted. Assuming that the physical response would be the same for all three epoxy networks, the experiment was performed on only one epoxy system, i.e. DGEBA/D230.

Samples conditioned at 45°C (S₄₅), 75°C (S₇₅₋₁, S₇₅₋₂), and 90°C (S₉₀) were used. After the PALS measurements on wet samples, S₄₅, S₇₅₋₁, and S₇₅₋₂ were then dried following 5 different drying cycles; S₄₅, dried at 75°C for 8 days; S₇₅₋₁, dried at 75°C for 8 days; S₇₅₋₂, dried at 75°C for 23 hrs, 90°C for 24 hrs, and 100°C for 52 hrs. Results were tabulated in Table 4-6.

Results showed that τ_3 and I_3 of dried samples were not much different from those of dry samples. From these findings, we could argue that regardless of temperatures at which the samples were conditioned, the free volume of the DGEBA/D230 were not affected by different sample-condition temperatures. Therefore, in terms of the size and the concentration of the free volume in a polymer network, moisture temperatures of the service environment does not affect its sorption behavior.

Table 4-5: τ_3 and I_3 results on epoxy systems.

Epoxy systems	Sample conditions	τ_3 (ns)	I_3 (%)
DGEBA/D230	Dry	1.776	15.415
	Wet (75°C)	1.742	12.941
	Dried	1.785	14.664
MY510/D230	Dry	1.683	15.469
	Wet (75°C)	1.701	12.793
	Dried	1.630	14.100
MY721/D230	Dry	1.702	14.613
	Wet (75°C)	1.693	13.015
	Dried	1.716	14.715

Table 4-6: Conditioned-temperature effects on the free volume. Presented here are data obtained on DGEBA/D230 epoxy network.

Sample condition	τ_3 (ns)	I_3 (%)
dry	1.774	15.479
S₄₅	1.742	12.996
S₇₅-1	1.745	13.048
S₇₅-2	1.742	12.948
S₉₀	1.731	13.014
S₄₅ (75°C / 8 days)	1.763	15.154
S₇₅-1 (75°C / 8 days)	1.781	14.421
S₇₅-2 (75°C / 23hrs)	1.776	14.481
S₇₅-2 (90°C / 24hrs)	1.793	14.299
S₇₅-2 (100°C / 52hrs)	1.751	14.543

4.5 Summary

Depression of T_g was observed in moisture saturated samples. There was an evidence that since the water molecule is polar, it formed hydrogen bonding with hydroxyl groups of the epoxy network. In a highly crosslinked epoxy network (MY721/D230), hydrogen bonding formation resulted in increase of T_g . T_g s obtained from the moisture saturated samples were far lower than dry T_g ; however, as the condition temperature increased, T_g also increased. Nevertheless, its dry T_g was never recovered even after the moisture was desorbed.

It is noteworthy that under the constant conditioning temperature, as $\Delta T = |T_e - T_g|$ increases, the diffusion coefficient decreased (T_e is an experiment temperature). In other words, as the conditioning temperature is further away from the T_g , the epoxy resin tends to be more glassy such that it will be more difficult for the diffusants to penetrate through the epoxy network.

When crosslinked epoxy systems absorb moisture, the water molecules tend to reside in 'empty space' between molecules, so called free volume. Dilatometry results on the moisture saturated samples showed that the slope of rubbery region was depressed such that the curve was leaning towards the x-axis. The total sample volume V consists of the sum of volume occupied by molecules V_o and free volume V_f . Therefore, when the water molecules occupy the free volume, V_f decreases resulting in decrease of V , where V_o is constant. After the moisture had been desorbed, the slope of rubbery region retained its dry slope.

PALS result also proved the water molecules occupying the free volume in the epoxy network. It was found that when the samples were saturated, there were no significant changes in τ_3 (the lifetime of *o*-Ps, related to the size of the free volume), but noticeable drop in I_3 (the intensity of *o*-Ps, related to the concentration of the free volume). When the moisture was desorbed, the concentration of the free volume was closely returned to its initial concentration. It is necessary to note that the sample condition temperature affected neither on the size nor on the concentration of the free volume.

5. MOISTURE EFFECTS ON MECHANICAL PROPERTIES

5.1 Experimental Procedures

When epoxies are utilized as composite matrices and adhesives, they are often exposed to extreme environments where high content of moisture are commonly observed. Predicting the durability of epoxies under such environments has been an important issue especially when epoxies are used in aerospace structural components. In order to examine the physical effects on the epoxies due to the absorbed moisture, mechanical testing was necessary.

Tensile testing was performed by using an Instron type 4200 series screw-driven tensile machine. Sampling rate was 10 pts/sec and the crosshead speed was 1.0 mm/min.

5.2 Samples

Dry and moisture saturated samples of DGEBA, MY510, and MY721 were tested. The width of the samples were 4.02 mm, the thicknesses were ranged from 1.20 to 1.46 mm, and the gauge lengths were 25.4 mm (1 inch).

5.3 Results and Discussions

5.3.1 Oxidation and Degradation

Samples have been in the moisture chambers at elevated temperatures over 2000 hours and it is suffice to say that there would be some oxidation on the surface of the samples due to the oxygen contained in the moisture and in the air. This assumption was proved to be true when the difference of the samples' color were compared between samples soaked at different temperatures.

As the soaking temperatures were increased, sample discoloration became severe such that the samples' color became darker as the temperatures of the soaking environment temperatures increased. Discoloration of the samples can be said to be an indication that there was a degree of oxidation. Change of sample's color is shown in Figure 5-1 through Figure 5-3.

Absorbed moisture caused not only the oxidation but altered the mechanical properties of the epoxies. Table 5-1 through Table 5-3 show the results of the mechanical tensile testing. Tensile testing results of DGEBA/D230 in Table 5-1 show that overall mechanical properties decreased except the % strain-at-break. This is due to the moisture acting as a plasticizer such that the crosslink network became more susceptible to the deformation. However, once the soaking temperature is past 60°C, the % strain-at-break started to decrease.

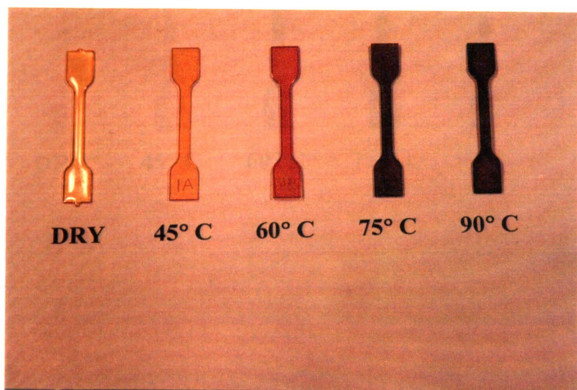


Figure 5-1: Comparison of the color change between dry and moisture saturated samples. As the soaking temperature increases, the color of the sample becomes darker. Shown here are DGEBA/D230 epoxy resins.

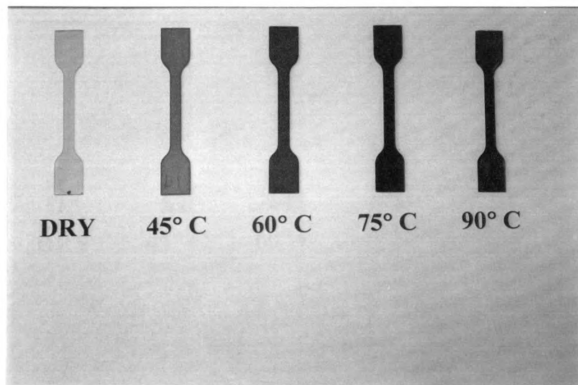


Figure 5-2: Comparison of the color change between dry and moisture saturated samples on MY510/D230 epoxy resins.

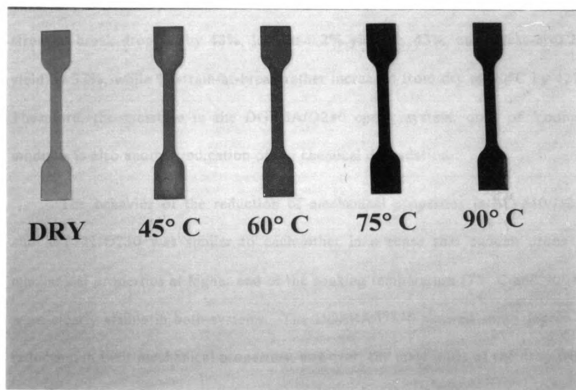


Figure 5-3: Comparison of the color change between dry and moisture saturated samples on MY721/D230 epoxy resins.

This is due to the chemical degradation of the crosslink network induced by the moisture such that while the moisture is behaving as plasticizer, increasing the % strain-at-break, it also serves as a cause for the chemical degradation. Young's modulus dropped from dry state to 45°C by 11%, to 60°C by 17%, to 75°C by 23%, and to 90°C by 25%. Load-at-Break dropped from dry to 90°C by 55%, stress-at-break dropped by 48%, load-at-0.2% yield by 45%, and stress-at-0.2% yield by 37%, while % strain-at-break rather increased from dry to 90°C by 42%. Therefore, the moisture in the DGEBA/D230 epoxy system, drop of Young's modulus is also another indication of the chemical degradation.

The behavior of the reduction of mechanical properties in MY510/D230 and MY721/D230 was similar to each other in a sense that sudden drops of mechanical properties at higher end of the soaking temperature (75° C and 90° C) were clearly visible in both systems. The DGEBA/D230 showed some degree of reduction in their mechanical properties; however, the magnitude of the drop from one temperature to next was not as considerable as those appeared in MY510/D230 and MY721/D230 systems.

As can be seen in Table 5-2, Young's modulus of MY510/D230 epoxy system from dry to 90°C dropped by 41% which is 16% more drop than that in DGEBA/D230 system. Load-at-break dropped from dry to 90°C by 83%, stress-at-break by 79%, load-at-0.2% yield by 90%, and stress-at-0.2% yield by 87%.

Table 5-1: Tensile testing results on DGEBA/D230 epoxy systems.

Temperature (°C)	% Strain at Failure (%)	Load at Failure (kN)	Stress at Failure (MPa)	Load at 0.2% Yield (kN)	Stress at 0.2% Yield (MPa)	Young's Modulus (MPa)
as cast (dry)	8.230	0.3295	61.58	0.2763	51.63	1678
45°C	9.469	0.3236	61.73	0.2188	42.40	1497
60°C	14.21	0.2341	43.01	0.2044	37.35	1395
75°C	13.27	0.1908	38.47	0.1617	32.60	1287
90°C	11.65	0.1497	32.16	0.1507	32.35	1257

Table 5-2: Tensile testing results on MY510/D230 epoxy systems.

Temperature (°C)	% Strain at Failure (%)	Load at Failure (kN)	Stress at Failure (MPa)	Load at 0.2% Yield (kN)	Stress at 0.2% Yield (MPa)	Young's Modulus (MPa)
as cast (dry)	11.280	0.3720	77.15	0.2493	51.72	1845
45°C	12.825	0.2829	54.37	0.1912	36.74	1428
60°C	17.030	0.2560	48.57	0.1650	33.03	1261
75°C	29.990	0.1961	39.02	0.1232	24.52	1053
90°C	1.498	0.0617	16.05	0.0250	6.669	1085

Table 5-3: Tensile testing results on MY721/D230 epoxy systems.

Temperature (°C)	% Strain at Failure (%)	Load at Failure (kN)	Stress at Failure (MPa)	Load at 0.2% Yield (kN)	Stress at 0.2% Yield (MPa)	Young's Modulus (MPa)
as cast (dry)	6.590	0.3884	79.78	0.2682	55.05	1911
45°C	8.952	0.4105	75.23	0.2527	46.31	1652
60°C	8.005	0.4096	74.66	0.2524	46.03	1505
75°C	3.155	0.2443	44.54	0.2338	42.62	1582
90°C	0.778	0.0530	10.48	0.0239	4.96	1376

strain-at-break at dry state was 11.28% and increased by 166% to 29.99% at 75°C and then dropped drastically to 1.498% by 87%. All these results show substantial drop in mechanical properties as soaking temperature increases.

MY721/D230, a tetra-functional epoxy, showed similar plunge in mechanical properties as seen in MY510/D230. Results showed that when comparing the tensile testing data of dry with 45°C, and 45°C with 60°C, there was a steady decrease in mechanical properties. When comparing data between 60°C and 75°C, the decrease was not steady anymore, and at 90°C, the decrease in mechanical properties ranged from 86% to 91% and the Young's modulus dropped by 28% from 1911 MPa to 1376 MPa.

Such decreases in mechanical properties in all three epoxy systems clearly exhibit that the moisture absorbed by the samples contributed severe damage to the crosslink networks of the epoxy systems such that chemical degradation of the network has become an obvious conclusion. In addition, sudden drops of the mechanical properties at 75°C and 90°C can be explained such that the moisture which contributed to the chemical degradation caused the chain scission at high temperature, lowering the mechanical properties.

In DGEBA/D230, di-functional epoxy system, the drop of the mechanical properties between the samples saturated at 75°C and those saturated at 90°C was not as drastic as those seen in MY510/D230 and MY721/D230 epoxy systems. Comparing between the MY510/D230 and MY721/D230, the percentage drop of

the mechanical properties of the MY721/D230 epoxy systems was greater than that of the MY510/D230. Therefore, it can be concluded that as the functionality of the epoxy increases, the network formed by the epoxy with higher functional groups become more susceptible to the chemical degradation, and results in the catastrophic failure due to the chain scissions induced by the moisture.

To aid visualizing the decrease in the mechanical properties of the moisture saturated samples, few bar graphs were constructed. % strain at break of each epoxy system at different soaking temperatures were shown in Figure 5-4. From this bar-graph, it can be easily noticed that % strain at break gradually increases as the soaking temperature increases. Then suddenly at a certain temperature, % strain at break plunges. The increase of the % strain at break in the beginning can be explained as due to the moisture acting as a plasticizer such that the mobility of the chemical chain is increased resulting in the increase in the % strain at break.

As the soaking time increases, however, the polymer network starts to degrade and eventually at a critical point, the network is encountered with chain scission. This reduces the structural integrity of the polymer network and resulting in a sudden drop of the % strain at break. This argument can also be supported by Figure 5-5 and Figure 5-6 where the change of load at break and Young's modulus are provided, respectively.

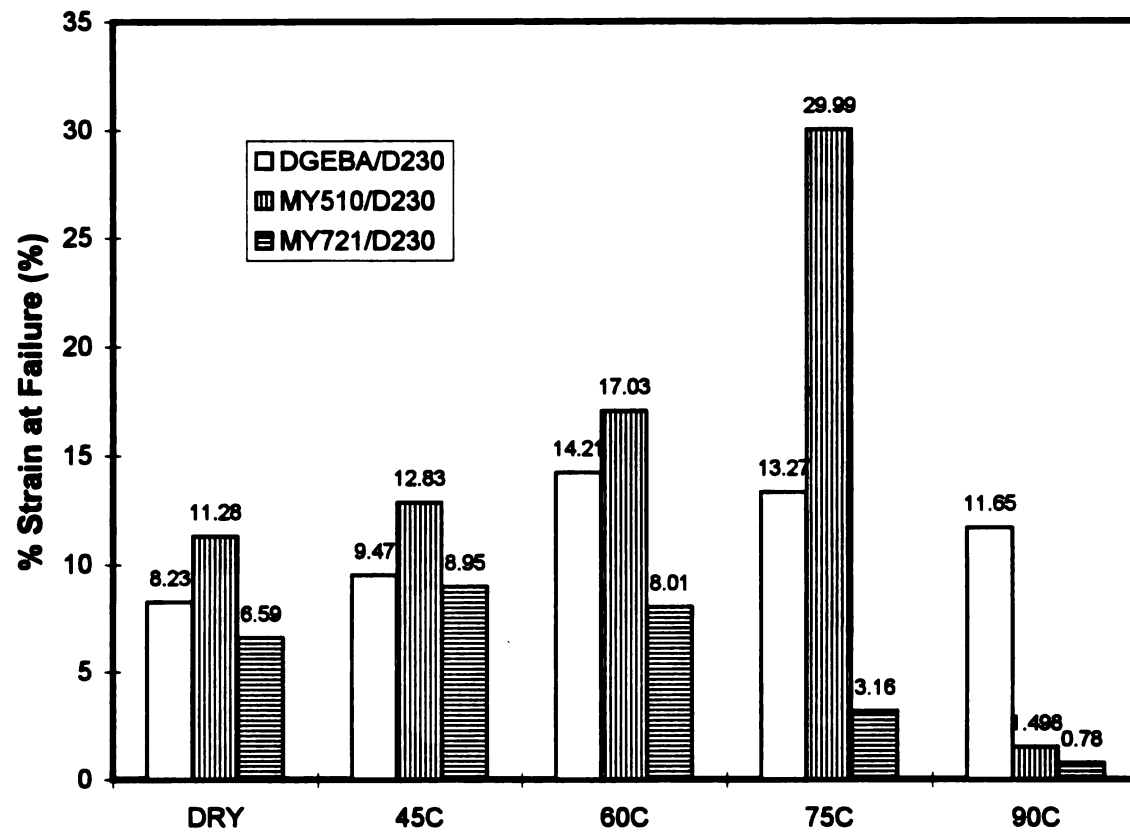


Figure 5-4: Change of % strain at failure (%) due to the moisture absorption.

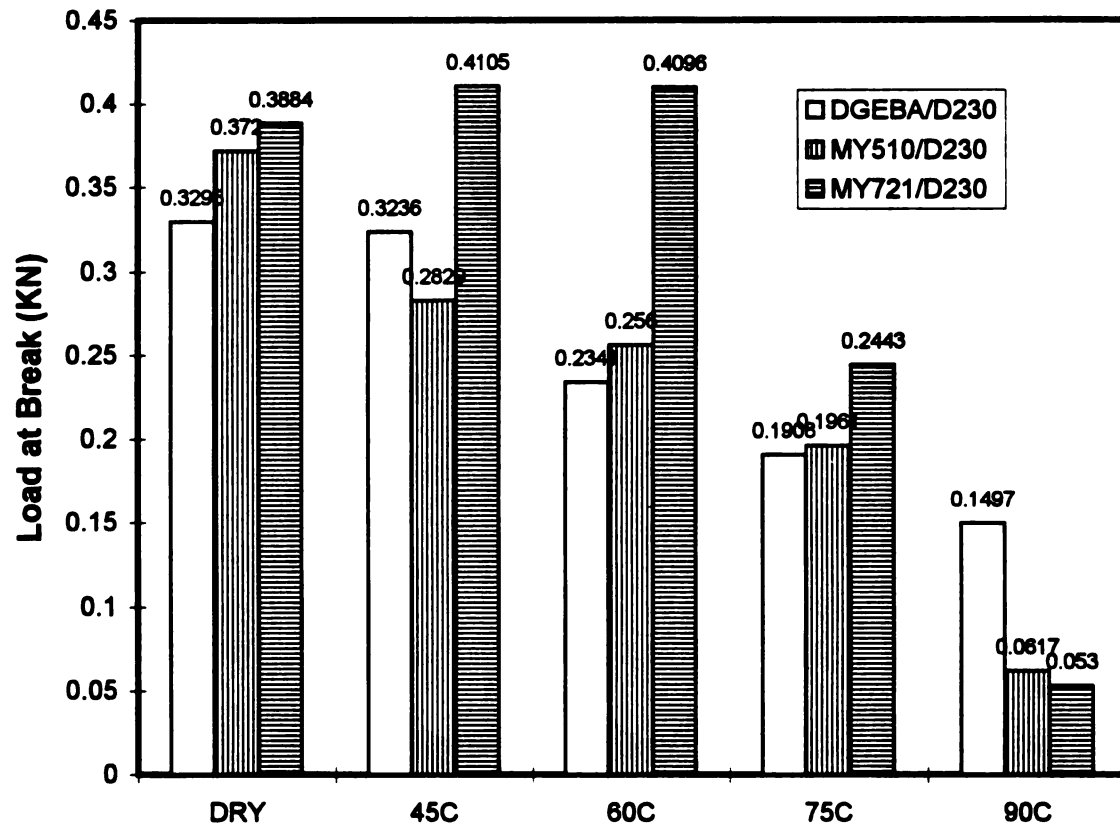


Figure 5-5: Variation of load at failure (kN) due to the moisture absorption.

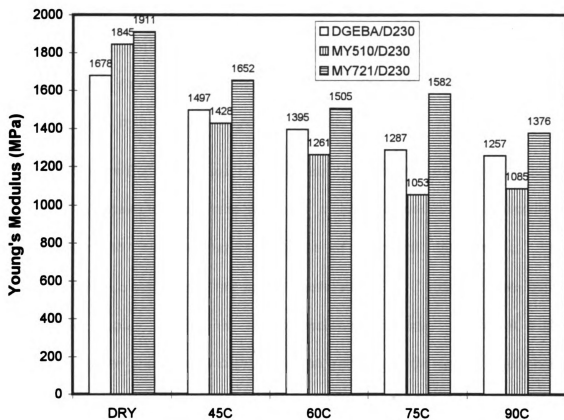


Figure 5-6: Variation of Young's modulus (MPa) due to the moisture absorption.

5.4 Summary

As the sample conditioning temperature increased, the degree of discoloration of the sample became severe such that a light colored, transparent sample when it is dry turned into a dark, almost black, and opaque sample. Prolonged submersion in the water caused discoloration, and it was suggested that the color change was a direct result of oxidation. Discoloration was not limited to just one epoxy resin but it appeared in all three.

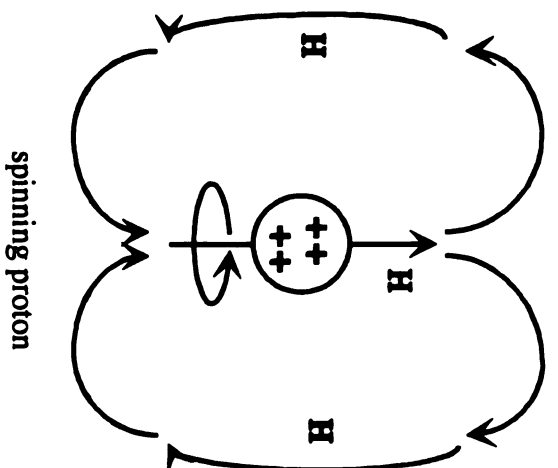
Besides the findings of color change during the immersion in water, it was also found that samples immersed in water at high temperatures, especially at 90°C encountered with substantial amount of chemical degradation. The degradation was so severe that the sample immersed at 90°C snapped even before the load was applied, during the sample mounting process. Water at higher temperatures gave much more damage to the samples with higher functionality such that the overall mechanical properties of MY721/D230 decreased in a great deal. Epoxy resins of high functionality are more susceptible to the chemical degradation than those of low functionality.

6. NUCLEAR MAGNETIC RESONANCE SPECTROSCOPY

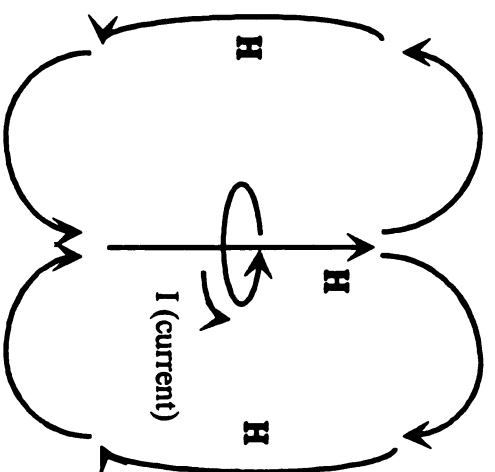
6.1 Introduction

Nuclear magnetic resonance (NMR) spectroscopy is the experimental study of the energy levels of certain atomic nuclei of molecules in a magnetic field [42]. The magnetic properties of the nuclei dominate in a magnetic field and all atomic nuclei possess a characteristic known as nuclear spin [43]. Certain atomic nuclei, having an odd number of either protons or neutrons possess a nonzero spin that can be observed by the NMR spectrometer. Such magnetic nuclei behave as though they were spinning on an axis [44]. A wide variety of nuclei, for instance, the principal isotopes of hydrogen (^1H), carbon (^{13}C), nitrogen (^{15}N), fluorine (^{19}F), and phosphorus (^{31}P) have suitable magnetic properties [43, 44].

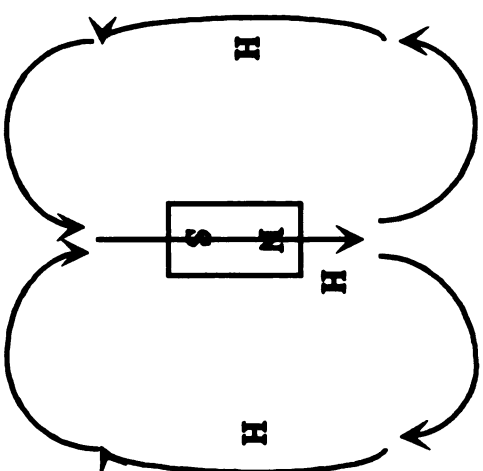
A proton is the simplest nucleus, and its odd atomic number (1) implies that it has a spin [44]. We can visualize a spinning proton as a rotating sphere of positive charge [44]. The movement of charge is similar to an electric current in a loop of wire. As the positively charged nucleus spins on its axis, it generates a magnetic field (H_n) that resembles to the field of a small bar magnet Figure 6-1. This magnetic field is called the magnetic moment of the nucleus. A magnetic moment is created by moving charge, and when a small bar magnet is placed in the field of a larger magnet, as shown in Figure 6-2, the magnetic moment tends to



spinning proton



loop of current



bar magnet

Figure 6-1: A spinning proton generates a magnetic field, called its magnetic moment. This magnetic field (H_o) resembles that of a small bar magnet. *Adapted from [43].*

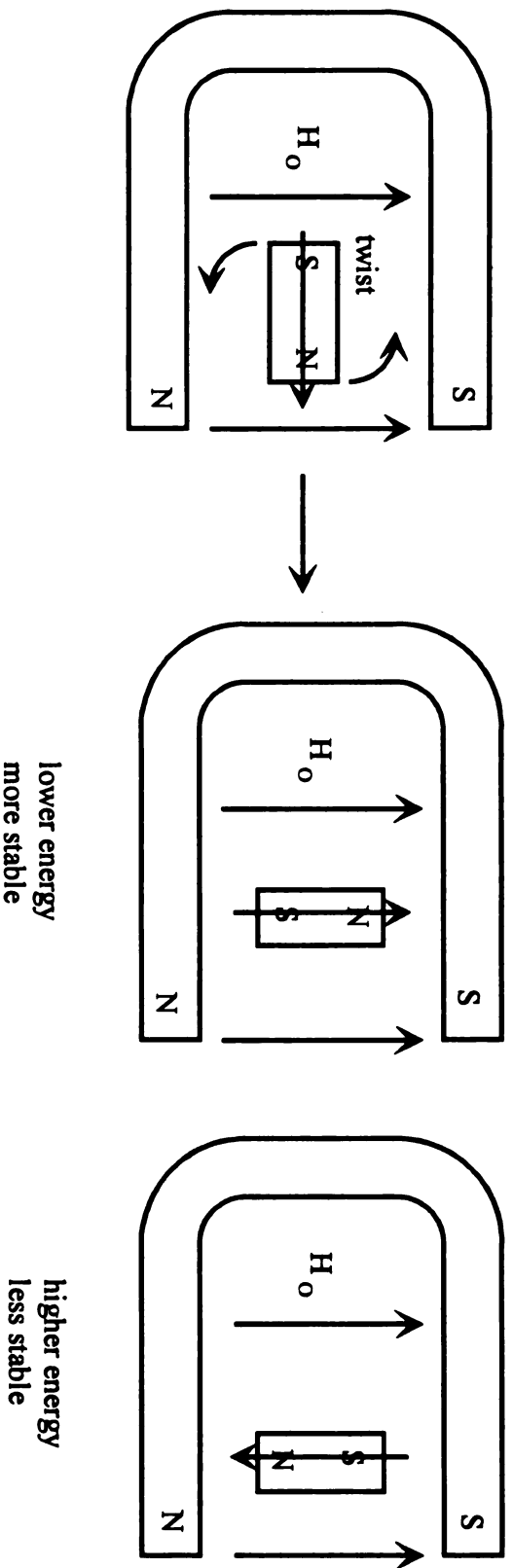


Figure 6-2: An external magnetic field (H_o) applies a force to a small bar magnet, twisting the bar magnet to align it with the external field. The arrangement of the bar magnet aligned *with* the field is lower in energy than the arrangement aligned *against* the field. Adapted from [43].

align itself with the field of the larger magnet - a lower-energy arrangement than an orientation against the field [43, 44].

The same effect can be observed when an external magnetic field (H_o) is applied to a proton, as shown in Figure 6-3. Quantum mechanics requires the magnetic moment of the proton to be aligned either *with* the external field or *against* the field. The state with the proton aligned *with* the field corresponds to a spin quantum number (I) of $+1/2$, called the **alpha-spin** (α -spin) **state**; the state with the proton aligned *against* the external magnetic field corresponds to a spin quantum number $I = -1/2$, called the **beta-spin** (β -spin) **state** [44]. Since the β -spin state is aligned against the external magnetic field, its energy state is higher than the α -spin state.

Quantum mechanics indicates that a nucleus with spin I , is characterized by an angular momentum with a spin quantum number I and is related to the magnetic moment, μ , by Eq. 6-1;

$$\mu = \gamma \hbar I$$

Eq. 6-1

where γ is the *gyromagnetic ratio* (rad/G-s), a constant that depends on the magnetic moment of the nucleus, and \hbar is Planck's constant divided by 2π .

Nuclei with a spin number of zero ($I = 0$) are not observable in NMR experiments. There are 118 nuclei that have been studied by NMR [43], but the

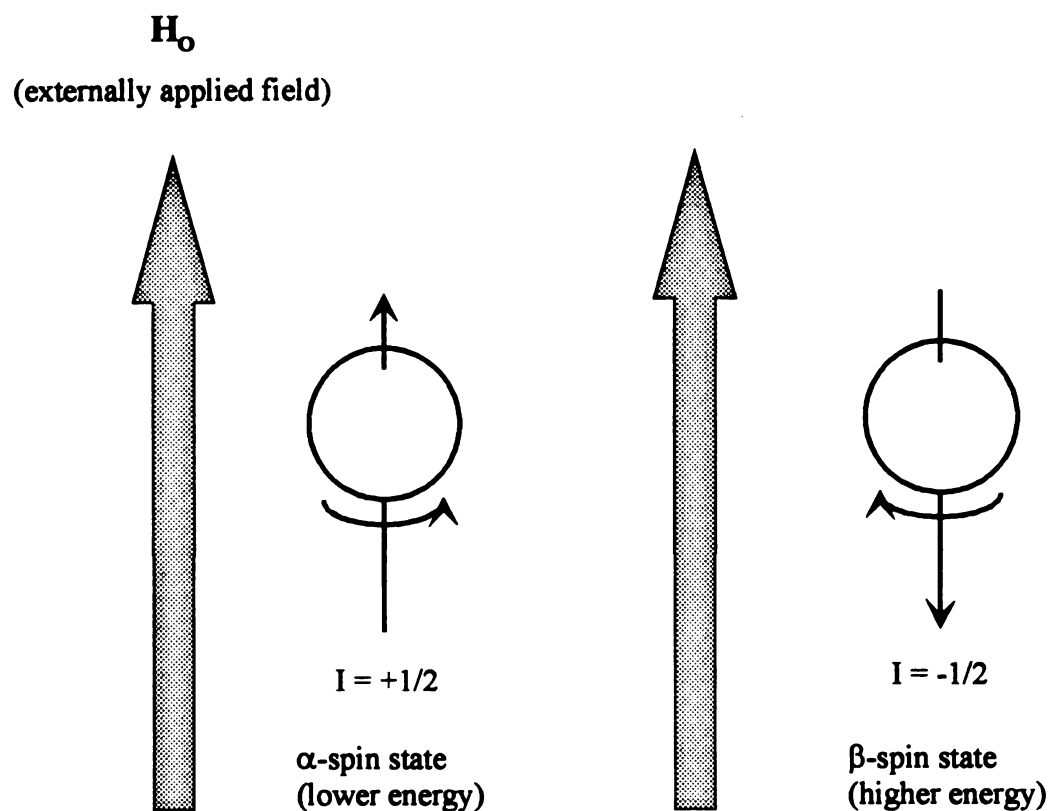


Figure 6-3: In the presence of an external magnetic field (H_o), a proton has a spin quantum number (I) of either $+1/2$ or $-1/2$. The state with spin $I = +1/2$ is called the α -spin state, aligned with the external magnetic field. The state with spin $I = -1/2$ is called the β -spin state, aligned against the external field. The β -spin state is higher in energy than the α -spin state. Adapted from [43].

nuclei of primary interest to polymer chemists are the proton (^1H , $I = 1/2$), deuteron (^2H , $I = 1$), ^{13}C ($I = 1/2$) (for the more common ^{12}C isotope, $I = 0$), and ^{19}F ($I = 1/2$) [43].

The two factors that determine the sensitivity and utility of a nucleus for NMR spectroscopy are the natural abundance and the gyromagnetic ratio [44]. For example, the ^1H isotope is 100% naturally abundant and has a high gyromagnetic ratio, and this makes ^1H the most sensitive nucleus for NMR study. On the other hand, the ^{13}C nucleus is present in natural abundance at a level of only 1.1% and has a gyromagnetic ratio that is 1/4 that of hydrogen to make it 1.6×10^{-2} less sensitive than hydrogen for NMR study [43].

In the absence of a magnetic field, the proton magnetic moments have random orientations, Fig. 6-4 (a) [43]. However, when a sample is placed in a homogenous magnetic field, the dipoles will align with the lines of induction or the force of the applied magnetic field and each proton assumes the α state or the β state (b). Because of the energy difference between the spin states, there are slightly more α spins than β spins. Molecules are constantly in thermal motion, and because the molecules interact with each other, the thermal motion will cause the magnetic moments of most of the protons to point randomly. However, the average or net magnetization will be preferentially aligned along the magnetic field (c). The average of all these magnetic moments is called the *thermal equilibrium magnetization*, M_0 . The intensity of the NMR signal is proportional

to M_o and is directly related to the magnitude of the applied field. The macroscopic nuclear magnetization, M , is the vector sum along H_o of the each spin moments. Because the nuclei have angular momenta and thermal motions, they will not align completely parallel to the field, and the torque from the applied field will cause the magnetic moments to precess about the field direction with a characteristic angular frequency. The precession frequency is known as the *Larmor frequency* (ω_o) and is proportional to the applied magnetic field, H_o . The Larmor frequency, ω_o is given by

$$\omega_o = \gamma H_o$$

Eq. 6-2

in radians per second.

The energy difference between the two spin states, α -spin state and β -spin state, is proportional to the strength of the magnetic field and can be expressed as in Eq. 6-3

$$\Delta E = \gamma \frac{h}{2\pi} H_o$$

Eq. 6-3

where ΔE is the energy difference between α and β states, h is Planck's constant, H_o is strength of the external magnetic field (in gauss), and γ is gyromagnetic ratio, $26,753 \text{ sec}^{-1} \text{ gauss}^{-1}$ for a proton. This equation shows that the energy

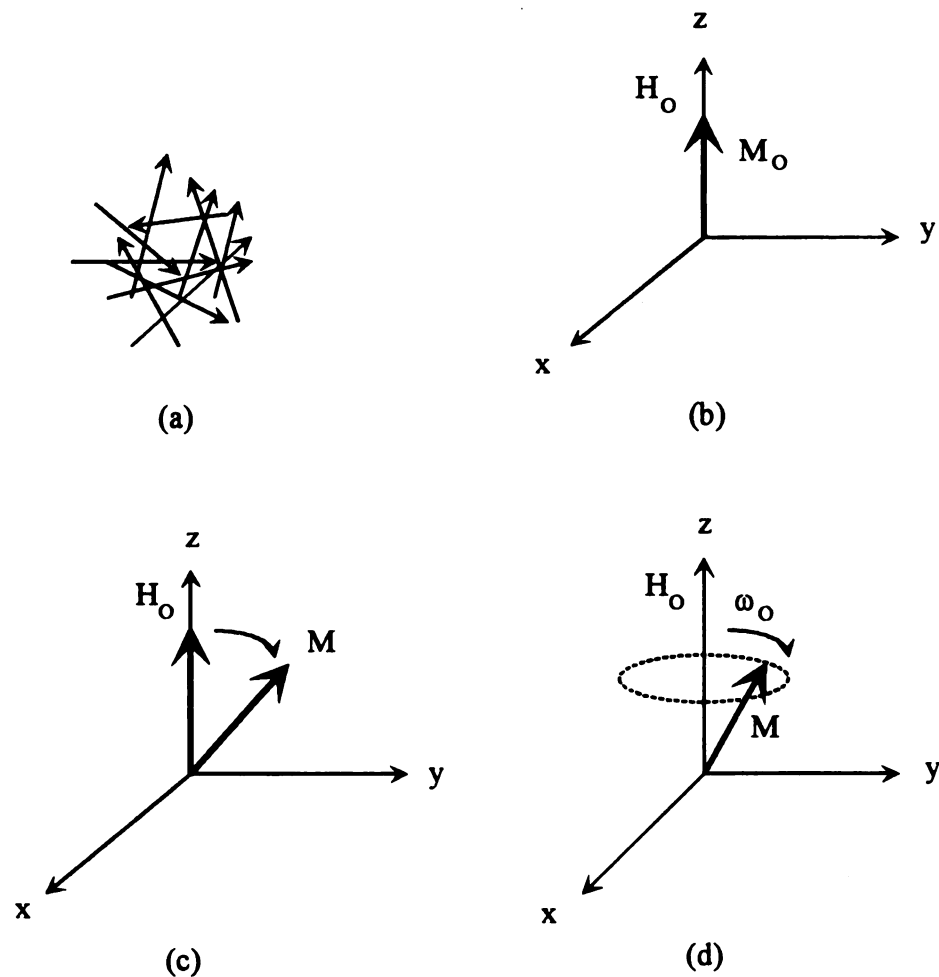


Figure 6-4: The nuclear spin generates a small magnetic field, and in the absence of an applied magnetic field, the orientation of these dipoles is random (a). When a sample is placed in a homogenous magnetic field, the dipoles will align themselves with the lines of induction or force of the applied magnetic field (b). However, thermal motion does not allow the alignment to remain, and the average alignment is at a small angle to the magnetic field (c). The magnetic moment precesses about the magnetic field at the Larmor frequency (d). *Adapted from [43].*

difference (ΔE) between the α -spin and β -spin states is proportional to the strength of the magnetic field (H_0) and to the gyromagnetic ratio (γ). The energy levels that occur in the presence of a static magnetic field appear as shown in Figure 6-5. When a proton is struck by a photon with just the right amount of electromagnetic energy, the proton's spin can flip flop from α to β or from β to α . A nucleus aligned with the field can absorb the energy needed to "flip" and align against the field.

The energy difference falls in the radiofrequency range ($10^7 - 10^8$ Hz). The nuclei can be induced into a higher energy state by absorption of a radiofrequency pulse of the appropriate frequency and strength [43]. This radiofrequency, rf, is produced by using an alternating current of variable frequency that is passed through a coil whose axis lies in the xy plane perpendicular to the applied magnetic field. This current excites an oscillating magnetic field that is also perpendicular to the applied field. As the frequency of the oscillating field varies, there is a point at which it exactly matches the precessional frequency of the nuclei, and energy from the radiofrequency is absorbed by the nuclei. When this absorption occurs, the system is said to be in resonance, as shown in Figure 6-6, and its absorption of energy is detected by the NMR spectrometer [43].

This absorption of energy is the resonance phenomenon. In resonance, energy is transferred from the rf radiation to the nuclei, which causes a change in the spin orientation of the nuclei or, in other words, a change in the spin

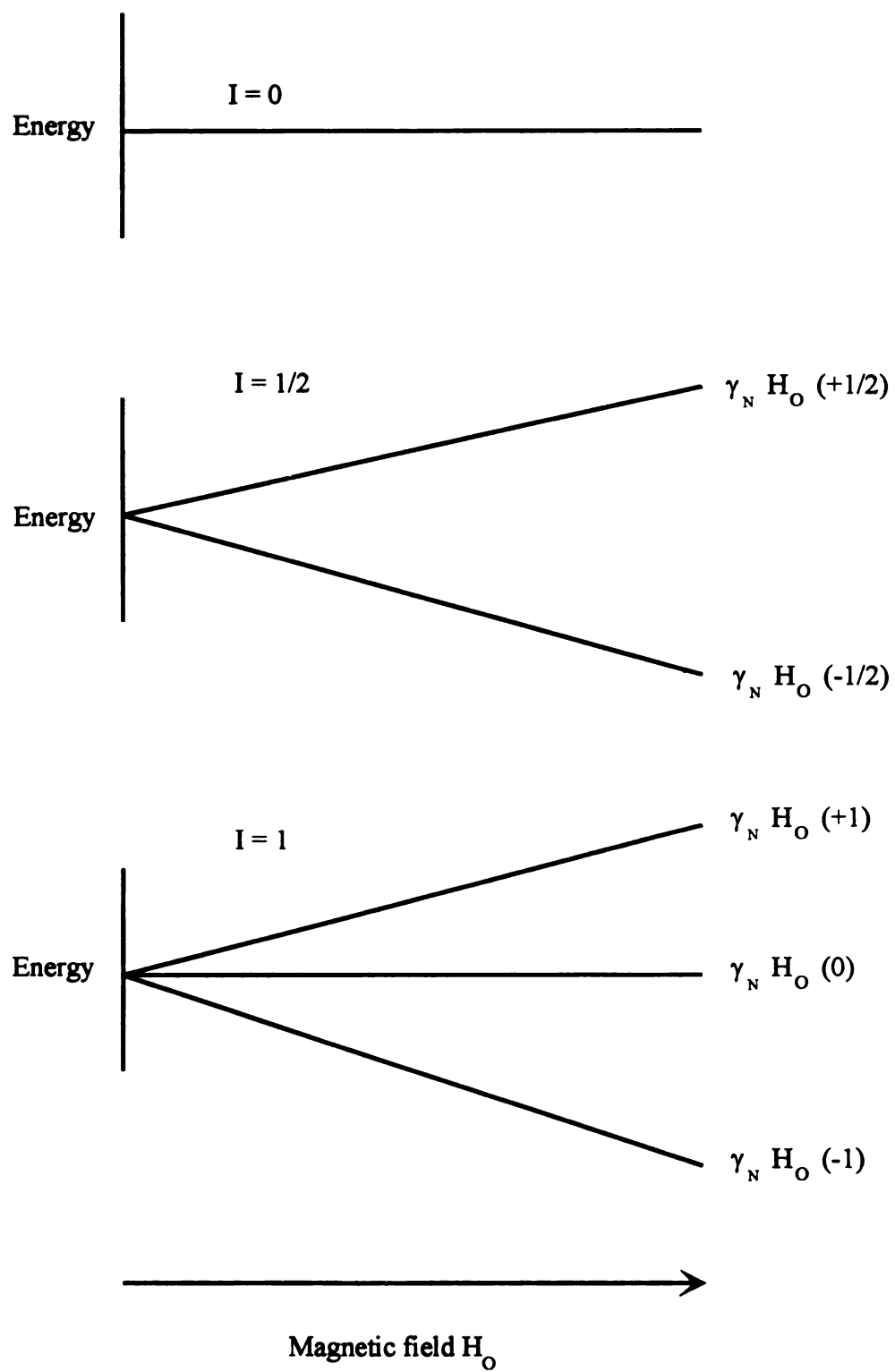


Figure 6-5: Quantized energies of nuclei in a magnetic field. *Adapted from [43].*

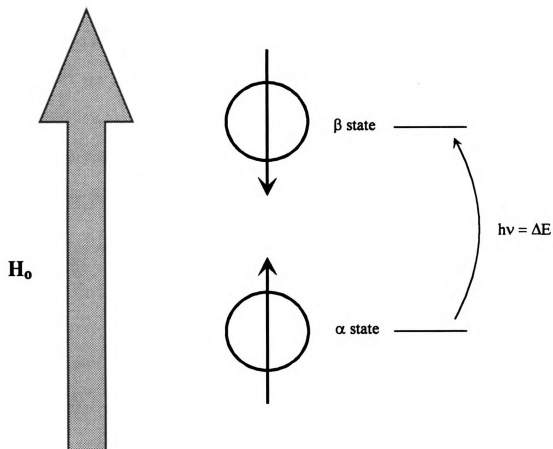


Figure 6-6: A nucleus in "in resonance" when it is irradiated with radio-frequency photons having energy equal to the energy difference between the spin states. Under these conditions, a proton in the α -spin state can absorb a photon and change to the β -spin state. *Adapted from [44].*

populations in the various energy levels. The rf field must oscillate with a frequency, ν , given by the equation of $E = h\nu$, showing that the energy E is in proportion to ν , the electromagnetic wave frequency. This equation is put together with the equation for the energy difference between the spin states to obtain a relationship between magnetic field and frequency. The Eq. 6-4 shows that the resonance frequency, ν , of a nucleus is in proportion to the applied magnetic field, H_0 , and the gyromagnetic ratio;

$$\nu = \frac{1}{2\pi} \gamma H_0$$

Eq. 6-4.

6.2 The Spin-Lattice Relaxation Time (T_1)

After the resonance rf pulse has been applied, a higher energy excited state is present [43]. This higher energy level corresponds to the nuclei that are elevated to the antiparallel position. To return to the equilibrium or ground state, this excess energy is passed to the surroundings by stimulated emission, and some of the antiparallel nuclei revert to the parallel or low-energy state. This decay of the magnetization proceeds to equilibrium in an exponential manner. The spin-lattice relaxation time, T_1 , measuring the longitudinal magnetic relaxation time is one of the methods to measure the decay of the magnetization [42].

The rate of return to equilibrium along the static field (z axis) is depended upon the rate of exchange of energy between the nuclei and the environment or,

lattice in NMR terminology (Figure 6-4). The longitudinal magnetic relaxation time, T_1 , is often called the *spin-lattice relaxation time* and depended upon the effectiveness of energy transfer from the excited nuclei to the lattice. Returning to the ground state is enhanced by the presence of rf energy in the lattice at the resonant frequency (stimulated emission). This rf energy comes from fluctuating magnetic nuclei and electrons in the lattice. Magnetic fluctuations that are at or near the resonant Larmor frequency generate rf magnetic fields which stimulate the transition from the high-energy to the low-energy states. This coupling mechanism allows the energy initially added by the rf pulse to be dissipated to the lattice [42].

The T_1 is unique for each molecule and its environment, and provides information about the molecular dynamics of the magnetic moments and the molecules around them. When the nuclear magnetization rotates at the Larmor frequency, the local fluctuating magnetic fields (perpendicular to the rf axis) are generated primarily by molecular motion [43]. Thus when the lattice exhibits considerable molecular motion at the appropriate frequency, the energy coupling is effective, and the T_1 is short. On this basis, the T_1 is short for liquids where the molecular motion is extensive over a broad range of frequencies but is quite long for solids where the motion is restricted and occurs over a narrow range of frequencies [43].

6.3 Cross-Polarization (CP)

Because of its inherent low sensitivity, the ^{13}C isotope addresses a challenge for NMR spectroscopy [43]. The observable ^{13}C signal is limited due to the low gyromagnetic ratio, the low natural abundance, and the long spin-lattice relaxation time of the ^{13}C nucleus. The sensitivity must be increased for the detection of the resonance of the ^{13}C nuclei. In response to this need, polarization-transfer methods are employed to transfer the large spin-state polarization of the protons to the weakly polarized ^{13}C nuclear species. If it is provided with perfect transfer of polarization from protons to ^{13}C , the ^{13}C signal will be improved by a factor of $\gamma_{\text{H}}/\gamma_{\text{C}} = 4$.

The $^{\text{C}}T_1$ spin-lattice relaxation times for solids are significantly longer than the $^{\text{H}}T_1$ times, so the maximum number of pulses that can be used is less. However, with polarization transfer, the delay time between cross-polarization pulse sequences is depended upon the shorter $^{\text{H}}T_1$ times, and further gains in signal enhancement becomes the extent of $(^{\text{C}}T_1/^{\text{H}}T_1)^{1/2}$ [43]. In addition, it would be possible to perform signal averaging experiments much more rapidly. This can be achieved as follows.

Let us designate the carbon coordinates as x'' and y'' since they are rotating at a different speed to x' and y' , the proton coordinates. Immediately following the 90° ^1H pulse and during the ^1H spin locking condition radiofrequency along

the coordinate x'' describing the ^{13}C magnetization is applied. However, the ^{13}C power level is altered so that

$$\gamma_H H_{1H} = \gamma_C H_{1C}$$

Eq. 6-5.

This is called the *Hartmann-Hahn* condition or match [43].

Cross-polarization is a double-resonance experiment in which the energy levels of the ^1H and ^{13}C spins are equalized to the Hartman-Hahn condition in the rotating frame [43]. Under this condition, energy may be exchanged between the two coupled spin systems. The result is a growth of the ^{13}C magnetization at the expense of the ^1H magnetization. The basic pulse sequence used for the cross-polarization experiment is shown in Figure 6-7. The method is comprised of four steps: (a) polarization of the ^1H spin system, (b) spin-locking of the protons in the rotating frame, (c) establishment of contact between the carbons and the protons, and (d) measurement of the magnetization of the carbon nucleus [43].

The application of a 90° ^1H pulse rotates the ^1H longitudinal magnetization into transverse magnetization (the xy plane is in the rotating reference frame as shown in Figure 6-7 (a)). The second step is the nearly immediate (within microseconds) application of a 90° phase-shifted proton pulse, which produces the effective field colinear with the proton magnetization and results in spin locking, Figure 6-7 (b). Spin locking is utilized because the magnetization of the protons

in the spin-locked state decays by a rotating frame spin-lattice relaxation time, $^H T_{1\rho}$. Therefore, the magnetization loss of the protons resulting from relaxation effects during the contact time is small [43].

Simultaneously with the spin locking of the protons, in the third step of the experiment Figure 6-7 (c), a pulse is applied in the ^{13}C channel, and this pulse is carefully adjusted so that the energy gap for spin flips agrees exactly to that of the protons. This pulse is maintained for a time, t_{CP} , and is called the *contact time*. This contact time allows for the exchange of energy between the abundant proton-spin reservoir and the rare carbon-spin system. This exchange, called *cross-polarization*, occurs when the Hartmann-Hahn match, which is defined as

$$\omega_H = \omega_C$$

Eq. 6-6

is contended with the rotating frame [43].

The fourth part of the CP experiment Figure 6-7 (d) is to terminate the ^{13}C pulse and to observe the FID (*free induction domain*, the observed signal in the time domain) while the ^1H field is used for decoupling. The resulting FID is Fourier transformed to give the frequency-domain spectrum [43].

In the CP experiment, the ^{13}C spin system is polarized by the ^1H spin system under the Hartmann-Hahn condition, Eq. 6-5. Thus, the longer $^C T_1$ (1-1000 s) is replaced by the shorter $^H T_1$ spin-lattice time (1-100 ms) [43].

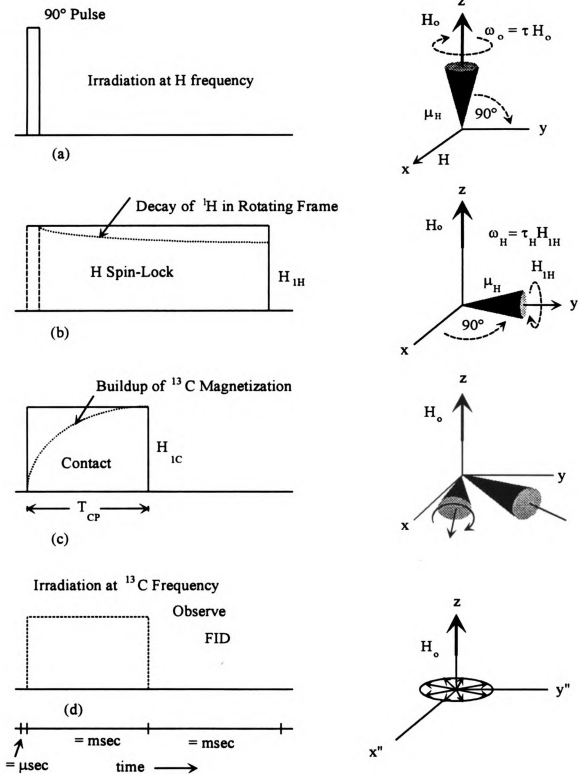


Figure 6-7: The timing sequence for the cross-polarization experiment. *Adapted from [43].*

The optimum recycle delay has been measured, and it is $1.25 {}^H T_1$ for the situation in which spin diffusion dominated the spin system [43]. For the case in which spin diffusion is not efficient, the optimum recycle delay must be longer ($4-5 {}^H T_1$) to avoid saturation.

A typical increase in carbon magnetization with contact time is shown in Figure 6-10. In the CP experiment, polarization is transferred from the magnetically rich protons to the magnetically poor carbons via their static dipolar interactions [42]. When both spins are locked in the rotating rf fields and their amplitudes are equalized by utilizing the Hartmann-Hahn condition, Eq. 6-5, the time constant for the transfer of polarization under conditions of spin locking is called the T_{CH} relaxation time. This transfer is spin-spin process, and generally has a magnitude in the range of $100\mu s$.

The result of CP is an initial growth of the ${}^{13}C$ magnetization at a rate that is inversely proportional to the cross-polarization-transfer rate constant (T_{CH}) Figure 6-10. After a suitable period (typically 1-10ms), a maximum ${}^{13}C$ magnetization is reached, after which the ${}^{13}C$ signal begins to decay at a rate in proportion to the inverse of the ${}^H T_{1\rho}$ time. The carbon magnetization, S , is given by

$$S = \exp\left(\frac{t_m}{{}^H T_{1\rho}}\right) \left[1 - \frac{\exp(-t_{CP})}{T_{CH}} \right]$$

Eq. 6-7

where t_{CP} is the contact time. Thus two opposing relaxation mechanisms operate during the contact time. For short contact times, the process is dominated by the T_{CH} process, and the carbon magnetization increases exponentially. At longer contact times, the ${}^H T_{1\rho}$ process dominates, and the magnetization decreases exponentially because of the proton spin-lattice relaxation in the rotating frame.

Provided that the carbons in a polymer repeat unit are subjected to the same motions, carbons with directly bonded protons are expected to cross-polarize more rapidly than carbons without direct interactions because the shorter interaction distance results in a larger local dipolar field. Rapid molecular motion attenuates the cross-polarization mechanism. For protonated carbons in rigid solids, most of the signal buildup occurs over about the first 100 μ s; for nonprotonated carbons, in the first few milliseconds [43].

The rate of signal decay depends on ${}^H T_{1\rho}$ [43]. If ${}^H T_{1\rho}$ is very short, the cross-polarization process is jeopardized because of the rapid decay process. By varying the contact time prior to observation of the spectrum, T_{CH} and ${}^H T_{1\rho}$ may be determined for the protons coupled with each resolved carbon resonance [43].

6.4 Proton Spin-Lattice Relaxation Times in the Rotating Frame

6.4.1 The rotating frame

The nucleus in the sample possesses a magnetic moment, charge and angular momentum, and as the magnetic moment interacts with magnetic field H ,

it will do so in such a way that the field will force the moment to line up with it [42]. If the nucleus was identical with a simple bar magnet, the moment would align along the direction of the magnetic field. The latter, by convention, is termed the z direction. However, unlike a simple bar magnet the nuclei have angular momentum and the effect is to force the nuclei; therefore, the magnetic moment to precess about the field H_0 . Figure 6-8 [42]. This motion is analogous to the spinning top which precesses about the earth's gravitational field. The precession velocity ω_0 of the moment (Larmor speed) is determined by the gyromagnetic ratio of the nucleus γ and the strength of the magnetic field as shown in Eq. 6-2. To express ω in units of hertz rather than radians, ω is divided by 2π , this equation is also shown in Eq. 6-4 [42].

Interaction of the electromagnetic radiation with the moment of the nuclei when inducing transitions between energy states can be understood by vector diagrams, since the magnetic moment is a vector quantity, if the coordinates used for the discussion are changed to *rotating frame coordinates* [42].

After the sample is put in the magnetic field, the magnetic moment of the nucleus precesses at the Larmor frequency with the direction of the magnetic field induced by the magnet, i.e. around z in Figure 6-9 (a). The coordinates x, y are the other coordinates of three-dimensional space in the laboratory of the laboratory 'frame'. From nucleus' point of view, they are rotating at the Larmor frequency. If we change the x, y coordinates to one rotating at the rotating frame

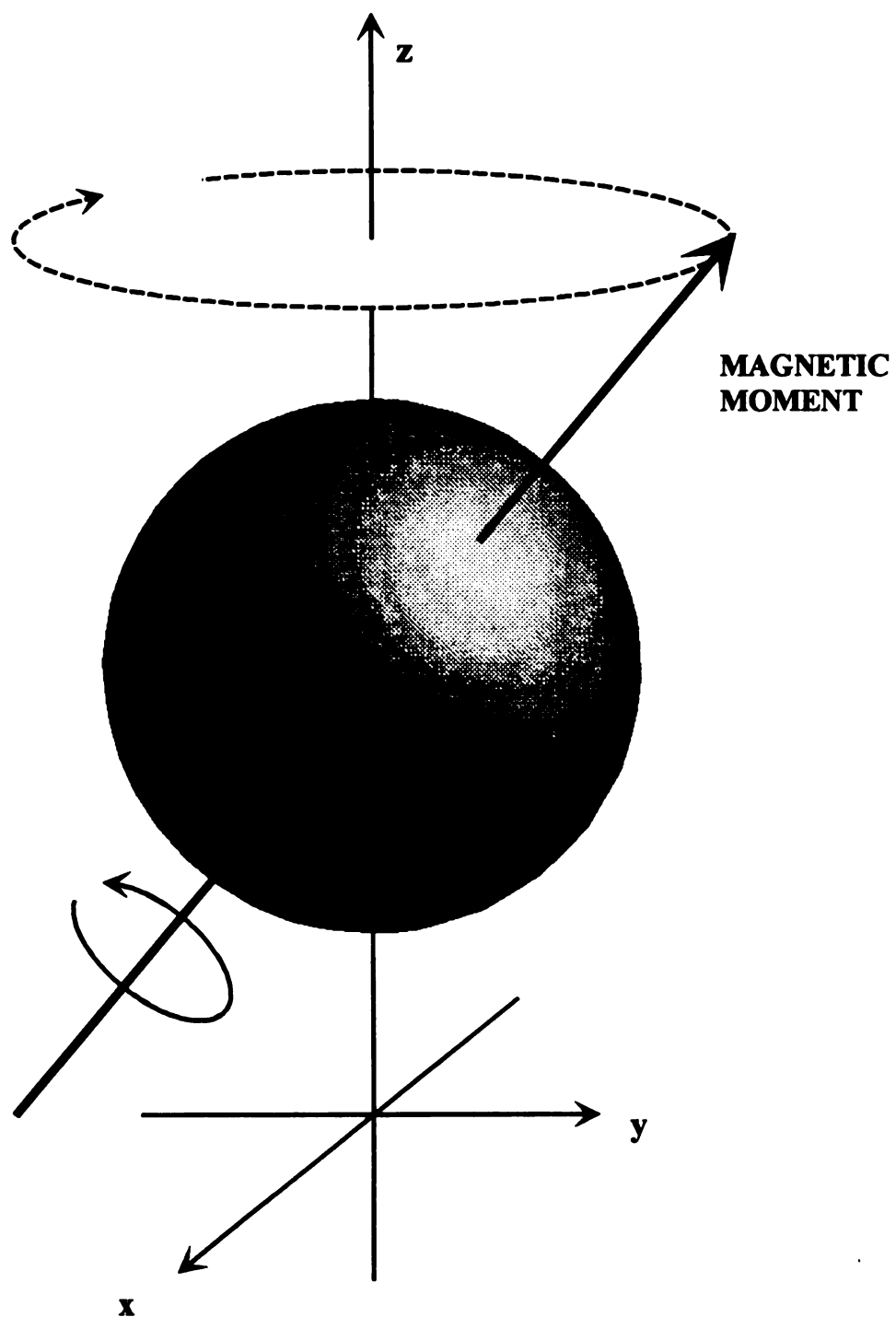
MAGNETIC FIELD

Figure 6-8: Diagram to show the motion of a spinning nucleus in a magnetic field of direction **z**. Adapted from [48].

(x', y') , i.e. at the Larmor frequency, the magnetic moment appears 'frozen' on the cone Figure 6-9 (a) [42]. In reality, there will be a large number of nuclei; each will have a magnetic moment frozen at a different position around the cone. The sum of these moments, the net magnetization, will lie along z -axis (now termed z' , Figure 6-9 (b)). It will be recalled that the radiofrequency irradiation at resonance is at the Larmor frequency as well. If this is applied in the laboratory frame at 90° to the magnetic field H_0 , the magnetic field from the electromagnetic irradiation (H_1) rotates in the x, y plane and at resonance is static 'frozen' along x' in the rotating frame Figure 6-9 (b) [42].

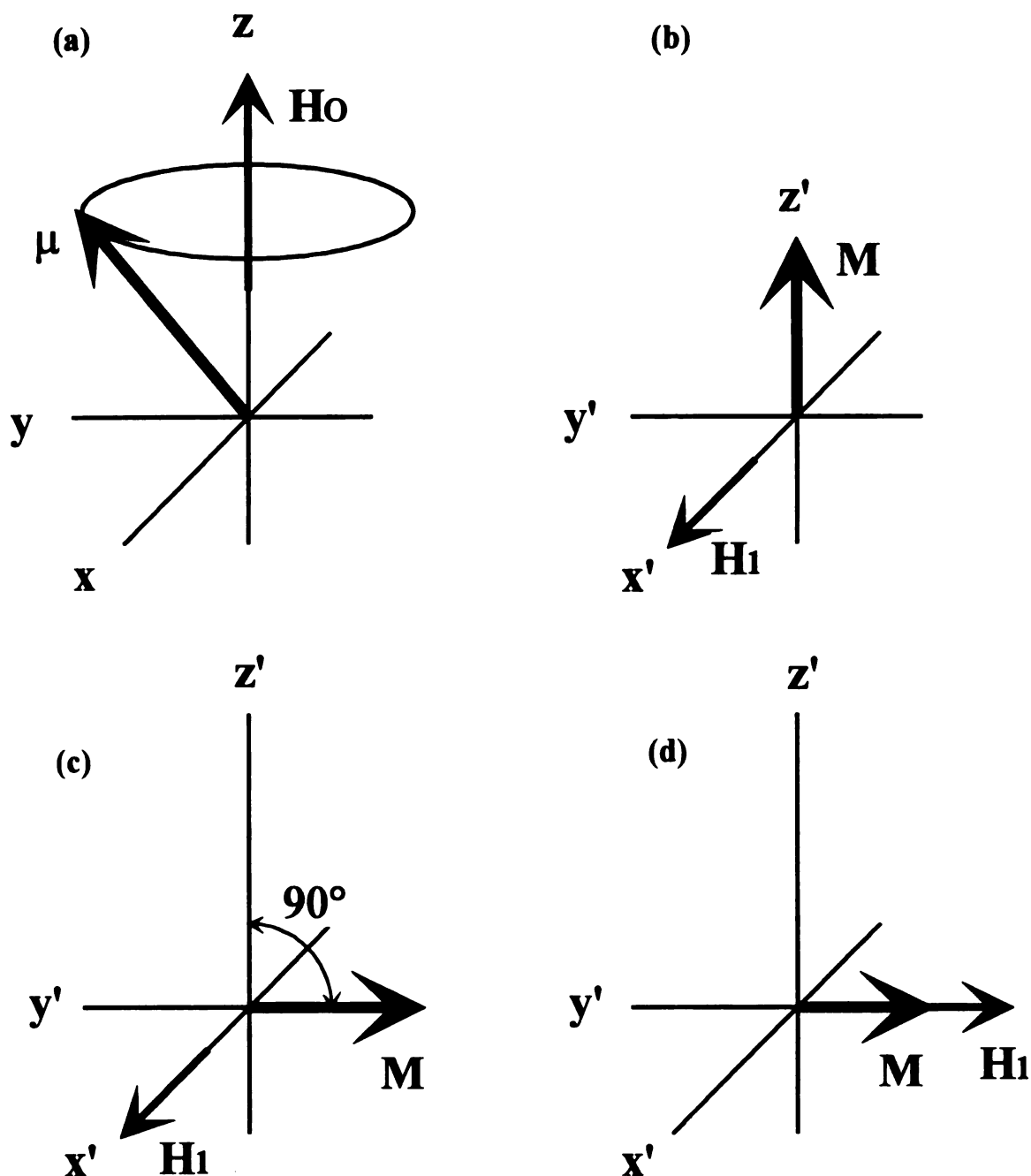


Figure 6-9: Changing coordinates to the rotating frame: (a) rotation of magnetic moment μ about laboratory coordinates; (b) change of coordinates to rotating frame and application of a radiofrequency induced magnetic field along x' ; (c) after application of field H_1 along x' (note the vector M moves through the $z'y'$ plane by 90° to become colinear with y'); (d) after changing the phase of the irradiation field so that H_1 is colinear with M and y' . *Adapted from [48].*

6.4.2 Proton spin-lattice relaxation times in the rotating frame

Proton $T_{1\rho}$ relaxation in the rotating frame, ${}^H T_{1\rho}$, is the T_1 process in the rotating frame that takes place for the proton nuclei [42]. When proton $T_{1\rho}$ relaxations are measured, because of spin diffusion, the observed relaxation times are averaged over all of the coupled protons. Individual proton $T_{1\rho}$ s, however, can be characterized by variations in the normal ${}^{13}\text{C}$ CP experiments. Measurements of ${}^H T_{1\rho}$ s have the advantage that they probe the molecular motion in the kilohertz range, whereas the T_1 s reflect motion in the megahertz range. On the basis of differences in the spectral density in the kilohertz region, the ${}^H T_{1\rho}$ s may be weakly depended upon the rf field [42].

The ${}^H T_{1\rho}$ s are obtained from the final slopes of the plots of observed carbon magnetization generated by log, equalized spin-lock cross-polarization transfers from protons to carbons [43]. After the initial increase carbon polarization, the carbon signal decreases by way of the ${}^H T_{1\rho}$ relaxation process. Under high-resolution conditions, the individual carbon resonance follow the protons to which they are most closely coupled. Therefore, it is possible to resolve ${}^H T_{1\rho}$ differences between protons on different types of carbons [43]. The measurement of individual ${}^H T_{1\rho}$ s involves the exordium of a variable contact time of cross-polarization. A semi-log plot of the carbon magnetization vs. the time of spin-lock cross-polarization transfer generates ${}^H T_{1\rho}$.

As an example, heterogeneities in blends of polymers can be detected because the $^1H T_{1\rho}$ s are sensitive to spin diffusion in polymer systems on the order of an internuclear distance of 1 nm. For single-phase systems of multicomponent systems, the rate of spin diffusion depends on the nature of the spatial mixing of the polymer chains. When the chains are intimately and homogeneously mixed, only one $^1H T_{1\rho}$ may be observed. If the mixing is nonuniform, several different $^1H T_{1\rho}$ s may be detected depending on the system [49].

6.5 Sample Preparation for the T_{CH} and $^1H T_{1\rho}$ Experiment

For each epoxy system, three different types of samples have been prepared; dry (unconditioned), wet (saturated at 75° C), and dried (wet samples that had been dried at 100° C under vacuum for 24 hours) samples. Samples were cut into the dimensions of $1.0 \times 0.4 \times 0.1 \text{ cm}^3$ so that they can fit into a sample spin tube. Both dry and dried samples were stored individually prior to NMR experiment at room temperature in polypropylene tubes containing desiccants, and in particular, each wet samples were stored in distilled water filled polypropylene tubes to minimize any moisture loss between the experiments.

6.6 Experimental Procedure

The experiments were conducted by Varian VXR-400 NMR spectrometer. The measurements were obtained by using combined techniques of cross-polarization and magic-angle spinning at the operating frequency of 100 Mhz.

The spinning speed was of the order of 4 kHz. Contact time for the cross-polarization relaxation time was from 10 μ s to 2500 μ s. Total acquisition time for one sample was 12.6 hours.

6.7 Results and Discussion

6.7.1 ^1H Spin-Lattice Relaxation Times in the Rotating Frame

$^H T_{1\rho}$ s on dry, wet, and moisture desorbed samples were obtained for each epoxy group samples as shown in Table 6-1 through Table 6-3. One of the I vs. contact time plots is shown in Figure 6-10.

$^H T_{1\rho}$ results show that the moisture saturated DGEBA/D230 sample has a higher $^H T_{1\rho}$ values over the range of the peak frequencies, compared to the unconditioned sample. The increased $^H T_{1\rho}$ values, however, returned to its initial values as the sample has been dried. Unlike the behavior shown by the DGEBA/D230 epoxy resin, MY510/D230 and MY721/D230 revealed different characteristics in their proton $T_{1\rho}$ relaxation in the rotating frame. Wet samples of MY510/D230 and MY721/D230 showed insignificant change in $^H T_{1\rho}$ comparing with $^H T_{1\rho}$ of dry samples. Even after the samples have been dried, $^H T_{1\rho}$ of dry, wet, and dried samples could not be differentiated from one another.

Table 6-1: T_{CH} and ${}^HT_{1\rho}$ of DGEBA/D230

Dry			75° C			75° C - Dried		
Peak freq.	T_{CH}	${}^HT_{1\rho}$	Peak freq.	T_{CH}	${}^HT_{1\rho}$	Peak freq.	T_{CH}	${}^HT_{1\rho}$
148.89	6.42	1436.6				146.25	760.21	753.52
62.08	11.44	572.18	64.08	4.10	4971.4	58.26	7.46	478.58
12.65			20.02	142.56	914.28	19.23	88.24	760.59
5.22	125.05	558.58	4.64	137.17	1011.3	4.82	106.36	620.86
-2.43	116.72	603.56	-2.19	136.94	914.76	-1.28	109.16	617.29

Table 6-2: T_{CH} and ${}^H T_{1\rho}$ of MY510/D230

Dry			75° C			75° C - Dried		
Peak freq.	T_{CH}	${}^H T_{1\rho}$	Peak freq.	T_{CH}	${}^H T_{1\rho}$	Peak freq.	T_{CH}	${}^H T_{1\rho}$
146.40	195.89	963.56	147.50	37.67	773.59	154.11	50.76	539.08
105.80	60.96	776.43	104.56	8.39	568.01	106.26	8.06	614.81
61.87	12.89	601.11	62.90	12.17	567.02	60.80	12.60	574.13
5.64	92.62	805.99	5.61	124.16	618.35	6.19	103.85	645.68
-1.67	100.49	686.97	-1.83	87.62	690.23	-1.70	107.94	608.20

Table 6-3: T_{CH} and ${}^H T_{1\rho}$ of MY721/D230

Dry			75° C			75° C - Dried		
Peak freq.	T_{CH}	${}^H T_{1\rho}$	Peak freq.	T_{CH}	${}^H T_{1\rho}$	Peak freq.	T_{CH}	${}^H T_{1\rho}$
122.40	11.86	620.69				120.52	33.88	426.20
63.90	12.77	635.83	61.32	14.78	522.46	65.54	11.56	550.82
6.03	112.37	765.78	6.52	102.01	887.58	6.49	94.062	840.55
-2.68	92.96	674.29	-2.37	94.10	656.99	-2.65	97.18	588.85

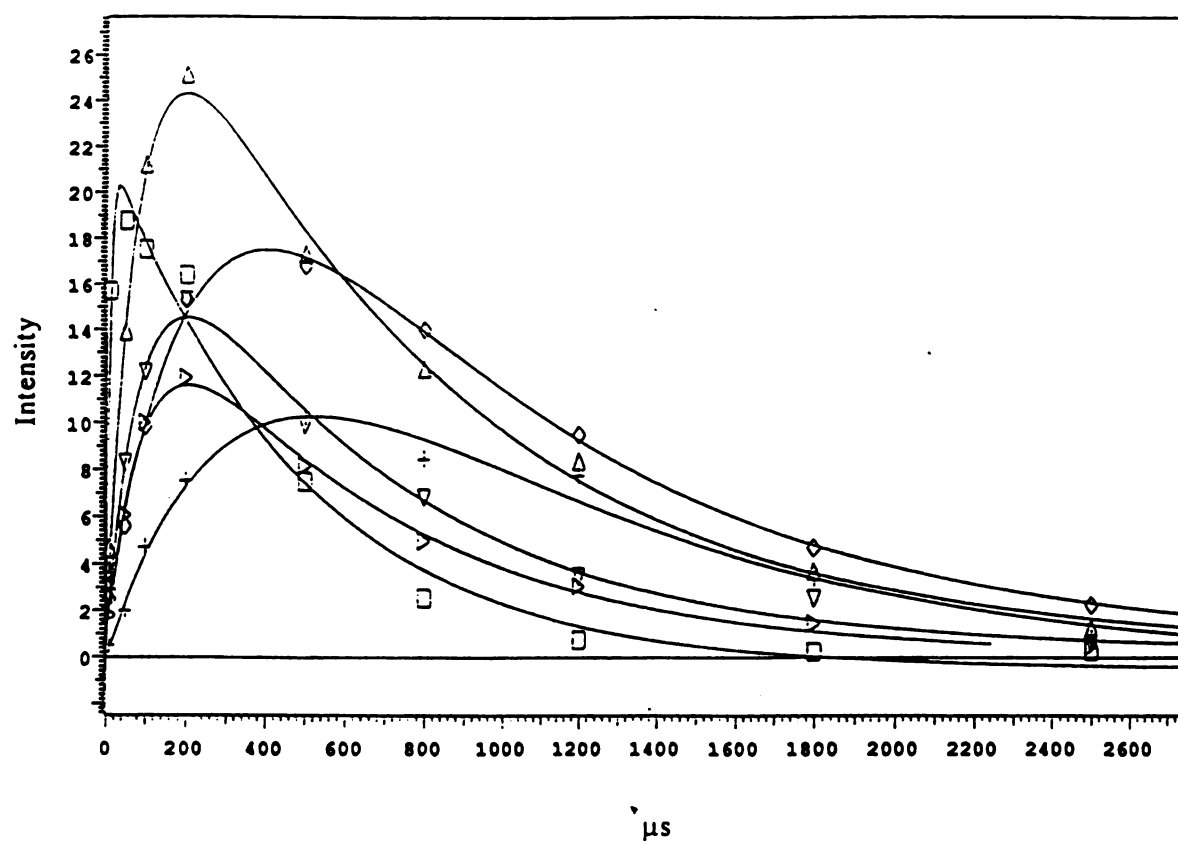


Figure 6-10: The change in carbon magnetization with contact time for the cross-polarization experiment. The initial rise is due to the cross-polarization contact time, T_{CH} , and the relaxation decrease is governed by the $^H T_{1\rho}$.

$^H T_{1\rho}$ provides information about the molecular dynamics of the magnetic moments and molecules around them. Also, the measurements of individual $^H T_{1\rho}$ involves the introduction of a variable contact time of cross polarization. When water molecules were introduced into the epoxy networks through sorption process, energy exchange occurs between ^1H and ^{13}C spin systems. The result is a growth of the ^{13}C magnetization at the expense of the ^1H magnetization. Thus, if mobile water molecules are present in the epoxy network, establishment of contact between the carbons and the protons will take some time. Therefore, as more mobile water molecules are present in the epoxy network, $^H T_{1\rho}$ will become longer.

$^H T_{1\rho}$ is a direct representation of the water molecule mobility. As mentioned above, $^H T_{1\rho}$ of moisture saturated DGEBA/D230 samples were distinctly higher than those of MY721 and MY510 epoxy glasses. In PALS experiment, it was said that τ_3 measures the size of the hole, and when comparing τ_3 of the three epoxy systems, τ_3 of DGEBA/D230 was the highest. In addition, VanderHart *et al* [41] reported that when water goes into the epoxy, a majority of water molecularly dispersed in the epoxy rather than aggregated in a waterlike state within voids (i.e. if voids are present, they can only accommodate one or two water molecules). Therefore, if the size of the hole is larger, the motion of water molecule will less likely be hindered. On the other hand, compared to DGEBA/D230, MY510 and MY721/D230 are tightly crosslinked polymer network

such that the size of free volume is smaller; therefore, it is less likely to show any significant increase in $^HT_{1\rho}$.

To further investigate the exact nature of the water in the crosslink network, quadrupole echo deuterium NMR spectroscopy was suggested.

6.8 Quadrupole Echo Deuterium NMR Experiment

Results from the conventional broad-line NMR spectroscopy were not satisfactory due to the broad signals it is giving out. For instance, when comparing spectra between dry and moisture desorbed samples to determine the nature of the moisture-epoxy chain interaction, it was difficult to affirm the water molecules were whether still linked to the chains after the desorption or all completely desorbed.

Quadrupole echo deuterium NMR provides an useful spectroscopic method for the study of water (i.e. deuterium oxide, D_2O) absorbed by polymers [50]. The quadrupole echo pulse sequence preserves the line shape of the inhomogeneously broadened deuterium NMR signal, thus by-passing the problems normally incurred with broad signals and receiver ringdown. Unlike conventional broad-line NMR counterpart, quadrupole echo deuterium NMR spectroscopy lends itself to Fourier transform method. Thus, it is possible to observe weak signals, using repeated spectral accumulation. In addition, the deuterium line shapes (acquired from Fourier transformation of the free induction decays) can be

analyzed in terms of models for molecular motion. Therefore, deuterium NMR spectroscopy is capable of providing highly specific and detailed information on a molecular level.

6.8.1 Results and Discussion

Figure 6-11 shows the quadrupole echo deuterium ^1H NMR spectrum of deuterium oxide (D_2O). It is shown as a sharp peak that the deuterium absorb at a chemical shift of $\delta 16000$ (16000 ppm). While this peak operates as a finger print for the deuterium in the epoxy network, the nature of the moisture can be studied by examining spectra of pure D_2O , D_2O saturated samples, and D_2O desorbed samples.

Experiments were conducted on samples saturated at 90°C only to examine the D_2O sorption and the desorption processes, disregarding the temperature effect on D_2O sorption behavior. As can be seen in Figure 6-12, mobile deuteriums, introduced to the epoxy resins by the sorption process are depicted as sharp peaks. All three systems clearly show the presence of the deuterium in their networks. After the desorption process (100°C for 4 days), however, there are no traces of deuterium presence in the epoxy resins. The results are shown in Figure 6-13.

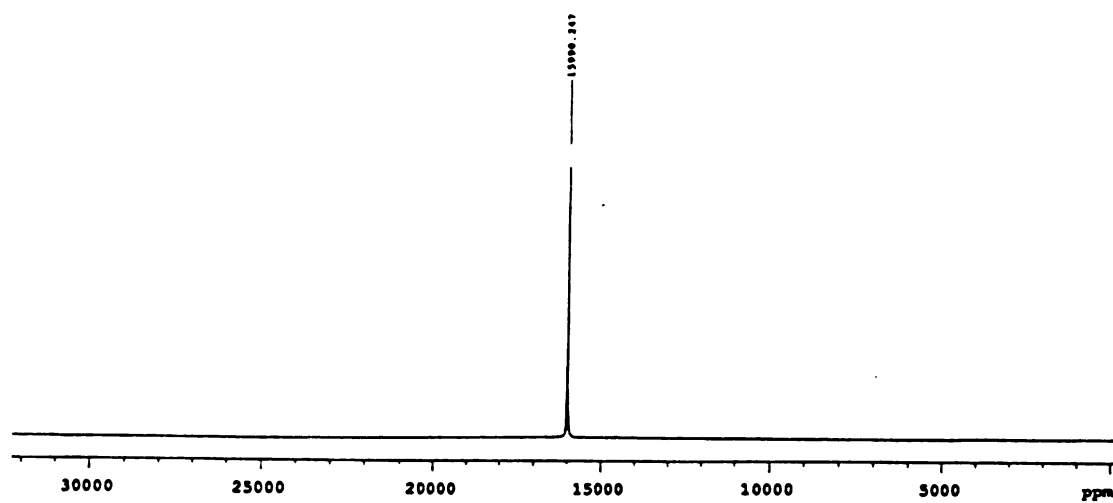


Figure 6-11: Quadrupole echo deuterium ^1H NMR spectrum of D_2O . The sharp peak at $\delta 16000$ is indicating the chemical shift of pure deuterium.

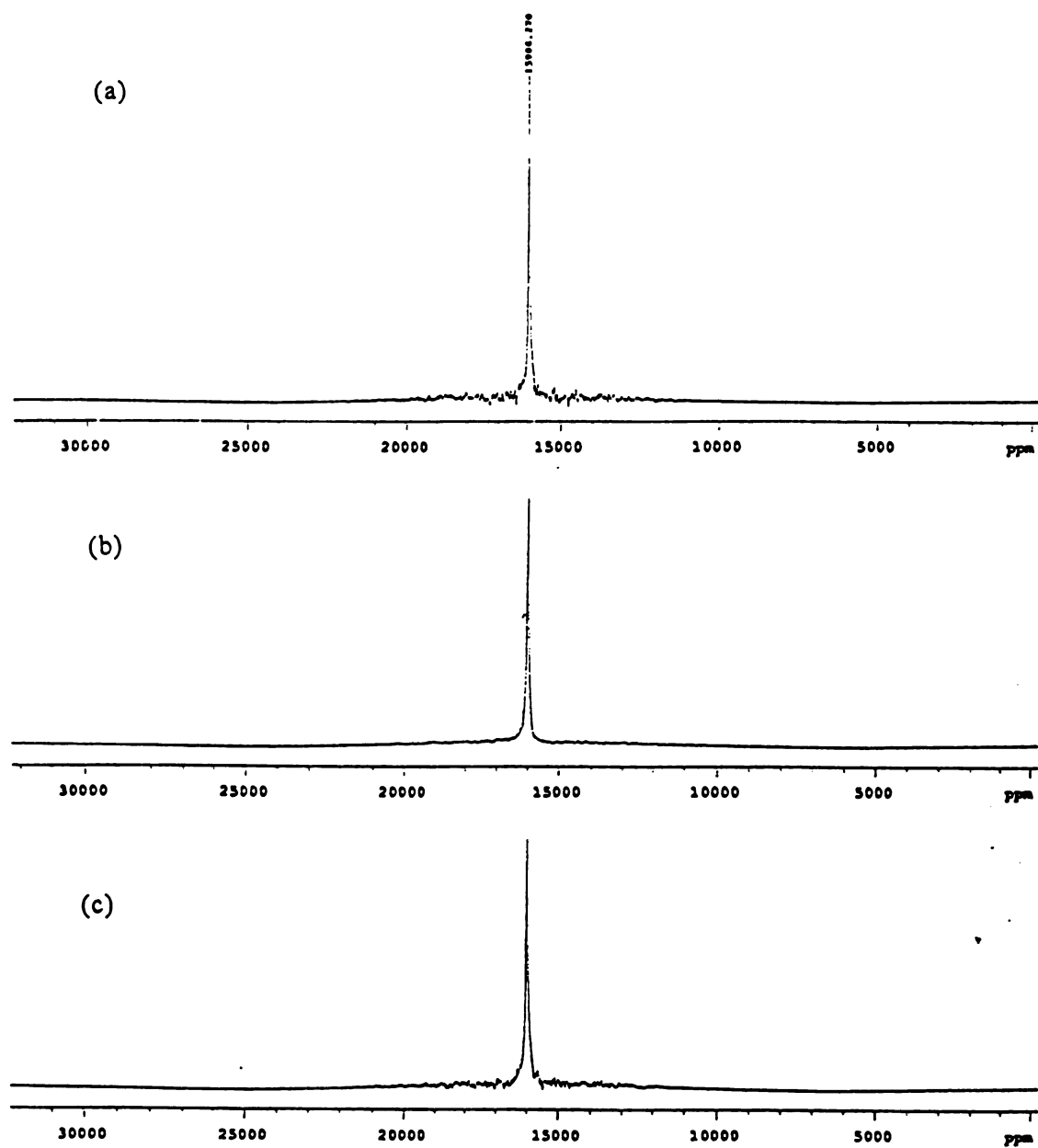


Figure 6-12: Quadrupole echo deuterium ^1H NMR spectra of samples saturated with D_2O at 90°C ; (a) DGEBA/D230; (b) MY510/D230; and (c) MY721/D230.

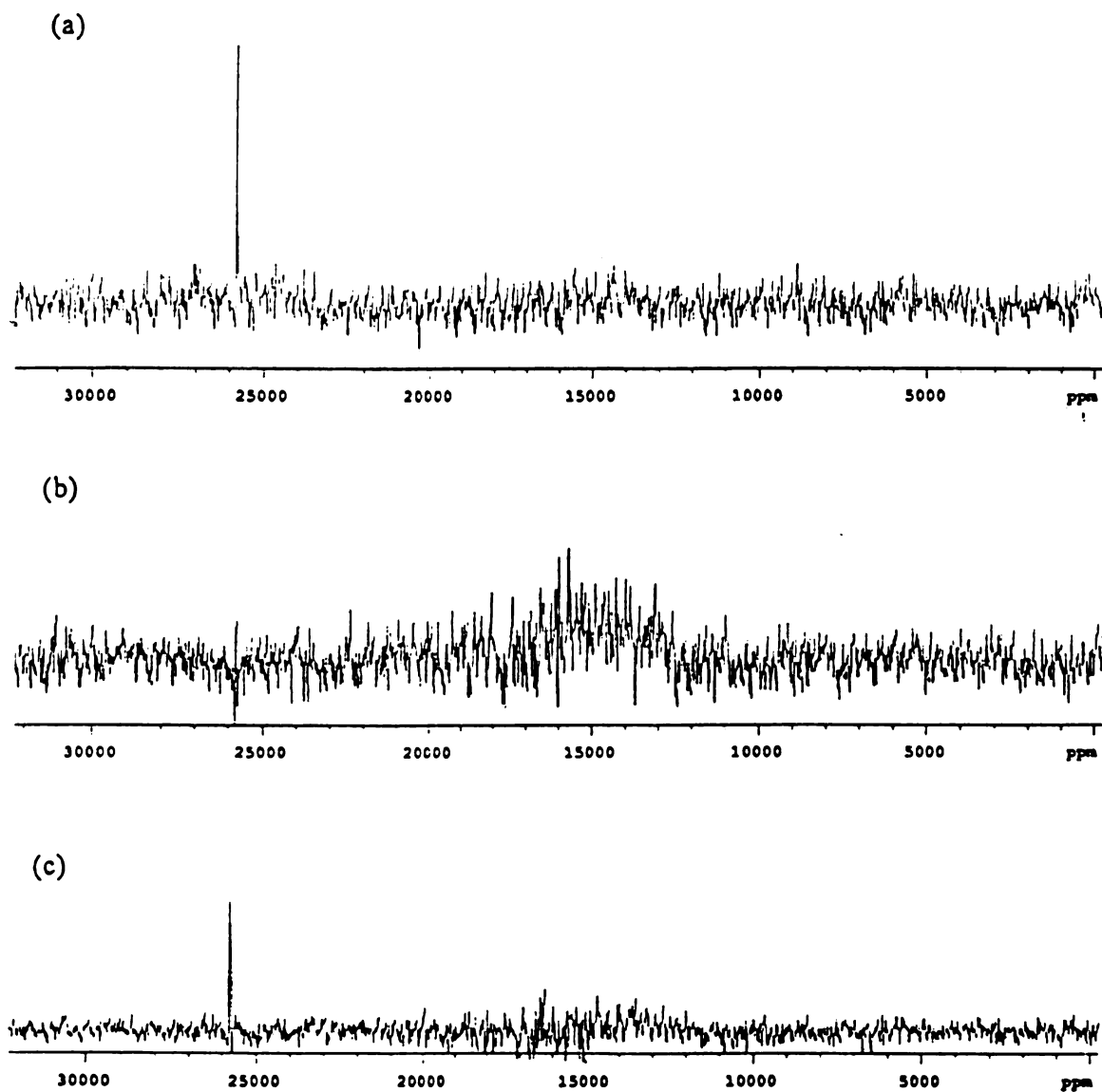


Figure 6-13: Quadrupole echo deuterium ^1H NMR spectra of D_2O desorbed samples (100°C for 4 days); (a) DGEBA/D230; (b) MY510/D230; and (c) MY721/D230.

6.9 Summary

Because the water molecules were highly mobile, DGEBA/D230 epoxy glass needed longer time to establish contact between the carbons and the protons. In addition, since the majority of water molecularly dispersed in the epoxy, rather than aggregated in a waterlike state within voids, as water molecules go into the epoxy network, it will certainly help the motion of water molecules if the size of free volume is large. From PALS results, it was found that DGEBA/D230 has larger free volume. Therefore, $^H T_{1\rho}$ of wet samples was significantly higher than that of dry samples. It is noteworthy that after the desorption process, $^H T_{1\rho}$ returned to its initial value, suggesting that the absorbed moisture was simply occupying free volume.

Similar results were found in quadrupole echo deuterium NMR experiment. Figure 6-13 shows no signs of deuterium present in the network after the samples have undergone the desorption process. Based on this finding, one can conclude that the moisture absorbed in the epoxy resins is not chemically bonded to the crosslink network, but rather is simply occupying the voids in the crosslink network such that when the samples were heated up, D₂O molecules were able to escape out of the epoxy resins.

7. CONCLUSIONS

Since the crosslink density increases with the resin functionality, it can be said that the resin functionality is directly related to the diffusion in an epoxy glass such that when an epoxy glass is formed by a reaction between hardener and a monomer with a higher number of functional groups, diffusivity of the epoxy glass becomes lower. It was also found that the highly crosslinked epoxy glass was more susceptible to the hygrothermal degradation.

Not only the crosslink density, but also the thickness variation affected the diffusion behavior in the epoxy network. Swelling effect made a great contribution in this phenomena such that thicker the sample, lower the diffusion coefficient and higher the equilibrium moisture content.

It is also noteworthy that under a constant conditioning temperature, as $\Delta T = |T_e - T_g|$ increases, the diffusion coefficient decreases, where T_e is an experiment temperature and T_g is a glass transition temperature. In other words, as the conditioning temperature is further away from T_g , it becomes more difficult for the diffusants to penetrate through the epoxy network.

As discussed earlier, crosslink density increases with a functionality, resulting in the increase of T_g . Moisture uptake, however, was depended upon not crosslink density, but available hydroxyl sites per mole in the epoxy resin such that MY510/D230 epoxy glass absorbed the most wt% of water, followed by the

MY721/D230 and the DGEBA/D230. Therefore, it can be concluded that the hydroxyl site availability in the epoxy network is the dominant factor determining the % weight gain of the moisture.

Moisture effects on physical properties were extensive such that plasticization of the polymer was observed. In addition, there was a prevalent conformational change in the polymer network during sorption and desorption processes. In terms of the localization of the water molecules in the epoxy network, positron annihilation lifetime spectroscopy (PALS) provided a great deal of information. It has shown that even though water molecules primarily tackle the hydroxyl sites, they occupy free volume between polymer molecules. Upon desorption, those water molecules, occupying free volume, simply desorbed away. The solid state NMR of ^1H spin-lattice relaxation times in the rotating frame and quadrupole echo deuterium NMR results also showed that there was no prominent evidence of water molecules chemically react with the polymer network.

Immersion of the epoxy resins in water at elevated temperatures for an extended period of time induced oxidation and chemical degradation resulting in discoloration of the specimens and significant decrease in mechanical properties. Discoloration and mechanical property drop were most severe with the immersion temperatures. In addition, epoxy resins of higher functionality were more susceptible to the chemical degradation than those of lower functionality such that the MY721/D230 epoxy resin suffered oxidation and degradation in a great deal.

Finally, the solid state NMR of ^1H spin-lattice relaxation times in the rotating frame and quadrupole echo deuterium ^1H NMR results revealed that even though the available hydroxyl sties are the driving force for the moisture absorption, the moisture absorbed in the epoxy resins were not chemically bonded to the network.

REFERENCES

8. REFERENCES

1. Chi-Hung Shen and George S. Springer, "Moisture Absorption and Desorption of Composite Materials", *Environmental Effects on Composite Materials*, ed. G. S. Springer, (1981), 15.
2. Andre Lee and Gregory B. McKenna, "The physical aging response of an epoxy glass subjected to large stresses", *Polymer*, **31**, 423 (1990).
3. Andre Lee and Gregory B. McKenna, "Effect of crosslink density on physical aging of epoxy networks", *Polymer*, **29**, 1812 (1988).
4. Y. Diamant, G. Marom, and L. J. Broutman, "The effect of network structure on moisture absorption of epoxy resins", *J. Appl. Polym. Sci.*, **26**, 3015 (1981).
5. V. B. Gupta and L. T. Drzal, "The physical basis of moisture transport in a cured epoxy resin system", *J. Appl. Polym. Sci.*, **30**, 4467 (1985).
6. Michael J. Adamson, "Thermal expansion and swelling of cured epoxy resin used in graphite/epoxy composite materials", *J. Mater. Sci.*, **15**, 1736 (1980).
7. E. Morel, V. Bellenger, and J. Verdu, "Structure-water absorption relationships for amine-cured epoxy resins", *Polymer*, **26**, 1719 (1985).
8. John B. Enns and John K. Gillham, "Effect of the extent of cure on the modulus, Glass transition, Water absorption, and Density of an amine-cured epoxy", *J. Appl. Polym. Sci.*, **28**, 2831 (1983).
9. R. T. Fuller, R. E. Fornes, and J. D. Memory, "NMR Study of Water Absorbed by Epoxy Resin", *J. Appl. Polym. Sci.*, **23**, 1871 (1979).
10. Ned D. Danieleley and Edward R. Long, Jr., "Effects of Curing on the Glass Transition Temperature and Moisture Absorption of Neat Epoxy Resin", *J. Polym. Sci. Chem. Ed.*, **19**, 2443 (1981).
11. C. Carfagna, A. Apicella, and L. Nicolais, "The Effect of the Prepolymer composition of Amino-Hardened Epoxy Resins on the Water Sorption Behavior and Plasticization", *J. Appl. Polym. Sci.*, **27**, 105 (1982).
12. P. Moy and F. E. Karasz, "Epoxy-Water Interactions", *Polym. Eng. Sci.*, **20**, 315 (1980).
13. I. Ghorbel and D. Valentin, "Hydrothermal Effects on the Physico-Chemical Properties of Pure and Glass Fiber Reinforced Polyester and Vinylester Resins", *Polym. Compos.*, **14**, 324 (1993).

14. Wen-li Wu and Barry J. Bauer, "Epoxy Network Structure. 3. Neutron-Scattering Study of Epoxies Containing Monomers of Different Molecular Weight", *Macromolecules*, **19**, 1613 (1986).
15. Wen-li Wu, Donald L. Hunston, Hsinjin Yang, and Richard S. Stein, "Epoxy Network Structure. 4. A Neutron Scattering Study of Epoxies Swollen in a Deuterated Solvent", *Macromolecules*, **21**, 756 (1988).
16. J. S. Vrentas and C. M. Vrentas, "Fickian Diffusion in Glassy Polymer-Solvent Systems", *J. Polym. Sci. Phys. Ed.*, **30**, 1005 (1992).
17. Donald S. Cohen, "Theoretical Models for Diffusion in Glassy Polymers", *J. Polym. Sci. Phys. Ed.*, **21**, 2057 (1983).
18. Donald S. Cohen, "Theoretical Models for Diffusion in Glassy Polymers II", *J. Polym. Sci. Phys. Ed.*, **22**, 1001 (1984).
19. B. De'Neve and M. E. R. Shanahan, "Water Absorption by an Epoxy Resin and its Effect on the Mechanical Properties and Infra-Red Spectra", *Polymer*, **34**, 5099 (1993).
20. J. J. Imaz, J. L. Rodriguez, A. Rubio, and I. Mondragon, "Hydrothermal Environment Influence on Water Diffusion and Mechanical Behavior of Carbon Fiber/Epoxy Laminates", *J. Mater. Sci. Lett.*, **10**, 662 (1991).
21. V. Bellenger, J. Verdu, and E. Morel, "Structure-Properties Relationships for Densely Cross-linked Epoxide-Amine Systems Based on Epoxide or Amine Mixtures", *J. Mater. Sci.*, **24**, 63 (1989).
22. Robert A. Yapel, J. Larry Duda, Xiaohong Lin, and Ernst D. von Meerwall, "Mutual and Self-diffusion of Water in Gelatin: Experimental Measurement and Predictive Test of Free-Volume Theory", *Polymer*, **35**, 2411 (1994).
23. John M. Zielinski and J. L. Duda, "Predicting Polymer/Solvent Diffusion Coefficients Using Free-Volume Theory", *AIChE J.*, **38**, 405 (1992).
24. Ryszard Steller and Danuta Zuchowska, "Free Volume Effects on Rheological and Thermal Properties of Polymers and Polymer Blends", *J. Appl. Polym. Sci.*, **43**, 1411 (1991).
25. J. S. Vrentas and C. M. Vrentas, "Evaluation of Free-Volume Theories for Solvent Self-Diffusion in Polymer-Solvent Systems", *J. Polym. Sci. Phys. Ed.*, **31**, 69 (1993).
26. Y. Limoge, "On the concept of Free Volume in Amorphous Materials", *Scripta Metall. et. Mat.*, **26**, 809 (1992).
27. Christopher S. Coughlin, Kenneth A. Mauritz, and Robson F. Storey, "A General Free Volume Based Theory for the Diffusion of Large Molecules

- in Amorphous Polymers above Tg. 4. Polymer-Penetrant Interactions", *Macromolecules*, **24**, 1526 (1991).
28. R. Kirchheim, "Sorption and Partial Molar Volume of Small Molecules in Glassy Polymers", *Macromolecules*, **25**, 6952 (1992).
 29. J. C. Moreland, G. L. Wilkes, and R. B. Turner, "Viscoelastic Behavior of Flexible Slabstock Polyurethane Foams: Dependence on Temperature and Relative Humidity. I. Tensile and Compression Stress (Load) Relaxation", *J. Appl. Polym. Sci.*, **52**, 549 (1994).
 30. Y. Kobayashi, K. Haraya S. Hattori, and T. Sasuga, "Evaluation of Polymer Free Volume by Positron Annihilation and Gas Diffusivity Measurements", *Polymer*, **35**, 925 (1994).
 31. Q. Deng, F. Zandiehnam, and Y. C. Jean, "Free-Volume Distributions of an Epoxy Polymer Probed by Positron Annihilation: Temperature Dependence", *Macromolecules*, **25**, 1090 (1992).
 32. J. Liu, Q. Deng, and Y. C. Jean, "Free-Volume Distributions of Polystyrene Probed by Positron Annihilation: Comparison with Free-Volume Theories", *Macromolecules*, **26**, 7149 (1993).
 33. Richard C. Macqueen and Richard D. Granata, "Positron Annihilation Spectroscopy Study of Moisture Absorption in Protective Epoxy Coatings", *J. Polym. Sci. Phys. Ed.*, **31**, 971 (1993).
 34. Antonio Apicella, Luigi Nicolais, Gianni Astarita, and Enrico Drioli, "Effects of Thermal History on Water Sorption, Elastic Properties and the Glass Transition of Epoxy Resins", *Polymer*, **20**, 1143 (1979).
 35. A. Apicella, L. Nicolais, G. Astarita, and E. Drioli, "Hygrothermal History Dependence of Moisture Sorption Kinetics in Epoxy Resins", *Polym. Eng. Sci.*, **21**, 18 (1981).
 36. Antonio Apicella and Luigi Nicolais, "Environmental Aging of Epoxy Resins: Synergistic Effect of Sorbed Moisture, Temperature, and Applied Stress", *Ind. Eng. Chem. Prod. Res. Dev.*, **20**, 138 (1981).
 37. David Shiaw-Guang Hu and Mark T. S. Lin, "Water-Polymer Interactions and Critical Phenomena of Swelling in Inhomogeneous Poly(acrylonitrile-acrylamide-acrylic acid)gels", *Polymer*, **35**, 4416 (1994).
 38. Myung Cheon Lee and Nikolaos A. Peppas, "Water Transport in Graphite/Epoxy Composites", *J. Appl. Polym. Sci.*, **47**, 1349 (1993).
 39. J. Zhou and J. P. Lucas, "Characteristics of Water in Graphite/Epoxy Composites", *Proceedings of the American Society for Composites, Ninth Technical Conference*, 1213 (1994).

40. Jiming Zhou and James P. Lucas, "Water-Environment Effects on Anomalous Absorption Behavior in Graphite-Epoxy Composite", PhD Thesis, Michigan State University, 1996.
41. R. J. Schadt and D. L. VanderHart, "Solid State Proton NMR of a Glassy Epoxy Exposed to Water", *Macromolecules*, **28**, 3416 (1995).
42. J. A. Pople, W. G. Schneider, and H. J. Bernstein, "High Resolution Nuclear Magnetic Resonance", McGraw-Hill, New York, 1959.
43. Jack L. Koenig, "Spectroscopy of Polymers", ACS Professional Reference Book, American Chemical Society, Washington, DC 1992.
44. L. G. Wade, Jr., Organic Chemistry, Prentice-Hall, Inc., Englewood Cliffs, NJ., 1987.
45. T. C. Wong and L. J. Broutman, "Moisture Diffusion in Epoxy Resins Part I. Non-Fickian Sorption Processes", *Polym. Eng. Sci.*, **25**, 521 (1985).
46. T. C. Wong and L. J. Broutman, "Water in Epoxy Resins Part II. Diffusion Mechanism", *Polym. Eng. Sci.*, **25**, 529 (1985).
47. J. Crank, "The Mathematics of Diffusion", Ch. 12, Clarendon Press, Oxford (1956).
48. Michael A. Wilson, *N.M.R. Techniques and Applications in Geochemistry and Soil Chemistry*, Pergamon Press, 1987.
49. J. Schaefer, M. D. Sefcik, E. O. Stejskal, and R. A. McKay, *Macromolecules*, **14**, 188-192 (1981).
50. R. J. Young, "Introduction to Polymers", 1st ed., Chapman and Hall, 1981.
51. Li Xie, David Gidley, Hristo Hristov, and Albert Yee, *Polymer*, **35**, 14-17 (1994)
52. Liu Yang, Hrist Hristov, Albert Yee, David Gidley, Didier Bauchiere, Jean Louise Halary, and Monnerie, *Polymer*, **36**, 3997-4003 (1995).

MICHIGAN STATE UNIV. LIBRARIES



31293015728698